2018

Quantitative Line Assignment in Optical Emission Spectroscopy

Jessica Chappell
University of Central Florida

QUANTITATIVE LINE ASSIGMENT IN OPTICAL EMISSION SPECTROSCOPY

by

JESSICA NICOLE CHAPPELL
B.S Southwest Baptist University, 2013
M.S. University of Central Florida, 2017

A dissertation submitted in partial fulfillment of the requirements
for the degree of Doctor of Philosophy
in the Department of Chemistry
in the College of Sciences
at the University of Central Florida
Orlando, Florida

Summer Term
2018

Major Professor: Matthieu Baudelet

ABSTRACT

Quantitative elemental analysis using Optical Emission Spectroscopy (OES) starts with a high level of confidence in spectral line assignment from reference databases. Spectral interferences caused by instrumental and line broadening decrease the resolution of OES spectra creating uncertainty in the elemental profile of a sample for the first time. An approach has been developed to quantify spectral interferences for individual line assignment in OES. The algorithm calculates a statistical interference factor (SIF) that combines a physical understanding of plasma emission with a Bayesian analysis of the OES spectrum. It can be used on a single optical spectrum and still address individual lines. Contrary to current methods, quantification of the uncertainty in elemental profiles of OES, leads to more accurate results, higher reliability and validation of the method.

The SIF algorithm was evaluated for Laser-Induced Breakdown Spectroscopy (LIBS) on samples with increasing complexity: from silicon to nickel spiked alumina to NIST standards (600 glass series and nickel-chromium alloy). The influence of the user's knowledge of the sample composition was studied and showed that for the majority of spectral lines this information is not changing the line assignment for simple compositions. Nonetheless, the amount of interference could change with this information, as expected. Variance of the SIF results for NIST glass standard was evaluated by the chi-square hypothesis test of variance showing that the results of the SIF algorithm are very reproducible.

To my family

ACKNOWLEDGMENTS

To my mom and dad, I want to thank you so much for the wisdom and guidance that you provided which has kept me focused on my pursuit of higher education. I wouldn't have been able to continue with this path if you hadn't been there for me every step of the way. To my brothers, thank you for supporting me and making me laugh when times were stressful. A special thanks to my grandma Chappell who passed my first semester of graduate school. I wouldn't be who I am today and continue to be without your love and spiritual guidance.

I would like to thank my research advisor, Dr. Baudelet, for his guidance throughout my graduate studies. I would also like to thank Dr. Sigman for all of his help and encouraging words throughout my time at the National Center for Forensic Science (NCFS). For my fellow graduate students at NCFS, of which there are too many to name, I cannot express how thankful I am for living life with you. To Danielle and Brian thank you for your friendship and counsel that you have provided from driving to pick me up when I wasn't well to watching movies together.

TABLE OF CONTENTS

LIST OF FIGURES

LIST OF TABLES

CHAPTER 1: INTRODUCTION

Elemental analysis is the qualitative or quantitative determination of major, minor and trace elements in a sample's composition. It is useful for many analytical applications such as environmental[1,2,3], biomedical[4,5], industrial[6,7], and forensics[8,9,10] analysis. Qualitative elemental analysis determines which elements are present while quantitative elemental analysis determines their concentration. Spectroscopic techniques for elemental analysis measure spectral line intensities that can be converted to the concentration of the elements present in a sample by a process known as calibration. The presence or the concentration of elements in the elemental profile allows for experimental data to be compared to databases of standards or known compounds for identification purposes.

Elemental analysis relies mainly on three techniques: absorption or emission of light by neutrals and ions, and mass spectrometry of singly-ionized species. This Ph.D. work focused on optical emission spectroscopy (OES) in the UV-Visible-Near Infrared region and as such, we will refer the reader interested in the other methods to the appropriate literature.

Two current techniques rely on OES: Inductively Coupled Plasma – OES (ICP-OES) and Laser-Induced Breakdown Spectroscopy (LIBS). Both techniques are of interest since laser ablation can be (in the former case) and is (for the latter) the sampling approach. Characteristics of LA-ICP-OES, and LIBS include little to no sample preparation, real time analysis, and analysis of materials in any state of matter. Laser ablation only samples a small amount of material, making

this technique relatively non-destructive. The characteristics of LIBS and LA-ICP-OES make these methods of analysis attractive for many applications.

The first step of elemental analysis is the assignment of spectral lines. Spectral interferences can taint spectral line assignment in laser ablation optical emission spectroscopy. They can originate from the instrumentation, line broadening, and shifting resulting in broadened spectral lines. The broadened spectral line cannot be resolved to identify the transition that produced the spectral peak without the use of an atomic emission database. Confidence in the spectral line assignment for a sample requires high spectral resolution, but high resolution cannot prevent all spectral interferences from occurring. These spectral interferences become a first source of uncertainty in line assignment for elemental analysis.

During this thesis, an algorithm has been developed to quantify spectral interferences in optical emission spectroscopy. It relies on the fundamentals of line emission and a Bayesian analysis of the emission spectrum. Therefore, before concentrating on the quantification of spectral interferences, chapter 2 will describe optical emission spectroscopy for the analytical techniques that are LIBS and ICP-OES as they rely on two different types of plasmas as their excitation source, still with similar theoretical description. Chapter 3 will focus on the fundamentals of the laser-induced plasma and its dynamics and thermodynamic equilibria, characterized by Planck, Maxwell and Boltzmann distributions, and Saha equilibrium.

Chapter 4 will address the importance of quantifying uncertainty in forensic analysis. The application to the uncertainties in optical emission spectroscopy will be discussed with examples such as line coincidence tables, calibration (and calibration-free) approaches, and chemometrics.

The quantification of spectral interferences developed in this thesis, called the statistical interference factor (SIF), will be extensively discussed in chapter 5. Chapter 6 will show the application of the SIF for LIBS analysis of a pure silicon sample and National Institute Standards and Technology standards of glass and a nickel-cobalt-chromium alloy. For each sample, the spectral interferences are identified and quantified to provide a more accurate analysis, reliability, and confidence of the results.

CHAPTER 2: BACKGROUND

Atomic emission spectroscopy (AES) is a type of optical emission spectroscopy; an analytical method of chemical analysis that measures the intensity of light emitted from an excitation source at a specific characteristic set of wavelengths for each emitter of interest. The emission of light by atoms or ions at a specific wavelength or frequency is unique to that element which results in a characteristic spectrum that can be utilized to identify that specific atom or ion. The identity of an element is determined by the wavelength of the emitted spectral line and the intensity is proportional to the number of atoms of the element present in the sample. There are many types of excitation sources that can cause a sample to emit light such as flame, plasma, arc, or spark.

Atomic emission occurs when a bound electron in a higher energy orbital returns to a lower energy orbital. The lowest energy state an atom can occupy is called its ground state which is also the most stable arrangement of electrons for an element. In Bohr's model, the energy of an electron E_n, in a specific orbital or quantum number n, is given by the following equation in Bohr's model, where *R* is the Rydberg constant, *h* is Planck's constant, n is the energy level of the atom, and *c* is the speed of light.

$$\boldsymbol{E_n = \frac{-Rhc}{n^2}} \qquad \textbf{(1)}$$

Figure 1 shows the Bohr's model of an element where an excited electron in a higher energy level is de-excited to a lower energy orbital resulting in loss of energy and the emission of a photon. The energy and the frequency of absorption and emission can be calculated using the difference between the two orbital energies. The probability per time unit of an atom in the upper energy level moving to a lower energy level is the emission probability of an emitter.

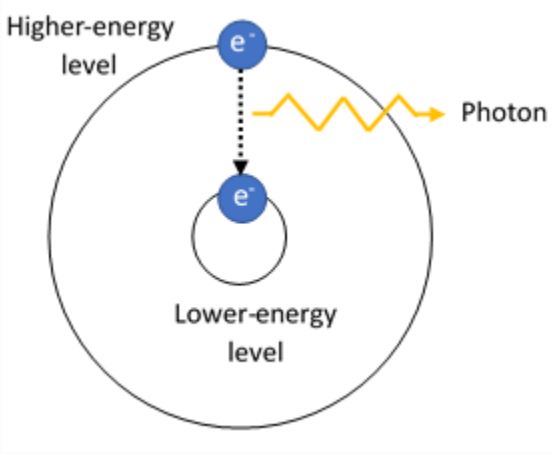

Figure 1: Bohr's model of an atom.

The combination of relativity and spin-orbit coupling results in a modification of the energy levels known as the fine structure. There are two possible spin orientations which results in the splitting of an energy level into two lines; one for the magnetic field of the electron and the other due to the magnetic moment of the electron with respect to its spin. Each electron within the atom has a spin S, and an orbital angular momentum l with magnetic moments. The total electronic angular-momentum quantum number J, is the sum of the spin and orbital angular momentum.

$$\boldsymbol{J = L + S} \qquad \textbf{(2)}$$

The spectral line defined by the emission of an emitter has a fine structure when there is a shift in the electronic atomic energy levels due to interactions between the electronic magnetic dipoles, orbital motion, and the nucleus. Optical emission spectroscopy quantitatively or qualitatively determines the elemental composition of a sample like AES and is based on the intrinsic plasma radiation.

Inductively-Coupled Plasma Optical Emission Spectroscopy

Inductively-coupled plasma optical emission spectroscopy (ICP-OES) is a type of atomic emission spectroscopy where a sample is excited in an inductively coupled plasma. ICP-OES provides qualitative or quantitative analysis through emission of atoms and singly-ionized ions. A schematic drawing of the ICP torch comprised of three concentric fused-silica tubes is shown in Figure 2. The three tubes are considered the outer, intermediate, and inner tubes. The ICP torch is placed within water-cooled two- or three- turn load coil connected to a radio-frequency (RF) generator[11]. Three types of gas flow, typically argon, are necessary for plasma formation in ICP-OES. Argon gas passes between the outermost and intermediate tubes tangentially at a rate of ~12-17 L/min generate the plasma[12]. The second gas flow, auxiliary gas passes through the intermediate tube and sample injector to change the position of the plasma relative to the tube and injector. A carrier gas or nebulizer gas flows through the inner tube bores through the base of the plasma and carries the sample to the plasma where emission is observed. The inductively coupled plasma is formed by the application of the radiofrequency (RF) power to the load coil

where an alternating current oscillates at a rate determined by the frequency of the RF generator. Electric and magnetic fields are created inside the top of the torch at the same high-frequency oscillation of the current. The argon gas flows through the torch and a spark from a Tesla coil produced charged particles inside the load coil area. The magnetic field accelerates the charged ions and electrons and collide with other atoms resulting in further ionization. Excited atoms and ions emit light when reverting to a lower energy state which is dispersed and detected yielding an emission spectrum.

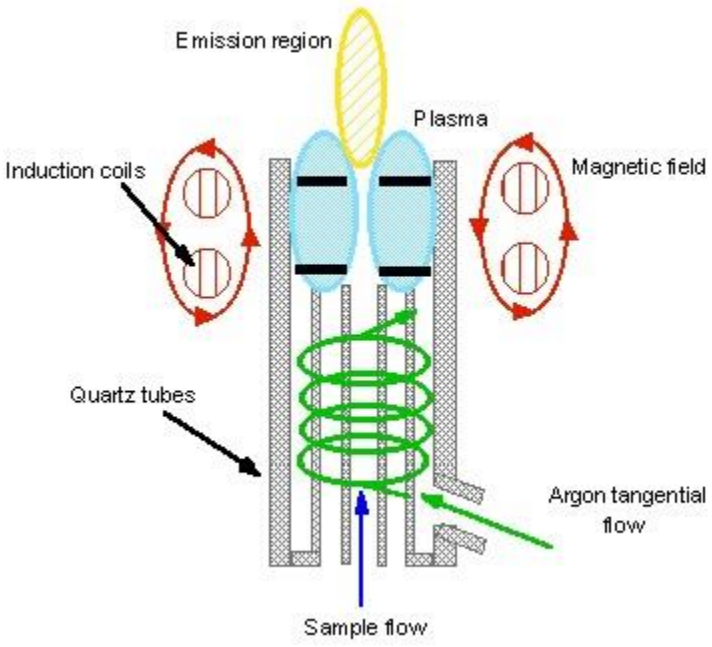

Figure 2: Schematic of an ICP torch[14].

ICP-OES is a multi-elemental technique that has high precision[14] and selectivity as well as low detection limits. The ability of the ICP to produce high temperature plasma, ~6,000 – 10,000 K,

allows for reproducible vaporization, atomization, excitation, and ionization of elements[15]. Sample preparation in ICP-OES is time and material consuming as the sample must be prepared in an aerosol form to be transported to the plasma; solids must be digested. Complex sample matrices affect accuracy and detection limits of trace elements[16]. Sample size requirement for ICP-OES is a few milligrams but the method is destructive. ICP-OES systematic errors occur from procedural steps or spectral interferences[17].

Laser-Induced Breakdown Spectroscopy

Laser-induced breakdown spectroscopy (LIBS) is a type of atomic emission spectroscopy that comprises of the formation of a laser-induced plasma on the surface of a sample to provide qualitative or quantitative analysis from atomic and ionic optical emission. Ablation of the sample's surface in LIBS occurs when a laser pulse is focused onto the surface of a sample with an irradiance generally greater than 1-10 MW/cm^2 [18]. Figure 3 shows schematically the laser-induced breakdown process in the common case of a nanosecond laser pulse.

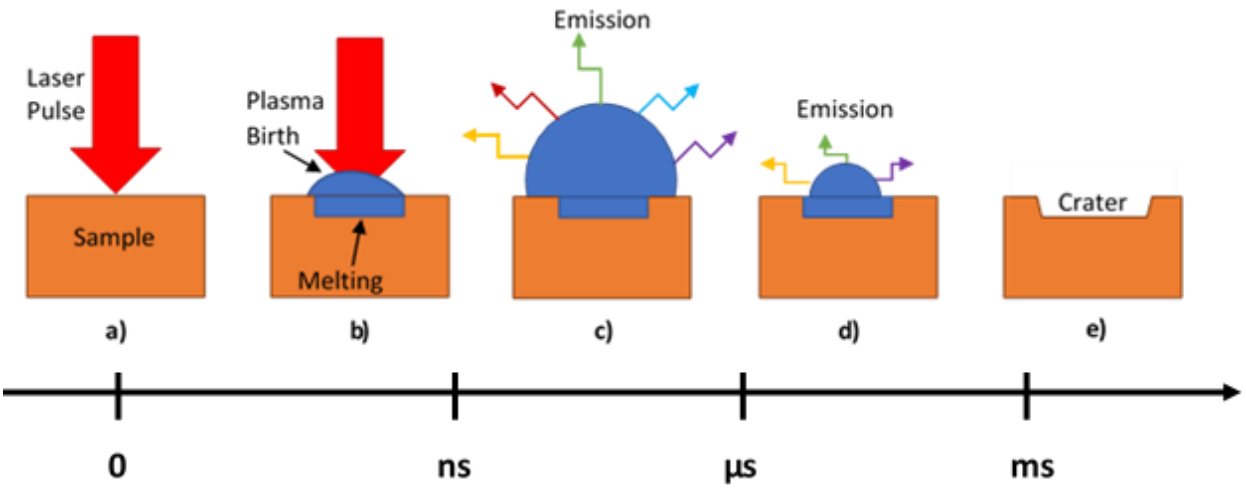

Figure 3: Schematic of LIBS ablation process (a) laser pulse (b) ionization and breakdown (c) plasma expansion and emission (d) plasma cooling (e) crater formation.

The sample's surface requires a focused laser irradiance that exceeds the breakdown threshold of a sample. The focused laser pulse strikes the sample's surface electrons with enough photoionization to remove electrons from the sample's neutral atoms (Figure 3a). The photoionization creates free electrons that can absorb energy and accelerate. Acceleration of these electrons result in collisional or impact ionization because there is enough energy to collide with other atoms and electrons. Breakdown of the sample's surface occurs when the electron density reaches approximately 10^{18} electrons/cm^3 and the formation of a plasma is present on the sample's surface (Figure 3b)[20].

Once a plasma initially forms, it expands. The plasma is highly luminous containing the ablated neutral atoms' and ions' emission signals (Figure 3c). When the laser pulse stops, the laser-

induced plasma starts cooling down, neutral atoms are formed from the recombination of ions and electrons (Figure 3d). Plasma cooling results not only in the recombination of atoms but also molecules. Once the plasma has disappeared, signs that ablation occurred are shown as a crater on the sample surface (Figure 3e). Sample material vapor will condense while the plasma is cooling around the ablation crater, the condensed material will be forced out of the crater's center by the vapor pressure change of the plasma resulting in ridges and droplets around the edge of the ablation crater[21]. Excited ions will emit light when the laser pulse is finished and the plasma cools by reverting to a lower energy state (Figure 3d). The emitted light is usually analyzed by a dispersion spectrometer yielding a spectrum with information on the sample's elemental composition.

Laser-induced breakdown spectroscopy requires little to no sample preparation[22] and can analyze materials in any state of matter[23]. LIBS requires little amount of sample with a sample size requirement of micrograms[24]. Even though a small portion of the sample has been ablated, the method is considered relatively non-destructive. LIBS performs real-time analysis[25] and can quickly analyze numerous samples. The cost of LIBS instrumentation is lower than other optical emission spectroscopy techniques. Handheld and field portable LIBS instruments provide on-site analysis not capable with inductively-coupled plasma[26,27]. Most LIBS system operate time-resolved detectors to capture a LIBS spectrum with minimal affects from background continuum. Background continuum is created by the emission of photons from the electron acceleration and deceleration from collisions, electron recombination, and ion recombination[19]. Issues that can affect spectral response in laser-induced breakdown spectroscopy include high background

continuum, self-absorption of peaks and line broadening. Time-resolved data collection, sampling within an inert atmosphere, and experimental geometry can minimize these effects[28]. These numerous characteristics of LIBS makes it attractive for elemental analysis.

Optical Emission Spectroscopy Instrumentation

ICP-OES and LIBS both involve a plasma, but the application is different between the two. Differences in how the plasma is utilized affect the components of the ICP-OES and LIBS instruments.

Inductively-Coupled Plasma Optical Emission Spectroscopy

ICP-OES requires the sample to be aerosolized before introduction into the plasma. Figure 4 depicts the main components of an ICP-OES system which include a pump, nebulizer, argon gas, ICP torch, power generator, spectrometer, and computer. The pump is used to consistently supply sample liquid to the nebulizer. Important features of the sample introduction method include tolerance to complex matrices, reproducibility, ability to analyze small amounts of sample, high transport efficiency, and low cost[29]. Nebulizers are the most common sample introduction system where the sample liquid is converted into an aerosol and transported to the plasma. The ICP torch can be configured two ways for observing emissions from ICP; radial or axial view and the two can be combined into a dual view.

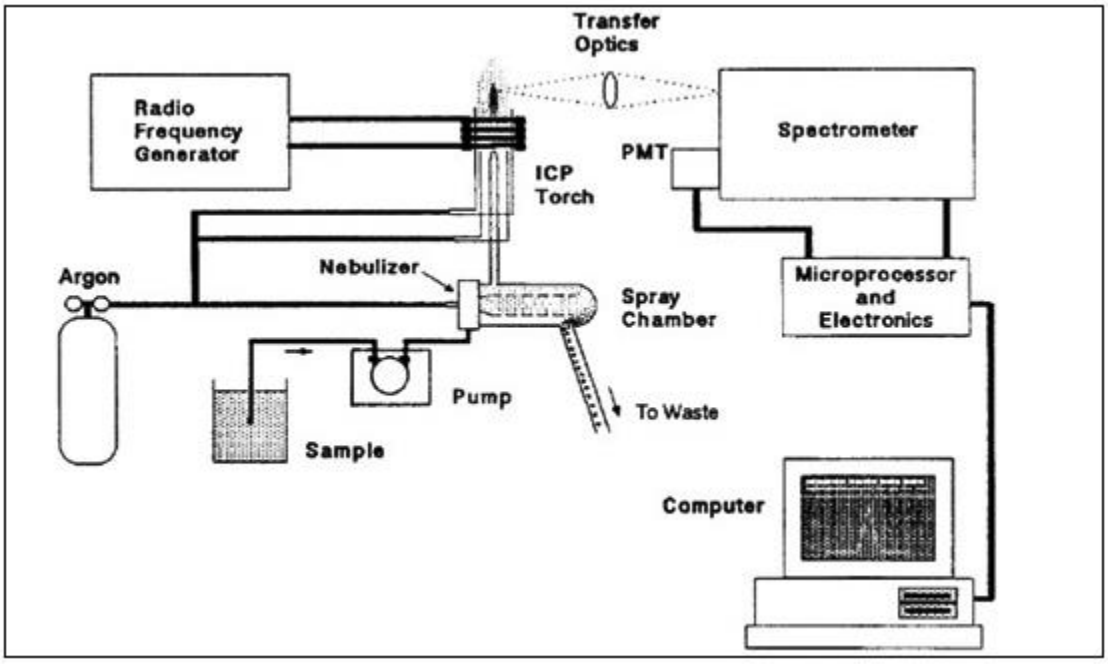

Figure 4: Schematic of an ICP-OES instrument[30].

When the plasma is in the vertical position, it is said to be in the radial view, where most emission originates (normal analytical zone) from the ICP discharge and is observed from the side of the plasma. The axial view is when the plasma is rotated to the horizontal position and the normal analytical zone is seen from the end of the plasma. Limits of detection are better when the ICP torch is in the axial view than the radial view[31].

An ICP-OES spectrum is obtained by pumping liquid sample in to the nebulizer where conversion to an aerosol occurs. The aerosol is carried to the plasma where desolvation, vaporization, ionization, excitation, and atomization process transpire. The excited atoms and

ions emit radiation which is detected by the spectrometer and turned into electrical signals. The computer reads the electrical signals and produces a spectrum of the wavelength of emitter's radiation versus the signal strength of the emitter's radiation at that wavelength.

Laser-Induced Breakdown Spectroscopy Instrumentation

A configuration of a LIBS apparatus is illustrated in Figure 5. The basic components of a LIBS system include the laser, focusing optics, sample holder, light collection system, detection system, and a computer. LIBS systems are comprised of the same basic components, but component specifications can change depending on the application. Laser specifications that are important include the pulse energy, pulse repetition rate, beam mode quality, size, weight, and cooling and electrical power requirements. The wavelength of the laser beam may or may not be an important parameter depending on the material of analysis[32].

The foundation of LIBS is the collection and analysis of an emission spectrum. The spectrometer which measures the intensity of light as a function of wavelength is an important component. Resolution and the spectral range are important properties of the spectrometer.

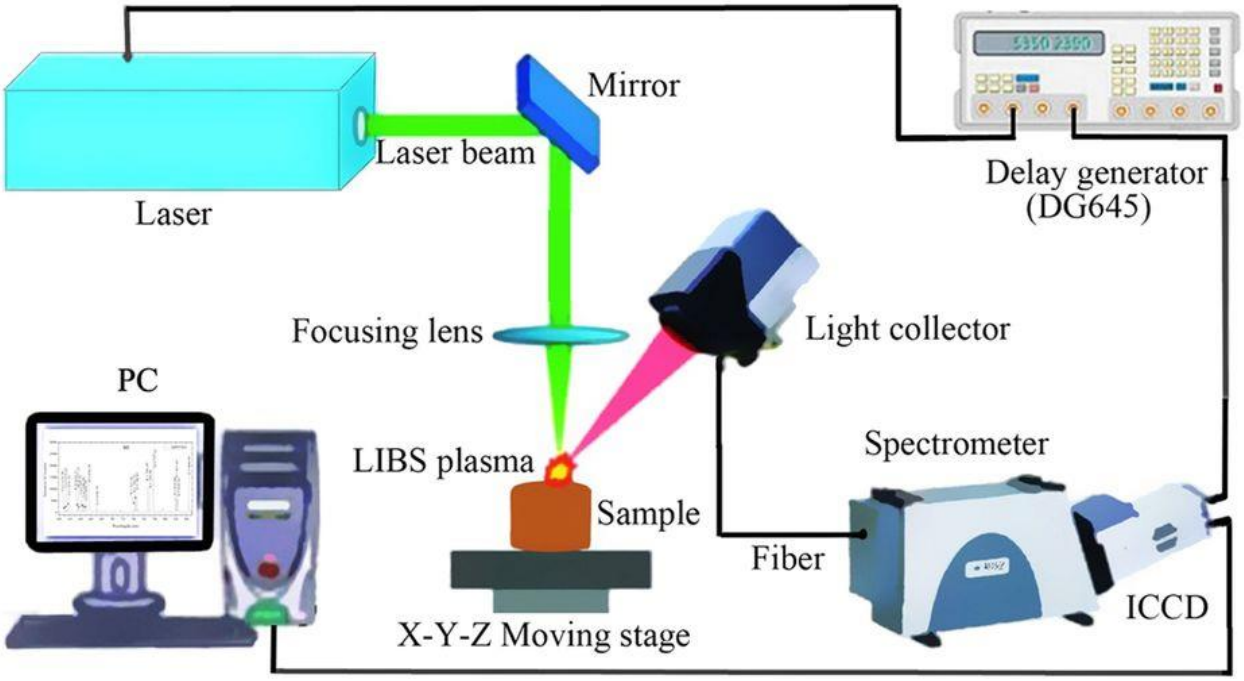

Figure 5: Schematic of a LIBS instrument[33].

A LIBS spectrum is obtained by focusing pulsed laser light onto the surface of a sample to ablate and vaporize a small amount of target material. A lens collects the plasma light and focuses it into the spectrometer slit where a diffraction grating separates the light into its separate spectral constituents. Measurement of the diffracted wavelengths' light are detected by a photodetector. The photodetector is comprised of pixels where each pixel is associated with a specific wavelength and converts the intensity of light incident into an electrical signal. A computer processes the electrical signal obtained from the photodetector and a spectrum is obtained in terms of wavelength of the diffracted light against the intensity of the diffracted light at each wavelength. A typical silicon spectrum is shown in Figure 6.

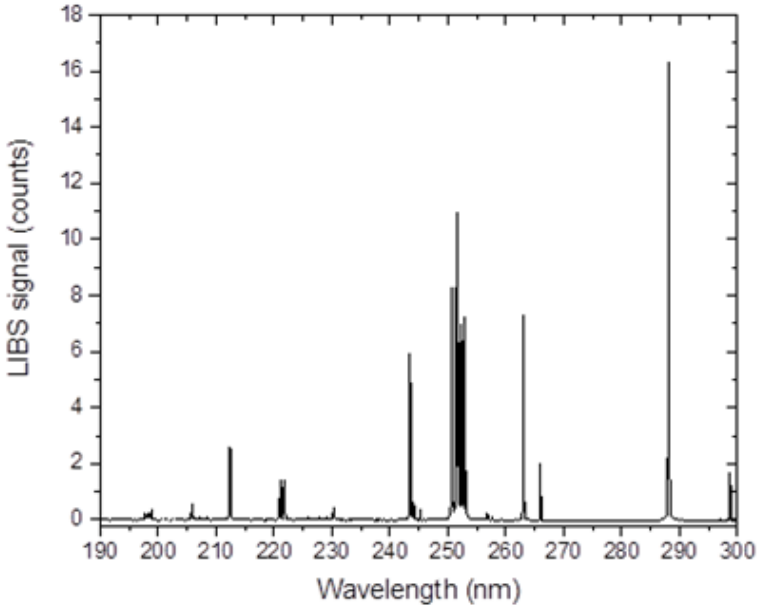

Figure 6: Experimental spectrum of silicon for the spectral range [190 nm – 300 nm].

Spectral Line Broadening and Spectral Profile

Relationships exist between the characteristics of the plasma (electron density and temperature) and the spectral line characteristics of linewidths, shapes, and shifts. Line shapes and shifts can be analyzed to determine the density of plasma species from the processes that increase the linewidth of a spectral line (broadening). Spectral lines have a small linewidth from natural broadening even when an electron transition from an upper energy level to a lower energy level when the atom is motionless. Broadening occurs from the fluctuations of different interactions of different atoms in a plasma. There are different broadening mechanisms that include natural, pressure or collisional, and Doppler.

Natural broadening is the result of the Heisenberg uncertainty principle, where the exact position and speed of an atom can never be known at the same time because it behaves as both a particle and a wave concurrently. When an atomic emission technique emits a photon, the frequency υ, wavenumber σ, and wavelength λ of the transition are given by:

$$\upsilon = \frac{\Delta E}{h} \quad \textbf{(3)}$$

$$\sigma = \frac{\upsilon}{c} \quad \textbf{(4)}$$

$$\lambda = \frac{1}{\sigma} \quad \textbf{(5)}$$

where ΔE is the energy level difference (in J), h is Planck's constant, and c is the speed of light. Spectral lines naturally broadened have a full-width at half-maximum (FWHM) considerably smaller than plasma and instrumental contributions[22,34] which is insignificant in laser induced plasma spectroscopy[35,36].

Doppler broadening is one of the two major line broadening mechanisms in laser plasmas. Doppler broadening is composed of emitted frequencies in a frequency range[37,38,39] due to emitters having different motions from their velocity distribution with respect to a detector. The speed in which an emitter moves is directly proportional to temperature, thus, an increase in temperature results in a rise of speed. The Doppler effect on frequency of the central wavelength of the emitter will be lowered when the emitter moves away from the detector and

increased when the emitter is moving towards the detector creating a spectral linewidth due to the difference in frequency[34]. Doppler broadening results in a Gaussian line profile where, Γ is the half-width at half maximum [HWHM], σ_0 is the central line in wavenumbers, M the atomic mass of the species[40].

$$\boldsymbol{I(\sigma) = \left(\frac{\ln 2}{\pi\Gamma}\right)^{1/2} exp\left[-ln2\left(\frac{(\sigma-\sigma_0)}{\Gamma}\right)^2\right]} \quad \textbf{(6)}$$

$$\boldsymbol{\Gamma = \left(\frac{(2\ln 2)k_B T}{Mc^2}\right)^2 \sigma_0} \quad \textbf{(7)}$$

Background shifts arising from radiative recombination processes and natural line broadening at wavelengths substantially in distance from the central wavelength are not influenced much by Doppler broadening[36]. The Gaussian line profile wings decreasing in intensity very quickly show this. Given the profile of the Gaussian line shape, the Doppler width $\Delta\lambda_0$ at FWHM can be calculated by the following equation which is dependent on the plasma temperature T and mass of the emitter M[22,34].

$$\boldsymbol{\Delta\lambda_0 = 7.16 * 10^{-7}\left(\frac{T}{M}\right)^{1/2}\lambda_0} \quad \textbf{(8)}$$

where λ_0 is the central wavelength of the spectral line. Doppler broadening dependence on temperature expresses how much kinetic energy of the atoms or ions are present in the plasma.

Pressure or collisional broadening is the other type of major line broadening processes that is produced when radiating ions and atoms collide and interact with neutral or charged particles. Depending on the species, different types of collisional broadening occur including Van der Waals broadening, Resonance broadening, and Stark broadening. Van der Waals broadening occurs from the interaction between the excited atoms with the induced dipole from neutral atoms in the ground state[37]. Resonance broadening is produced from the interactions between an excited atom and an identical atom in its ground state[41]. Resonance broadening effects on background shifts can be minimized if the partial pressure of the species of interest are small[42]. Interactions between emitters with charged ions or electrons result in Stark broadening[22]. The electric field of the energy level of the ion or element splits into sublevels based on the species' quantum number to contribute to the species' emission. The sublevels of a species have electron transitions that occur which shift the wavelength of the emitted line[22,34]. Symmetrical or asymmetrical lines can be produced from Stark broadening where symmetrical have relatively large splitting resulting in broad lines and asymmetric results in less broad lines[36]. Stark shift is not affected by motion or opacity[43]. Collisional broadening results in a Lorentzian profile[22,44]. The Lorentzian line profile has the form where γ represent the decay constant for the transition from the upper to lower energy level and the FWHM can be calculated by the following equations.

$$\boldsymbol{I}(\upsilon) = \frac{(\boldsymbol{\gamma/2})^2}{\boldsymbol{4\pi^2}(\upsilon-\upsilon_{\boldsymbol{0}})^2+(\boldsymbol{\gamma/2})^2} \quad \textbf{(9)}$$

$$\Delta\boldsymbol{\lambda_0} = \frac{\boldsymbol{\gamma}}{\boldsymbol{2\pi}} \quad \textbf{(10)}$$

Instrumentation broadening can occur when there is an imbalance in the type of broadening. The combination of Doppler and collisional and pressure effects on spectral broadening are less effective than instrumentation effects[36]. A low-resolution spectrometer that cannot resolve emission lines close to one another would cause instrumentation broadening. The use of a high-resolution spectrometer does not remove all line broadening which contributes to spectral interferences[45]. An emission line obtained from an optical emission spectroscopy technique can exhibit both Doppler and collisional broadening resulting in the need for a compromise between the Lorentzian and Gaussian line profiles. A Voigt profile is the convolution of Gaussian and Lorentzian line profiles[46] which better characterizes the line shape from plasmas.

Line broadening can be induced from the absorption of emitted photons from the same species is called self-absorption. Broadening occurs at the center of an emitted line because there is a greater probability of reabsorption from the photons at the central wavelength than at wavelengths further away from the center as shown in Figure 7.

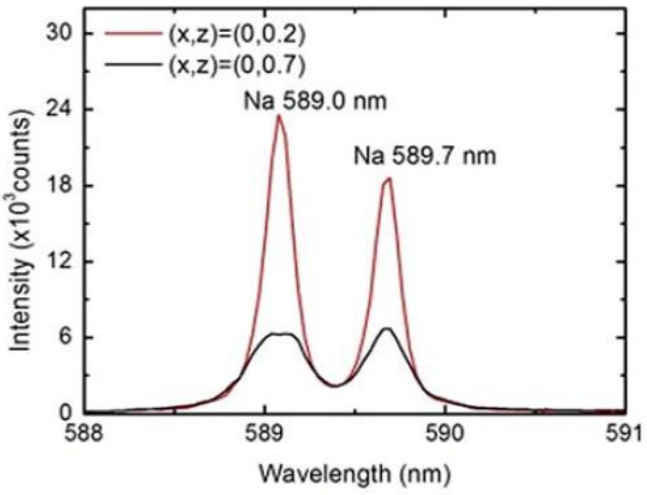

Figure 7: Spectral peak absorption of sodium [47].

A profile of a self-absorbed peak is shown in Figure 7 where the center wavelength of the emission line is less intense than the surrounding wavelength's intensities and the width is broadened. Broadening mechanisms increase the wavelength range of a spectral line creating difficulty in spectral line assignment.

Spectral Line Assignment

The detection of elements in a sample relies on the qualitative analysis of optical emission spectroscopy by line assignment. The assignment of spectral lines is possible by comparison of experimental spectral lines to reference database lines. Databases used in optical emission spectroscopy include the National Institute of Standards and Technology Atomic Spectra Database (NIST)[48], Atomic Line List Harvard-Smithsonian Center for Astrophysics (Kurucz)[49],

Massachusetts Institute of Technology Wavelength tables (MIT)[50], and Kelly Atomic Line database[51]. The information contained in each database includes more than just the wavelength of the emission line. Reference database calculated, or experimental emission lines provide information on the probability of a transition occurring and the energy levels involved in the transition. Spectral interferences can influence spectral line assignment and will be further discussed in chapter 4.

CHAPTER 3: CHARACTERIZATION OF PLASMA

Physics of Plasma

The transient nature of laser-induced plasmas in addition to complex processes that occur make their characterization difficult. These processes are photoionization, collisional ionization, radiative recombination, collisional excitation, radiative decay, and Bremsstrahlung process are a few of the complex processes that occur in laser-induced plasmas[40]. Nonetheless, the characterization of the laser induced plasma is important to understanding its resulting spectrum.

Thermodynamic Equilibrium (TE)

Thermodynamic equilibrium (TE) is the most restrictive assumed state for the laser induced plasma thermodynamic system to simplify its characterization. In TE, plasmas can be described by a single temperature, which influences the population density of electrons and atoms. Thermodynamic equilibrium is based on two assumptions: density of the plasma particles is high enough that the plasma volume relations holds true and that radiation doesn't have imposed equilibrium conditions[40]. When no net energy transfer occurs between particles through collisional processes such as collisional excitation and de-excitation, local thermodynamic equilibrium is expected[22,34,53]. TE is expected if rate equations for the steady state solution can be obtained if the velocity distribution of colliding particles is thermal.

The characterization of plasma by TE depends on the electron density of the plasma and a minimum density is required for TE existence because the collisional rates must exceed the

radiative processes[22,34,54]. Thermodynamic equilibrium can still occur if the collision rates exceed the radiative rate if the plasma is optically thick at all frequencies. An optically thick plasma will compensate for the radiative emission by self-absorption[54].

Local Thermodynamic Equilibrium (LTE)

If the plasma system can be explained by a single temperature from the Maxwell velocity distribution function, Boltzmann population distribution, Saha-Eggert equation, Planck's function, and any other processes based on temperature, the plasma is assumed to be in local thermodynamic equilibrium (LTE). LTE only occurs if a given process involved in the transfer of energy from one particle to another corresponds to the reverse process[53]. Like thermodynamic equilibrium, LTE is described by a single plasma temperature and a minimum electron density is required for the obtention of enough collisions to allow energy transfers. The McWhirter criterion gives the lower limit of the electron density n_e (in cm^{-3}), where the change in energy ΔE (in eV) is the largest energy transition that holds for the electron temperature T (in K)[55].

$$\boldsymbol{n_e = 1.6 * 10^{12} T^{1/2} (\Delta E)^3} \qquad \textbf{(11)}$$

Spectral information obtained from plasmas with high electron densities are difficult to interpret due to overlapping of spectral lines from line broadening, oscillator strengths, and continuous absorption coefficients[35]. Local thermodynamic equilibrium better characterizes the laser-induced plasma than thermodynamic equilibrium because it accounts for the inhomogeneity and

transient nature of the laser-induced plasma and the ideal blackbody behavior is not seen because of the intrinsic emission of light[56].

Maxwell Velocity Distribution Function

The velocity of an atom is given by the Maxwell velocity distribution function.

$$\boldsymbol{f}(\upsilon) = \boldsymbol{n} * \left(\frac{\boldsymbol{m}}{\boldsymbol{2\pi k_B T}}\right)^{\boldsymbol{3/2}} \boldsymbol{\exp}\left(\frac{\boldsymbol{m\upsilon^2}}{\boldsymbol{2k_B T}}\right) \quad \textbf{(12)}$$

where m is the mass of the particles, k_B the Boltzmann constant, n is the population density, T is the kinetic temperature, and υ is the average velocity of the electron, ion or molecule. The kinetic temperature is equal between each plasma constituent {electrons, ions, and molecules} when in LTE[52].

Boltzmann Population Distribution

An energy level for an atom has bound discrete energy states. There exists above the dissociation limit where the electron has become unbound and a continuum describes the density of energy states $\rho(E)$[57]. When in local thermodynamic equilibrium, the relative population $N(E_i)$ for a given bound state i, with an energy E_i known as the Boltzmann factor, where k_B is Boltzmann's constant and is the T temperature.

$$\boldsymbol{N(E_i) = \exp(\frac{-E_i}{k_B T})} \quad \textbf{(13)}$$

Molecules, atoms, and ions that can occupy more than one quantum state at a given energy defines the concept of degeneracy. The relative population between energy levels of a molecule, atom, or ion is explained by the Boltzmann distribution when the plasma is in thermodynamic equilibrium[34,57]. The Boltzmann population distribution formula is:

$$\boldsymbol{\frac{N_k}{N_l} = \frac{g_k}{g_l} \exp\left(-\frac{\Delta E_{kl}}{k_B T}\right)} \quad \textbf{(14)}$$

where N_k is the population density of the upper energy level, N_l is the population of the lower energy level, g_k and g_l are the degeneracy (statistical weights) for the upper and lower energy level respectively, ΔE_{kl} is the difference in energy between the upper and lower energy level, k_B is the Boltzmann constant, and T is the excitation temperature[40]. The statistical weight or degeneracy is calculated by Equation 15 where J is the total angular momentum quantum number.

$$\boldsymbol{g = 2J + 1} \quad \textbf{(15)}$$

The partition function $Z(T)$ accounts for the degeneracy g_i of the relative population densities at each energy level E_i.

$$\boldsymbol{Z(T) = \sum_i g_i \exp(-E_i / k_B T)} \quad \textbf{(16)}$$

The partition function is the sum of all the possible energies and their state as a function of temperature. Probability that an atom is in a specific energy state can be provided by the Boltzmann equation with the partition function included where N_k is the population of the upper energy level, g_k the degeneracy of the upper energy level, the Boltzmann factor, $Z(T)$ the partition function, and N the sum of all of the possible energy levels for a specific atom, ion, or molecule at a given temperature T[58]. The sum of all possible energy levels is given in Equation 17 where m_{max} is the number of excited levels (0, 1, 2, 3, …), and $N_m$the energy of the excited level m.

$$\boldsymbol{N = \sum_{m=0}^{m_{max}} N_m} \quad \textbf{(17)}$$

$$\boldsymbol{\frac{N_k}{N} = \frac{g_k}{Z(T)} \exp\left(-\frac{\Delta E_{kl}}{k_B T}\right)} \quad \textbf{(18)}$$

An emitted spectral line from a species has an intensity I described in Equation 19, where A_{kl} is the transition probability of the upper energy state k and lower energy state l (in s^{-1}), h is Planck's constant, N_k is the population of the upper energy level, and υ_{kl} is the frequency of the transition.

$$\boldsymbol{I = A_{kl} h \upsilon_{kl} N_k} \quad \textbf{(19)}$$

A relationship between the intensity of a spectral line and population of the excited state is given once the Boltzmann Equation 19 variable is substituted into the intensity of the emitted spectral line Equation 21.

$$\boldsymbol{I = A_{kl} h\upsilon_{kl} N \frac{g_k}{Z(T)} \exp\left(-\frac{\Delta E_{kl}}{k_B T}\right)} \quad \textbf{(20)}$$

$$\boldsymbol{h\upsilon_{kl} = \frac{hc}{\lambda_{kl}}} \quad \textbf{(21)}$$

$$\boldsymbol{I = g_k A_{kl} \frac{hc}{\lambda_{kl}} \frac{N}{Z(T)} \exp\left(-\frac{\Delta E_{kl}}{k_B T}\right)} \quad \textbf{(22)}$$

Saha-Eggert Ionization-Recombination

Atoms can be ionized if there is enough energy transferred to the plasma and the population density of atoms in the process of ionization are described by the Saha-Eggert equation. The singly-ionized process for a neutral atom shows that the rate of ionization is equal to the rate of recombination:

$$\boldsymbol{A \rightleftarrows A^+ + e^-} \quad \textbf{(23)}$$

The Saha equation defines the population density of atoms in ionization as:

$$\frac{n_e n_{a,i}}{n_{a,0}} = \frac{2Z_{a,i}(T_i)}{Z_{a,i-1}(T_i)} \frac{(2\pi m_e k_B T_i)^{3/2}}{h^3} \exp\left(-\frac{E_{a,0}-\Delta E_0}{k_B T_i}\right) \quad \textbf{(24)}$$

where n_e, $n_{a,i}$ and $n_{a,i-1}$ are the density of the electron, ion, and neutral species respectively. $Z_{a,i}(T_i)$ and $Z_{a,i-1}(T_i)$ are the partition functions for the ion and neutral species, m_e is the mass of the electron, T_i is the temperature of the ion, $E_{a,0}$ is the ionization energy of the neutral species, and $\Delta E_a$is the plasma correction factor for the ionization energy of the neutral atom. The correction factor ΔE_a in the Saha-Eggert equation considers the effects of electric fields produced by charged particles which slightly lower the ionization level and can be calculated by the following equation where Z_{eff} is the nuclear charge which acts on the optical electron and ε_0 is the permittivity of the vaccuum[59].

$$\Delta E_a = 3Z_{eff} \frac{e^2}{4\pi\varepsilon_0} \left(\frac{4\pi N_e}{3}\right)^{1/3} \quad \textbf{(25)}$$

The correction factor reduces the ionization energy of an ion because the binding energy of the bound states would be less than the ion would correlate to electron-ion pairs with more energy than the next ion and the free electron at zero kinetic energy[60].

Planck's Law

Excited particles produce emissions of radiation by the release of their excitation energy. In thermodynamic equilibrium, the release of the excitation energy can only occur if there is

absorption of radiation that occurs at the same time. This results in radiation always being present with species. The radiation of particles present depends on temperature and the energy density of photons in a vacuum is described by Planck's Law[53].

$$\boldsymbol{dE(v) = \frac{8\pi h\upsilon^3}{c^3}\left(\frac{hv}{e^{k_B T_{ph}}-1}\right)^{-1}} \quad \textbf{(26)}$$

where c is the speed of light (in m/s), v is the frequency of the photon (in 1/s), T_{ph} is the temperature of the photon (in K), $k_B$is Boltzmann's constant, and h is Planck's constant. The energy of photons that escape the plasma can differ from Planck's law. Local thermodynamic equilibrium can still be valid for the plasma if the loss of energy from radiation is smaller than the energy involved in other processes and the plasma can still be accurately represented by the Maxwell velocity distribution, Boltzmann population distribution, and the Saha-Eggert equation[55,61].

There are many different methods to calculate the different types of temperature of electronic, excitation, ionization, vibrational, rotational, and heavy particles or molecules that occur in laser induced plasmas. Laser-induced plasma different types of temperatures may not agree with each other in the beginning processes of the plasma due to the plasma's inhomogeneity but as the plasma starts cooling, equilibrium between the types of temperatures is obtained[40].

Plasma Temperature and Electron Density Calculation

Boltzmann Plot Method

The most widely used method for determining the excitation temperature of the plasma is by the ratio of relative intensities of two spectral lines that are emitted by the same emitter[34,62]. When determining the electron temperature by the Boltzmann plot method, a requirement is that the plasma is optically thin. An optically thin plasma allows for emitted photons to escape without further interactions between species. Measurement of the intensity of the escaped photons in an optically thin plasma is more accurate than in an optically thick plasma where photons cannot escape from the plasma[63,64,65]. A plasma is optically thin with respect to an element when the ratio of the observed intensities is similar to the ratio theoretically determined from the statistical weights of the upper energy level and their profile of emission. Verification of optically thinness requires the knowledge of the transition probabilities and statistical weights of the upper energy level. Once the plasma has been verified for being optically thin with respect to the chosen element, the electron temperature can be used to calculated for that element by the Boltzmann plot method. Two spectral lines emitted by the same ion can calculate the excitation temperature assuming the level population obeys the Boltzmann population distribution function.

At least two atomic or ionic lines from one element with adequate strength and differences between upper energy levels is required for the Boltzmann plot method. The Boltzmann plot method is a fast and simple method to determine the excitation temperature because only two emission lines are needed for calculation. When only a few spectral lines are available from a

single element, it is difficult to determine the plasma temperature from the Boltzmann plot[13]. Self-absorption affects species differently which could cause inequality of plasma temperatures obtained by the Boltzmann plot method[66,67].

The intensity ratio of the two element's spectral lines k and l calculate the excitation temperature T_{exc} by the following equations[68].

$$\frac{I_k}{I_l} = \frac{g_k}{g_l}\frac{A_k}{A_l}\frac{\lambda_l}{\lambda_k} exp\left(-\frac{(E_k - E_l)}{k_B T_{exc}}\right) \quad \textbf{(27)}$$

$$\ln\left(\frac{I_k \lambda_k}{g_k A_k}\right) - \ln\left(\frac{I_l \lambda_l}{g_l A_l}\right) = -\frac{(E_k - E_l)}{k_B T_{exc}} \quad \textbf{(28)}$$

$$T_{exc} = \frac{E_k - E_l}{\left[\ln\left(\frac{I_k \lambda_k}{g_k A_k}\right) - \ln\left(\frac{I_l \lambda_l}{g_l A_l}\right)\right] k_B} \quad \textbf{(29)}$$

In Equations 27-29, I is the intensity of the spectra line at wavelength λ, g is the statistical weight associated with the upper energy level, A is the transition probability, and E is the upper energy level. To minimize sensitivity and effect of spectral response, two lines should be chosen as close as possible in wavelength and with the largest upper energy level difference. The uncertainty or relative error in the temperature calculation can be obtained by the following equation[68,69].

$$\frac{\Delta T_{exc}}{T_{exc}} = \frac{k_B T_{exc}}{E_k - E_l} \frac{\Delta\left(\frac{R_l}{R_k}\right)}{\frac{R_l}{R_k}} \quad \textbf{(30)}$$

$$R = \ln\left(\frac{I\lambda}{gA}\right) \quad \textbf{(31)}$$

The uncertainty in R on the uncertainty in the excitation temperature can be minimized by large values of the change in upper energy level of the transition. Given the transition probabilities and statistical weights for measured intensities of multiple spectral lines from the same element with different excitation state, the plasma temperature can be determined by the Boltzmann plot.

The Boltzmann plot consists in plotting the two spectral emission lines $\ln\left(\frac{I_k\lambda_k}{g_k A_k}\right)$ and $\ln\left(\frac{I_l\lambda_l}{g_l A_l}\right)$ and taking the slop of the line to extract the temperature. The Boltzmann plot method requires only two spectral lines for temperature calculation, but accuracy of the plasma temperature is increased by the consideration of multiple spectral lines. Equation 30 can be rearranged, and the natural log taken to determine the Boltzmann plot equation in the linear form $y = mx + b$ which is used to extract the temperature of a plasma.

$$I = g_k A_{kl} \frac{hc}{\lambda_{kl}} \frac{N}{Z(T)} \exp\left(-\frac{\Delta E_{kl}}{k_B T}\right) \quad \textbf{(32)}$$

$$\ln\left(\frac{I_{kl}\lambda_{kl}}{g_{kl}A_{kl}}\right) = -\frac{1}{k_B T} E_k + \ln\left(\frac{hcN}{Z(T)}\right) \quad \textbf{(33)}$$

$$\downarrow \qquad \downarrow \qquad \downarrow$$

$$y \quad = \quad mx \quad + \quad b$$

The value of temperature T is obtained from the slope $m = -\frac{1}{k_B T}$ of the Boltzmann plot when the ln $\left(\frac{I_{kl}\lambda_{kl}}{g_{kl}A_{kl}}\right)$ is plotted against the energy of the upper level of each emission line related to its ionized or neutral atom. An example of a Boltzmann plot of Fe I lines with the natural log of the magnitude of the emission lines for neutral iron, a linear fit is obtained and by the slope the temperature was determined to be roughly 21,000 ± 1,300 K by Camacho *et. al*[70].

The assumption of the LTE is correctly identified when the data from the Boltzmann plot shows high linearity because the Boltzmann distribution characterizes the population of the excited states accurately[71]. Difficulties arise in experimentally obtaining absolute intensity values for spectral lies so the intercept from the Boltzmann plot is rarely used. Relative intensities from the most intense peak are used instead of absolute intensity values[63]. The calculated temperature from the Boltzmann plot vary depending on the elemental reaction within the plasma. If the plasma is in local thermodynamic equilibrium, the excitation temperature is more accurately calculated for neutral atoms than for ions. Large amounts of deviations from the best linear fit line of the Boltzmann plot, remove the assumption of LTE[72]. The voiding of the LTE assumption for a sample means that radiative decay processes occur more than electron collisions in the plasma event. A correction factor b_i can be used to correct for non-equilibrium effects on temperature. The ratio of experimental population density N_i^{exp} to the population density theoretically calculated from the Saha and Boltzmann distributions at the excitation temperature N_i^{LTE} calculate the correction factor b_i[72,73,74].

$$\boldsymbol{b_i = \frac{N_i^{exp}}{N_i^{LTE}}} \quad \textbf{(34)}$$

The atomic and ionic transitions have different correction factors based on collisional and radiative arguments[74].

$$\boldsymbol{b_{i,atom} = 1 + \left(\frac{6.55x10^{13}E_{\infty}(E_{\infty}-E_i)^{2.607}}{N_e T^{0.107}}\right)} \quad \textbf{(35)}$$

$$\boldsymbol{\frac{1}{b_{i,ion}} = 1 + \left(\frac{1.27x10^{11}E_i^3 T^{1/2}}{N_e}\right)} \quad \textbf{(36)}$$

The correction factor b_i is substituted into the Boltzmann equation which shifts the Boltzmann plot data towards linearity and LTE. With the use of the corrected Boltzmann equation, the temperature can be determined by the slope.

$$\boldsymbol{\ln\left(\frac{I_{kl}\lambda_{kl}}{g_{kl}A_{kl}b_i}\right) = -\frac{1}{k_B T}E_k + \ln\left(\frac{hcN}{Z(T)}\right)} \quad \textbf{(37)}$$

Assessment of local thermodynamic equilibrium by the Boltzmann plot method alone can produce incorrect conclusions. A straight line can fit the data in a Boltzmann plot even when the population of the energy level is significantly different from its equilibrium value due to experimental constraints[75]. Characterization of the plasma temperature affects the electron density of the plasma.

Electron Density

The temperature of the plasma, the plasma electron density can be calculated from the peak broadening of a line expressed as the full-width at half-maximum (FWHM)[68].

$$\Delta\boldsymbol{\lambda_{1/2}} = \mathbf{2}\boldsymbol{w}\left(\frac{\boldsymbol{n_e}}{\mathbf{10^{16}}}\right) + \mathbf{3.5}\boldsymbol{A}\left(\frac{\boldsymbol{n_e}}{\mathbf{10^{16}}}\right)^{\mathbf{1/4}}\left[\mathbf{1} - \boldsymbol{B}\boldsymbol{N_D^{-1/3}}\right]\boldsymbol{w}\left(\frac{\boldsymbol{n_e}}{\mathbf{10^{16}}}\right) \quad \textbf{(38)}$$

The right side of the equation is split into two terms: the first comes from electron broadening and the second from ion interactions. Parameter B is a coefficient for ionic and neutral lines with a value of 1.2 or 0.75 respectively, n_e is the electron density, N_D is the number of particles in the Debye sphere, A is the ion broadening parameter, and w is the electron impact parameter[60]. The electron density can only be calculated from its full-width at half-maximum if Stark broadening is more influencing on the plasma than Doppler or instrumental broadening[76]. Knowledge of the plasma temperature and electron density allow for characterization of the laser induced plasma at equilibrium.

CHAPTER 4: UNCERTAINTIES AND THEIR MEASUREMENTS IN OES

Forensic Analysis Need

In the report, "Strengthening Forensic Science in the United States: A Path Forward" by the National Research Council, it was mentioned very clearly that "few forensic science methods have developed adequate measures of the accuracy of inferences made by forensic scientists[77]." Optical Emission Spectroscopy being used as an analytical tool for forensic analysis, the measurement of accuracy needs to account for all uncertainties for the results obtained. Studies need to be conducted to estimate the error rates in order to improve and strengthen the method by understanding the sources of uncertainties.

One cause of uncertainty in optical emission spectroscopy elemental profiles is the presence of spectral interferences. Line broadening and shifting due to plasma processes described in chapter 2 as well as the instrumentation affect spectral resolution, leading to challenges in line assignment. The first step to confident spectral line assignment is high spectral resolution though prevention of all spectral interferences is not possible. Spectral interferences can be classified as spectral line coincidence[78], overlap with a broadened line wing[79], spectrometer stray light[80] and background continuum[80].

Types of Spectral Interferences

When a monochromator or spectrometer cannot separate two emission lines from each other, line coincidence occurs. For instance, the Si I line at 252.852 nm ($3s^2 3p^2\ (^3P_2) \leftarrow 3s^2 3p4s\ (^3P^\circ_1)$) is

known to be interfered within 0.001 nm by many other transitions, more especially the one from Sb I at 252.853 nm ($5p^3(2D^\circ_{5/2}) \leftarrow 5p^2(3P)6s\ (3P_{3/2})$)[76]. The overlap of two spectral lines that coincide is hard to avoid, especially when one of them is the matrix and the other a trace element. Approaches to separate the analyte from the interfering matrix have been proposed, such as, using larger acquisition delays, incorporating Stark broadening parameters, and a range of tolerance around the central wavelength of the analyte emission line can reduce incorrect line assignment from line coincidence[81].

Spectral interferences can be caused by a strong broadened line of an element in the matrix near the emission line which overlap each other. Interferences by the overlap with a nearby broadened line wing possibly will be avoided by using background correction[82], by chemical separation, or by moving to another emission line that is free from interferences[80].

Stray light occurs when wavelengths of background light outside of the instrumental bandpass reach the detector. Stray radiation that doesn't come from the species of interest but is recorded in the detector result in incorrect measurement of the incident light of the species of a particular wavelength. There are numerous sources of stray that include reflections or scattering from optical components, grating imperfections, and diffraction from mirror apertures[83]. Stray light can increase and shift the background continuum in a spectrum. Spectral continuum is a characteristic of a plasma in optical emission spectroscopy due to the radiative recombination of electrons with other ions. The more electron density present in a plasma the greater the

background emission will be. Stray light can be classified into two categories: near and far. Far stray light comes from stray light due to grating effects. Near stray light originates from a strong line near the species' emission line[84]. Instrument design such as interference filters[85] or double monochromatization lead to reduction of stray light[86].

Spectral Interference Uncertainty Importance

It is important to identify and characterize the uncertainty in optical emission spectroscopy elemental profiles to provide a more accurate analysis[87]. Quantification of uncertainty will provide an error rate associated to the optical emission spectroscopy technique and can lead to reduction of error[88]. Error rates provide validation of the optical emission spectroscopy technique[89]. Accuracy, validation, and reduction of errors lead to reproducibility of a method and quality assurance[90]. Quality assurance can identify where weaknesses are and limitations to a method. Thus, the quantification of uncertainty by an error rate produces confidence in the results obtained from a method. The assessment of spectral interferences in optical emission spectroscopy is difficult because it requires the identification and estimation of all parameters involved in the interference process[91,92].

Approaches to Spectral Interference Uncertainty

Line Coincidence Tables

The Q-concept method for quantification of spectral interferences was developed by Boumans *et al*[92]. Spectral interferences from line coincidence and overlap with broadened line wing can be quantified by the Q-concept method using ICP line coincidence tables. The sensitivity of the

interferent $S_I(\lambda)$is calculated as where $x_I(\lambda)$ is the wavelength array of the interference and c_I is the concentration of the interferent[92].

$$\boldsymbol{S_I(\lambda) = \frac{x_I(\lambda)}{c_I}} \quad \textbf{(39)}$$

The Q-value of the interferent is obtained by the ratio of the sensitivity of the interferent to the sensitivity of the analysis emission line.

$$\boldsymbol{Q_I = \frac{S_{I(\lambda)}}{S_A}} \quad \textbf{(40)}$$

When the bandwidth changes, so do the sensitivity ratios. To quantify spectral interferences from line coincidence and overlap with broadened line wing, the Q-value is determined by the following equations where B corresponds to the background and W to the wing background.

$$\boldsymbol{Q_B = \frac{x_B}{c_I S_A}} \quad \textbf{(41)}$$

$$\boldsymbol{Q_{total} = Q_I + Q_W + Q_B} \quad \textbf{(42)}$$

There is no need for specialized software for Q-concept analysis[93] as ICP line coincidence tables are already in existence[92,94,95]. Larger Q-values can be obtained than determined when an

interfering line is further in distance, from the central peak position. The Q-concept method cannot distinguish spectral interferences if the Q-value is close to the detection limit of the instrument[93]. Incorrect ratios between the analytical emission line and the interfering line are possible with the Q-concept method due to different excitation conditions of the optical emission spectroscopy technique[93].

Calibration

Instrument response of a sample compared with the response of a set of standard elements results in a calibration graph. The calibration graph plots the instrument response (signal intensity) against the concentration of the standard element solution. Use of a calibration curve corrects for line overlap and matrix effects based on the apparent concentration of the interferent of an un-interfered analyte line[93]. Line overlap results in the incorrect measurement of the intensity of a line which results in a parallel shift of the calibration curve while matrix effects change the calibration curve slope. A linear least squares fit is applied to the data and the equation obtained gives the concentration of an element of interest without interference from an overlapping line in the form y = mx + b.

$$\boldsymbol{C_i = A_0 + A_1\left(I_i - \sum h_{ij} I_j\right)} \qquad \textbf{(43)}$$

where C_i is the concentration of the element of interest, I_i the measured line intensity, h_{ij} the correction factor for all interfering elements, and I_j the measured intensity of the interfering element. Matrix effects can be corrected where k_{ij} is the correction factor for the interferant:

$$\boldsymbol{C_i = A_0 + A_1 I_i\left(1 \pm \sum k_{ij} I_j\right)} \quad \textbf{(44)}$$

The error rate of the spectral interferences by interelement correction of spectral line overlap and matrix effects by a calibration curve is the relative standard deviation of the measurement. There is no need for sophisticated software to produce a calibration curve for an optical emission spectroscopy spectrum. Calibration curves can be imprecise if elements are missing from the standards. It is easy to correct for missing standards but depending on the number of standards needed, very time consuming.

There are two types of analysis when describing calibration curves: univariate and multivariate. Univariate calibration aims to find a relationship between the concentration of an element with the peak intensity at a specific wavelength. Multivariate calibration involves the application of chemometrics where the object is to develop a model to predict the concentration of elements in an optical emission spectrum.

Calibration-Free Approach

Calibration is based on the empirical spectral relationship between the intensity and the concentration of an analyte while calibration-free methods model the physics of the plasma. Calibration-free methods consider matrix effects with the analyte simultaneously rather than in calibration where it is considered an external influence[58]. Calibration-free optical emission spectroscopy is then a standardless method. The quantification of spectral interferences becomes difficult as matrix effects are present as an internal influence and interelement corrections cannot be determined based solely on the relationship between spectral line intensity and concentration of analyte but on other parameters such as the plasma temperature. The accuracy of quantitative analysis by calibration-free optical emission spectroscopy is affected by the estimation of plasma temperature and self-absorption effects [83].

Chemometrics

Chemometrics combines mathematical and statistical methods to increase the understanding of chemical information or correlation of parameters to spectral data. There are many different chemometric methods that have been used to analyze optical emission spectroscopy data including but not limited to correlation analysis, principal component analysis (PCA), partial least squares analysis (PLS), artificial neural networks (ANN), and support vector machine (SVM). Chemometrics can be used for calibration or classification. Classification allows for discrimination of samples. Advantages to chemometrics include decrease in computation time and automation.

Correlation Analysis

The composition of a sample can be determined using correlation analysis between experimental and library reference spectra[97]. This approach uses unique identifiers which indicate differences in spectral peak positions and intensities for different materials. Linear correlation determines the relationship between the spectral wavelength x and intensities y with a linear correlation coefficient r[98,99].

$$\boldsymbol{r = \frac{\sum_i (x_i - \bar{x}) \sum_i (y_i - \bar{y})}{\sqrt{\sum_i (x_i - \bar{x})^2} \sqrt{\sum_i (y_i - \bar{y})^2}}} \quad \textbf{(45)}$$

where $\bar{x}$ and y are the means of the spectral wavelengths and intensities respectively. The correlation coefficient will have a value between -1 and 1. A positive correlation occurs when the data has a positive linear slope meaning that the variables of spectral wavelengths and intensities increases together. A negative correlation has a negative linear slope where the spectral wavelengths and intensities decreases at the same time. The statistic of how well the correlation fits the data is estimated by the correlation significance a where $erfc$ is the complementary error function and N the number of data points.

$$\boldsymbol{a = erfc\left(\frac{|r|\sqrt{N}}{\sqrt{2}}\right)} \quad \textbf{(46)}$$

$$\boldsymbol{erfc(x) = \frac{2}{\sqrt{\pi}} \int_x^{\infty} e^{-t^2}\, dt} \quad \textbf{(47)}$$

The smaller the correlation significance, the more strongly correlated the variables of wavelength and intensity are. Linear correlation doesn't account for distribution of the spectral wavelengths and intensities making it a poor statistic for determining correlation[100].

Rank correlation analysis considers the distribution of the variables being tested making it a good statistic for determining correlation. The equation for rank analysis is very similar to linear correlation with ranks replacing the original data of spectral wavelengths and intensities. The least intense pixel in the experimental spectrum is given a 1 while the most intense pixel is given the rank of N (total number of data points). The non-parametric correlation coefficient r_s is given by the following equation where R and R' correspond to the ranks of the original wavelength and intensity respectively[101].

$$\boldsymbol{r_s = \frac{\sum_i (R_i - \bar{R}) \sum_i (R'_i - \overline{R'})}{\sqrt{\sum_i (R_i - \bar{R})^2} \sqrt{\sum_i (R'_i - \overline{R'})^2}}} \qquad \textbf{(48)}$$

Correlation analysis whether rank or linear requires a library of representative spectra which can be difficult to determine depending on sample composition and knowledge of every element within the sample. The computation time for correlation analysis is very quick and doesn't require coincidence tables. Quantifications of the interferences in experimental spectra cannot be calculated even if the method can differentiate between similar spectra.

Labutin *et al* proposed an automated spectral line assignment by correlation of model spectra to experimental spectra[102]. Modeled spectra were used as a reference with simulations from different temperatures and electron densities. The line assignment was dependent on a factor α not found in the model spectra. The authors credited this parameter to the fact that only certified elements were modeled. The parameter is defined by the ratios of intensity of the *i*th line to the maximum intensity of a given spectral peak. This automated line assignment is simple and fast but requires model spectra form prior knowledge of samples compositions. Spectral interferences were not discussed by the authors.

A novel approach to quantify spectral interferences in optical emission spectroscopy has been developed that builds on the atomic line databases already in existence. The algorithm builds on the fundamental knowledge of plasma emission to quantify spectral interferences for individual line assignment in optical emission spectroscopy while using the full spectral information.

CHAPTER 5: STATISTICAL INTERFERENCE FACTOR

Algorithm Development

The algorithm developed to quantify spectral interferences is determined by the comparison of detected peaks from an experimental spectrum to a database of choice of atomic and ionic emission lines. This quantification is represented by the statistical interference factor (SIF). Figure 8 shows the flowchart for the calculation of the SIF.

The first step of the algorithm is the introduction of an optical emission spectrum, the extracted peaks' parameters of the experimental spectrum, and the database of choice. These inputs allow for calculation of the SIF which comprise of a global matching factor for each emitter and the individual peak analysis. Individual SIF values are obtained for each individual peak. A Bayesian inference approach is used to identify the optimal number of emitters and calculate the likelihood of combinations of emitters for the entire experimental spectrum. Prior knowledge of the sample composition, background gas, plasma conditions, and instrumental conditions are applied to the Bayesian statistics to provide the optimal posterior SIF values for the spectral interferences in a sample.

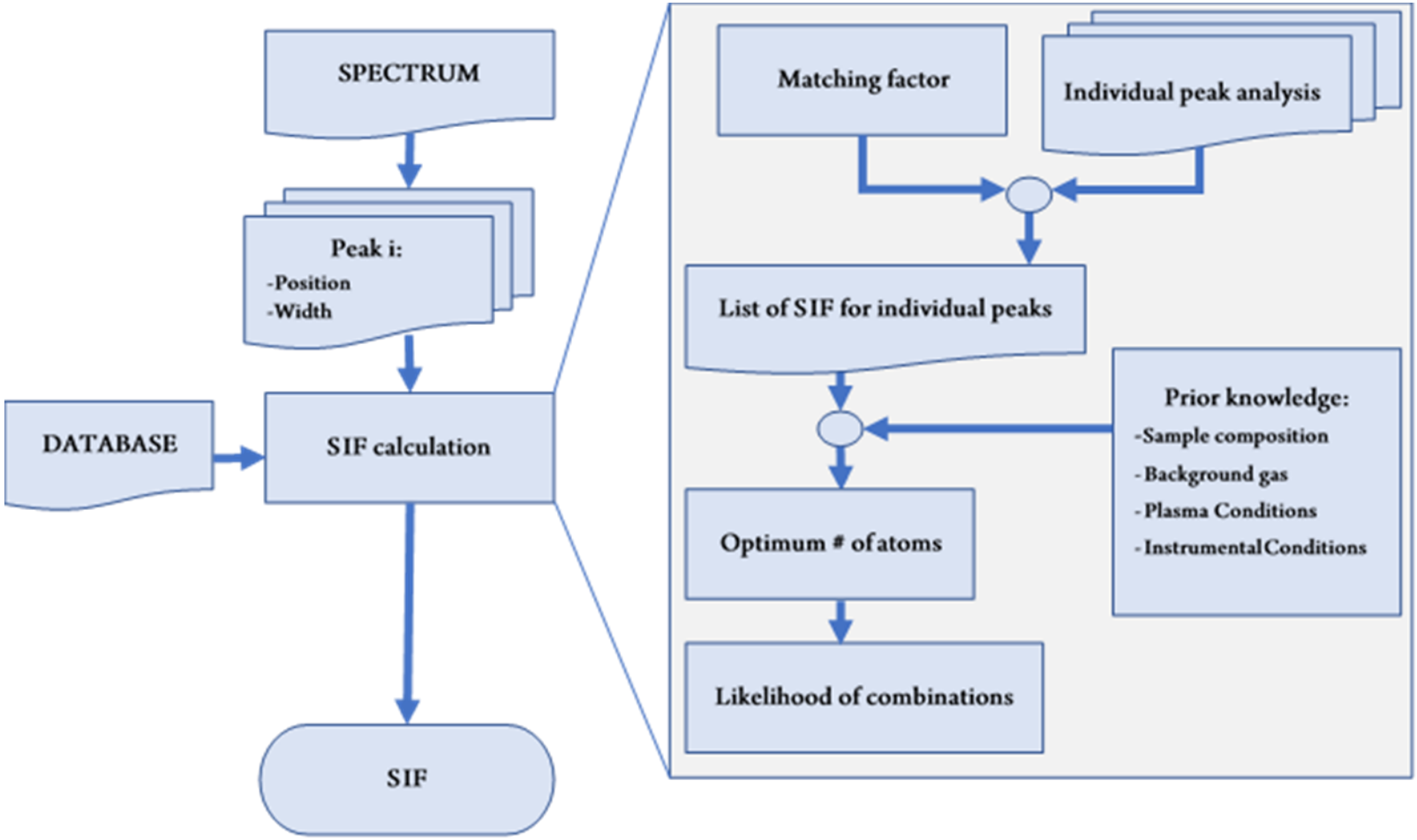

Figure 8: Flow chart of the SIF algorithm[111].

Sample/Spectral Data

An experimental spectrum is the first input for the determination of the SIF. For demonstration of the algorithm developed to statistically quantify spectral interferences, a silicon wafer was analyzed by LIBS. A LIBS spectrum is considered a multimodal distribution of emission from elements listed in a database. Each transition within the experimental spectrum has a weight proportional to a calculated strength. A specific set of weighted distributions make up a spectrum that allows for emission peaks to have their own profile. The statistical weight is not equally distributed to each emitter from the database. The emission probability of a transition, probability of the population of energy levels, and plasma parameters influence the emitter's statistical weight.

The information obtained from the LIBS instrument for an experimental spectrum are the wavelength and corresponding intensity of emission. The experimental silicon spectrum from 185 nm to 1050 nm is shown in Figure 6. Most of the silicon emission lines were detected below 300 nm in our conditions.

The silicon spectral intensity data was normalized between 0 and 1 using the following equation where z_i is the *i*th normalized intensity value, y_i is the *i*th intensity value and y is the vector of all intensity values.

$$z_i = \frac{y_i - \min(y)}{\max(y) - \min(y)} \quad (49)$$

Peak Detection/Peak Fitting

A peak in a LIBS spectrum represents the presence of an atom in a given excited state. The first input of the SIF algorithm is the parameters that define each peak of the experimental spectrum with no assumption of instrumental functions, resolution, or broadening effects. The peak information includes the position, width, shape, and integral value (Figure 9). The position of the peak defines the central wavelength λ_0 and the width of the peak (FWHM) provides the subsection range of the wavelength-ordered spectral database that will be used for comparison for each individual peak. The intensity of the peak is described by the peak's height I_{max}. The shape of the peak is used to identify which type of fit should be applied to the experimental spectrum. The fit is used to interpolate the emission intensity given by the peaks' integral value.

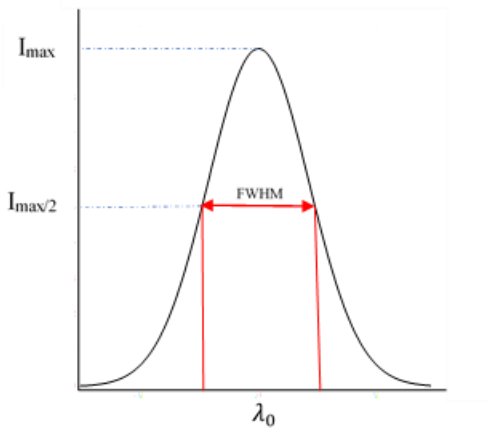

Figure 9: Spectral peak information.

Even if the SIF algorithm does not rely on peak detection but just on information from a list of peaks given by the user, peaks present in the silicon spectrum were detected by the MATLAB findpeaks function[104]. The findpeaks function is based on finding local maxima with a minimum height greater than a user defined threshold. The minimum height threshold of signal-to-noise ratio of 3 greater than its two neighbor data values was used throughout this algorithm. There were eighty-four peaks (•) in total identified for the silicon sample.

Experimental peaks are fitted in the SIF algorithm by a pseudo-Voigt profile to determine the interpolation values. A pseudo-Voigt fit is an approximation of the Voigt profile that is the linear deconvolution of the Gaussian and Lorentzian distributions. Gaussian profile can approximate instrumental contributions and Doppler broadening. A disadvantage of the Gaussian probability distribution profile is that it does not consider Stark broadening. The Gaussian distribution equation is defined in Equation 50. The Gaussian fit of the experimental silicon 212.42 nm is shown in Figure 10.

$$\boldsymbol{G(x) = \frac{A}{\sigma}\sqrt{\frac{4*\log(2)}{\pi}}\, e^{((-4*\log(2))*\frac{(x-\mu)^2}{\sigma^2})}} \qquad \textbf{(50)}$$

Likewise, the Lorentzian probability distribution profile does not consider Doppler or collision broadening but describes Stark broadening. The Lorentzian distribution equation is defined in Equation 51: Figure 10 shows the Lorentzian fit of the experimental silicon 212.42 nm peak.

$$\boldsymbol{L(x) = \frac{A\sigma}{2\pi[(x-\mu)^2+\sigma^2]}} \quad \textbf{(51)}$$

Fitting by a Voigt allows for both broadening and shifting effects to be taken into account and provide a theoretical description of the LIBS peak shape[105]. The linear deconvolution equation for the pseudo-Voigt is defined in Equation 52.

$$\boldsymbol{V(x) = \eta * L(x) + (1-\eta) * G(x)} \quad \textbf{(52)}$$

where η is the computed parameter from the FWHM of the Gaussian and Lorentzian functions, $L(x)$ is the Lorentzian profile and $G(x)$ is the Gaussian profile. The pseudo-Voigt fit was applied to the same experimental silicon 212.42 nm peak (Figure 10).

A chi-square goodness of fit test was applied to the Gaussian, Lorentzian, and pseudo-Voigt fit of the experimental 212.42 nm peak with the hypothesis that the fit values were different than the experimental LIBS signal. The chi-square goodness of fit by a model is determined by the following equation[106].

$$\boldsymbol{\chi^2 = \sum \frac{(observed-expected)^2}{expected}} \quad \textbf{(53)}$$

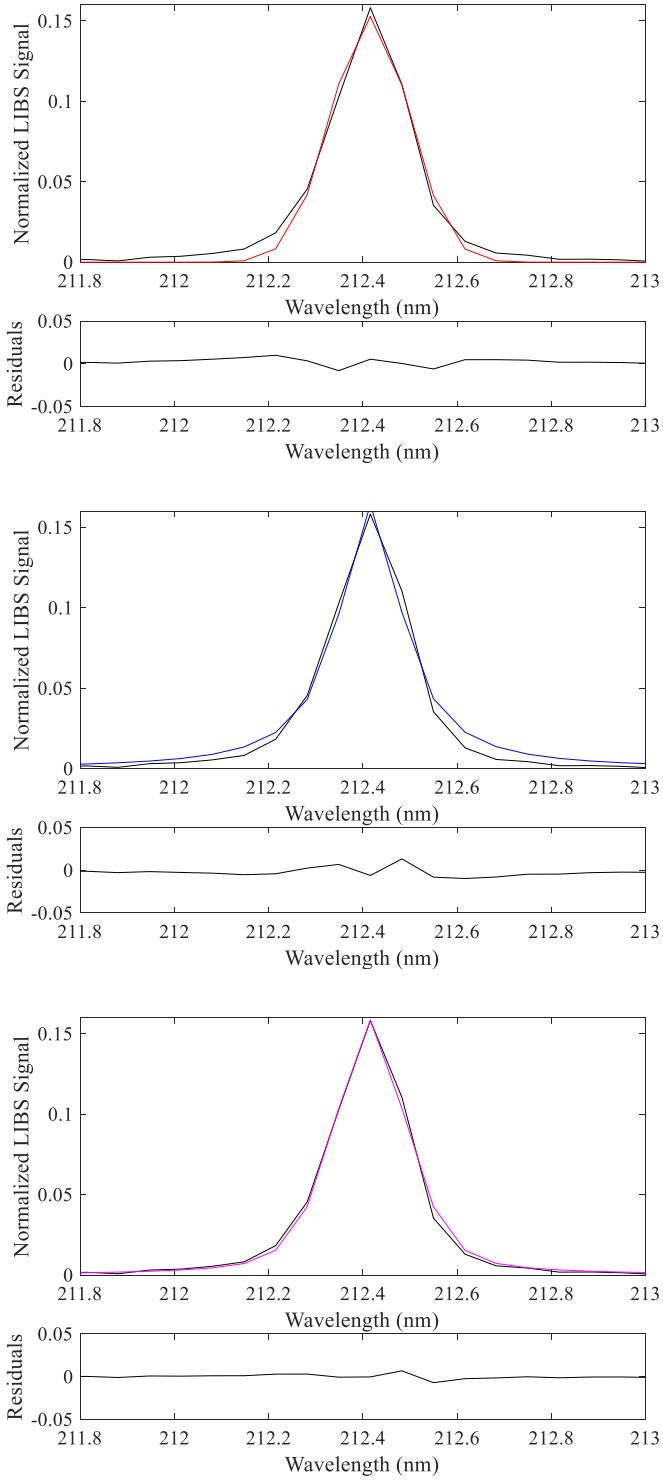

Figure 10 : Curve fitting with residuals (top) Gaussian (middle) Lorentzian (bottom) Pseudo-Voigt

The chi-square test statistics obtained were 0.0438, 0.0674, and 0.0066 for the Gaussian, Lorentzian, and pseudo-Voigt respectively. At a 95% confidence level, the tabled chi-square statistic for 70 degrees of freedom is 48.758[107]. The null hypothesis is rejected for all three fits which are considered the same as the experimental data. Since, all three fits rejected the null, their chi-square test statistics were compared to one another. The Lorentzian fit had the highest chi-square value which relates to the highest amount of error between the fit and experimental data from instrumentation or broadening effects. The Gaussian fit had the second highest chi-square value while the pseudo-Voigt fit had the smallest. The pseudo-Voigt fit had the smallest chi-square statistic which results in a better fit of the experimental data because it considers the instrumentation and broadening effects that show a Gaussian distribution and the shifting effects reflected by a Lorentzian distribution. A pseudo-Voigt function requires less computation time than the Voigt function when numerous convolutions are needed for calculation with minimal loss of accuracy[108].

The full width at the half maximum (FWHM) of the peak for the pseudo-Voigt function are related to the FWHM of the deconvoluted Gaussian and Lorentzian distributions. The FWHM of the Lorentzian function (f_L) and the Gaussian function (f_G) are related by the parameter η[105]. The Γ variable is approximated by a derivation from computer-generated convolutions by a series expansion where f_G is the FWHM of the Gaussian function and f_L is the FWHM of the Lorentzian function[105].

$$\eta = 1.36603(\Gamma_L/\Gamma) - 0.47719(\Gamma_L/\Gamma)^2 + 0.11116(\Gamma_L/\Gamma)^3 \quad (54)$$

$$\Gamma = (\Gamma_G^5 + 2.69269\Gamma_G^4\Gamma_L + 2.42843\Gamma_G^3\Gamma_L^2 + 4.47163\Gamma_G^2\Gamma_L^3 + 0.07842\Gamma_G\Gamma_L^4 + \Gamma_L^5)^{1/5} \quad (55)$$

The peak information obtained for the eighty-four peaks were used to compare against the Kurucz database hosted by the Harvard-Smithsonian Center for Astrophysics (Kurucz)[49]. The Kurucz database is available in an electronic format which is why it is used for the SIF calculation. The Kurucz database includes information such as the energy of the upper E_{upper} and lower E_{lower} levels in (eV), the total electronic angular-momentum quantum number of the upper J_{upper} and lower J_{lower} levels, transition probabilities (s^{-1}), wavelength of the transition (nm), and the element involved in the transition that are used as parameters in the SIF even if there is a large variance for the parameters whereas several of the other atomic line databases do not contain this information. Table 1 shows a subset of twelve Kurucz database values that can be found within the width of the silicon experimental 212.42 nm peak[49]. The Kurucz database is reduced to neutral and singly-ionized emitters due to their greater probability than higher ionization states in LIBS conditions of being at the origin of the spectrum[22]. This reduction of possible emitters allows for simplicity and faster computation times. There is a total of one-hundred forty-seven neutral and singly ionized emitters found within the Kurucz database from 180 nm to 1050 nm.

Table 1: Kurucz database subset for experimental 212.42 nm peak.

Wavelength (nm)	Transition Probability (s^{-1})	Element and Ion	E_{lower} (eV)	J_{lower}	E_{upper} (eV)	J_{upper}
212.4088	1.02E+07	26.01	7.568723	2.5	13.4043	1.5
212.4109	1.67E+02	23	0.275277	2.5	6.11082	1.5
212.4122	7.20E+08	14	0.781011	2	6.61652	3
212.4124	1.45E+05	20	2.709192	2	8.5447	1
212.4128	8.68E+05	26.01	7.804716	3.5	13.6402	4.5
212.4158	1.65E+06	23	0.068563	4.5	5.90398	3.5
212.4209	7.70E+06	26.01	7.636356	5.5	13.4716	6.5
212.4210	1.10E+04	24.01	8.73243	3.5	14.5677	4.5
212.4221	2.37E+06	21	0.020873	2.5	5.85611	1.5
212.4230	2.72E+04	24.01	6.282361	3.5	12.1176	3.5
212.4324	2.23E+04	28.01	11.09242	5.5	16.9274	4.5
212.4326	5.88E+03	23	0.068563	4.5	5.90351	4.5

As shown in the flowchart for the algorithm (Figure 9), the partial SIF ${}^{p}SIF_{i\to j}^{e}$ attributed to each individual transition $i \to j$ of an emitter e for a single peak p is calculated as the product of the transition strength by the emitter matching factor and the intensity of the fitted spectral line at the wavelength $\lambda_{i\to j}$ of the transition $i \to j$:

$$ {}^{p}SIF_{i\to j}^{e} = S_{i\to j}^{e} * MF^{e} * {}^{p}I\left(\lambda_{i\to j}\right) \quad \textbf{(56)} $$

with $S_{i\to j}^{e}$ the strength of the transition $i \to j$ for the emitter e, MF^{e} the emitter matching factor for the emitter e and ${}^{p}I\left(\lambda_{i\to j}\right)$ the signal value from the emission profile of the peak p centered at the wavelength $\lambda_{i\to j}$.

Statistical Interference Factor (SIF)

The SIF relies on the statistical weight, or strength, of the transitions in the database. This strength can be adapted to the amount of knowledge the user has. The lowest amount of knowledge for the strength considers all transitions are equi-probable, meaning there is absolutely no knowledge from the user. Second level of knowledge of the SIF for an individual SIF for an individual experimental peak considers the emitter's probability of transition, $A^e_{i\to j}$ (s^{-1}) of the transition $i \to j$ for the emitter e is found within the Kurucz database. The emitter with the highest probability of transition would have the highest probability of being the experimental peak's emitter.

Building on the first and second levels of understanding, the third level of knowledge considers the population of the upper energy level of an emitter's transition. The Boltzmann equation provides the population of the upper energy level involved in an atom's transition which assumes local thermodynamic equilibrium and is defined by the parameter of an excitation temperature. The equation for the strength $S^e_{i\to j}$ of the transition $i \to j$ with the addition of the population of the upper energy level for the emitter e is defined by the following equation.

$$\boldsymbol{S^e_{i\to j} = \frac{g^e_i A^e_{i\to j}}{Z^e(T)} \exp\left(\frac{-E^e_i}{T}\right)} \qquad \textbf{(57)}$$

The variables involved in Equation 57 include, the degeneracy g_i^e of the upper energy level energy E_i^e (cm^{-1}) involved in the transition, $A_{i\to j}^e$ the emission probability (s^{-1}), and $Z^e(T)$ the partition function of the emitter e at the excitation temperature T (eV). Addition of the population of the upper energy results in the probabilities of some emitters from the second level of knowledge being reduced or increased.

The fourth level of knowledge includes the knowledge of all parameters involved in the LIBS process such as electronic density and ionic densities in the plasma and can provide a deeper understanding of the strength of an emitter's transition for the SIF. The inclusion of more parameters in the SIF will increase the computation time.

Compromising the number of parameters and the computation time involved in calculating the SIF, the individual peak SIF uses the strength of an emitter's emission which considers the population of the upper energy level. The individual peak SIF is defined by the product of matching factor $MF_{i\to j}^e$, strength of transition $i \to j$ for the emitter e $S_{i\to j}^e$ and intensity of the fitted spectral line at the wavelength $\lambda_{i\to j}$ for the transition $i \to j$ for a single peak ${}^pI(\lambda_{i\to j})$.

$$ {}^{p}\boldsymbol{SIF}_{\boldsymbol{i\to j}}^{\boldsymbol{e}} = \boldsymbol{S}_{\boldsymbol{i\to j}}^{\boldsymbol{e}} * \boldsymbol{MF}^{\boldsymbol{e}} \ * \ {}^{p}\boldsymbol{I}\left(\boldsymbol{\lambda}_{\boldsymbol{i\to j}}\right) \quad \textbf{(58)} $$

A statistical interference factor is evaluated for all of the transitions within each experimental peak's width individually. The interpolated experimental value from the pseudo-Voigt fit of the emission for every wavelength of transition is multiplied by the strength that describes each transition within an individual peak and the matching factor of the corresponding emitter defined in Equation 58.

Figure 11 illustrates the different transitions found from the Kurucz database for the experimental Si I 212.41 nm line and the individual weight attributed before and after multiplication by the experimental emission. The experimental spectrum is shown as the solid black line. The shaded area represents the peak's FWHM. Left, the black square lines (symbol ■) represent the strength for each transition. Right, the red circle lines (symbol ●) represent the individual SIF of each transition for this spectral line taking into account the matching factor and the line profile. There is one transition seen to be the main contributor to the emission line Si I 212.41 nm in Figure 11.

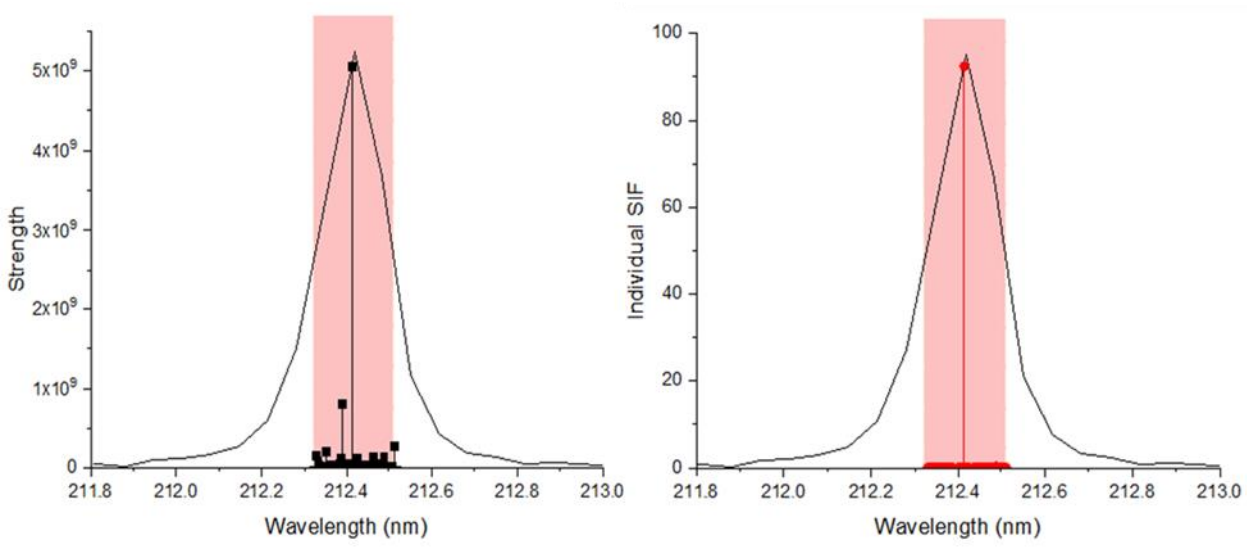

Figure 11: List of transitions for the individual peak 212.42 nm (left) strength of transition (right) individual SIF of transition.

The large probability of emission, large population of the upper energy level in LIBS conditions, and large matching factor for the spectral window 210 nm to 224 nm contribute the experimental peak 212.41 nm to neutral silicon. Table 2 shows three other contributions, Ni II, Fe II, and Al II possible for the experimental 212.41 nm peak besides Si I, their probability of transition, and their individual SIF. Neutral silicon has a probability of transition one power of ten greater than Al II, Fe II, and Ni II. Nickel II has the second highest individual SIF of $7.83 \times 10^8\ s^{-1}$ when the strength of the emission line comes from the Kurucz probability of transition. The matching factor for Ni II in the 210 nm to 224 nm window is 16.90 %. The strength of the Ni II transition with the population of the upper energy added when multiplied with the small matching factor results in a very miniscule individual SIF for peak 212.41 nm. Aluminum II and Fe II have

similar results to Ni II. Both Al II and Fe II have a smaller probability of transition than Ni II and Si I and small matching factors which lead to small individual SIFs of 1×10^{-6} %.

Table 2: Four transitions within experimental 212.42 nm peak.

Emitter	**Emission Wavelength (nm)**	**Probability of Transition (s^{-1})**	**Individual SIF (%)**
Si I	212.41	5.04×10^{9}	92.39
Ni II	212.39	7.83×10^{8}	1×10^{-6}
Al II	212.46	1.29×10^{8}	1×10^{-6}
Fe II	212.42	1.08×10^{8}	1×10^{-6}

Matching Factor

The matching factor (MF) is the first step in the SIF and provides a semi-quantitative evaluation of the emission of each atom in the Kurucz database compared to the experimental spectrum. The foundation of the matching factor is built on the fact that individual emission lines of the same element should be highly correlated[109]. The matching factor takes into consideration if a peak from an emitter is missing from the spectrum. Its calculation is derived from the ratio between the sum of detected peaks' strength to the sum of the theoretical peaks' strength that should occur in the spectral range for a specific emitter.

$$MF^e = \frac{\sum_{detected} S^e_{i\to j}}{\sum_{database} S^e_{i\to j}} \quad \textbf{(59)}$$

There is a relationship between the number of peaks found within the database to explain the experimental spectrum and the matching factor value. The lower the number of detected peaks between the experimental spectrum and the database, the lower the matching factor will be, and the converse holds true.

A typical spectrum of silicon between 210 nm and 224 nm is shown in Figure 12. Eighteen theoretical emission lines for the neutral silicon atom are found within this window. The eighteen neutral silicon emission lines from the Kurucz database and their upper energy transition are shown in Table 3 that produce the experimental peaks of the 210 nm to 224 nm spectral range.

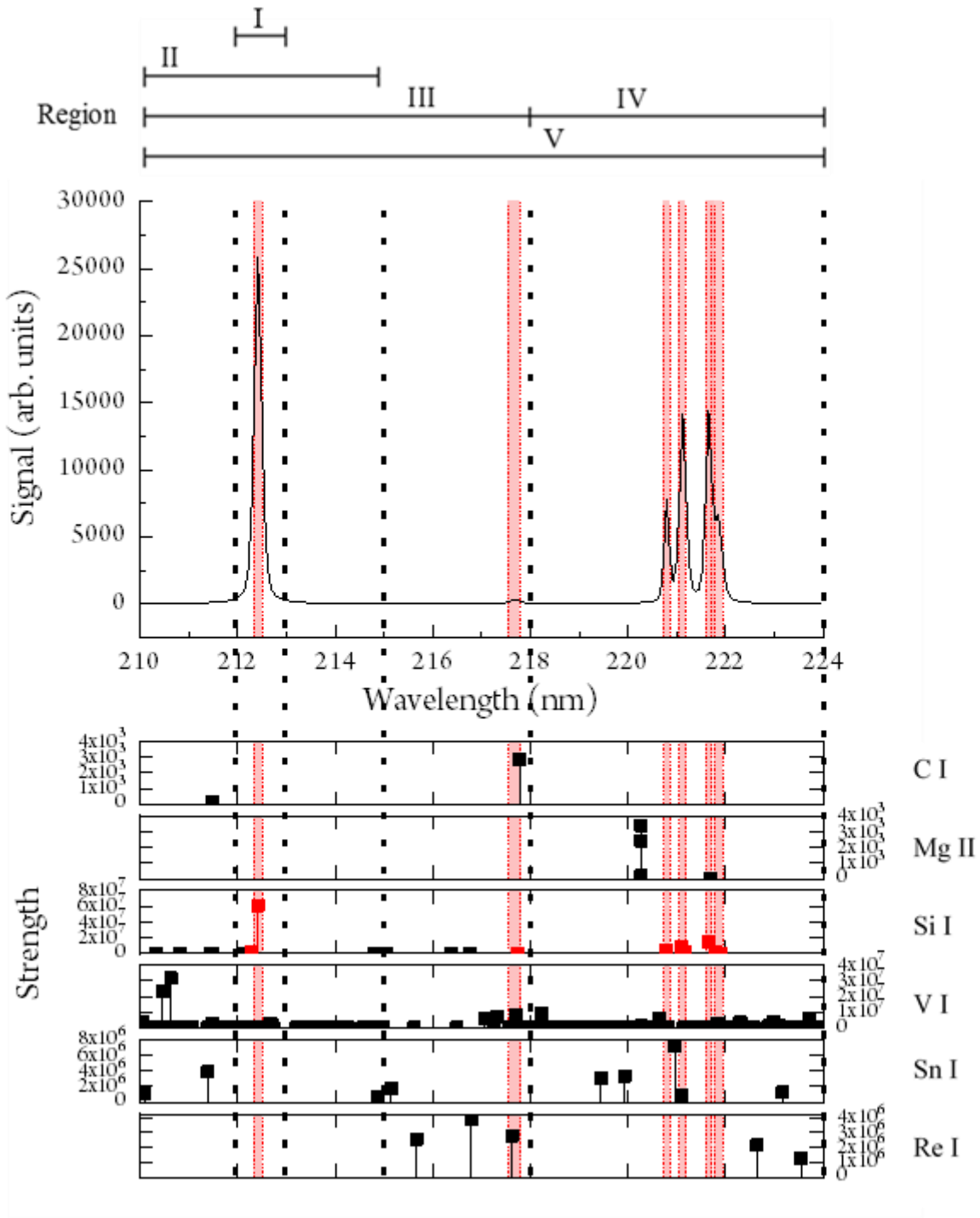

Figure 12: Measurement of matching factor of six emitters for the spectral range [210 nm – 224 nm] of silicon emission within five regions of interest[103].

Table 3: Neutral silicon transitions within spectral range [210 nm – 224 nm].

Wavelength (nm)	Transition	Strength
210.32	$3p^2\ ^1S_0 \leftarrow p6d\ ^3D°_1$	9.48E+04
210.82	$3p^2\ ^1S_0 \leftarrow p8s\ ^3P°_1$	3.74E+03
211.46	$3p^2\ ^3P_1 \leftarrow p3d\ ^1D°_2$	3.37E+03
211.48	$3p^2\ ^1S_0 \leftarrow p6d\ ^1P°_1$	1.28E+04
212.12	$3p^2\ ^3P_2 \leftarrow p3d\ ^1D°_3$	1.88E+04
212.30	$3p^2\ ^1D_2 \leftarrow p3d\ ^1P°_1$	2.18E+06
212.41	$3p^2\ ^1D_2 \leftarrow p3d\ ^1F°_3$	6.12E+07
214.79	$3p^2\ ^1S_0 \leftarrow p5d\ ^1D°_3$	7.37E+03
215.05	$3p^2\ ^1S_0 \leftarrow p7s\ ^1P°_1$	2.18E+04
216.38	$3p^2\ ^1S_0 \leftarrow p7s\ ^3P°_1$	5.42E+03
216.77	$3p^2\ ^1S_0 \leftarrow p5d\ ^3D°_1$	1.89E+05
217.74	$3p^2\ ^1S_0 \leftarrow p5d\ ^1P°_1$	8.61E+04
220.80	$3p^2\ ^3P_0 \leftarrow s3p^3\ ^3D°_1$	3.82E+06
221.09	$3p^2\ ^3P_1 \leftarrow s3p^3\ ^3D°_1$	8.37E+06
221.17	$3p^2\ ^3P_1 \leftarrow s3p^3\ ^3D°_2$	2.78E+06
221.67	$3p^2\ ^3P_2 \leftarrow s3p^3\ ^3D°_1$	1.50E+07
221.81	$,3p^2\ ^3P_2 \leftarrow s3p^3\ ^3D°_3$	2.65E+06
221.89	$3p^2\ ^3D_2 \leftarrow s3p^3\ ^3D°_1$	1.75E+05
	Total Detected	9.63E+07
	Total	9.66E+07
	MF (%)	99.70

The matching factor is calculated for all emitters in the Kurucz database for the spectrum input of eighteen emission lines and the list of transitions within each peak width (shaded areas in Figure 12).

The 210 nm to 224 nm spectral region for the experimental silicon spectrum is broken into five different regions. Table 4 displays the five regions and their wavelength range.

Table 4: Five spectral regions of spectral window [210 nm - 224 nm].

Region	I	II	III	IV	V
Wavelength (nm)	212 – 213	210 – 215	210 – 218	218 – 224	210 – 224

The six emitters with the larger matching factor, C I, Mg II, Si I, V I, Sn I, and Re I were analyzed for each region. Two of the six emitters, Si I and V I have emission lines from the Kurucz database within all experimental peak widths. The matching factor for element for each region is given in the table below. The LIBS conditions used for the silicon wafer analysis were not able to detect all of the transitions in the Kurucz database with low transition probabilities. This inability of detection results in the matching factor being smaller than 100%.

Table 5: Matching factor for five spectral regions of spectral window [210 nm – 224 nm].

Region MF (%)					
	I	**II**	**III**	**IV**	**V**
C I	0	0	94.74	0	94.74
Mg II	0	0	0	0.37	0.37
Si I	96.53	96.34	96.02	100	97.37
V I	4.87	0.38	10.09	7.72	9.32
Sn I	0	0	0	6.05	4.12
Re I	0	0	30.42	0	22.37

Figure 12 shows the 210 nm to 224 nm spectral region for the experimental silicon spectrum broken into the five separate regions. Neutral silicon is expected to have a matching factor larger

than 90% for all regions, as we analyze a LIBS spectrum of silicon. Region IV has a matching factor of 100% for silicon. The six neutral silicon emission lines from the Kurucz database from Table 3 from 218 nm to 224 nm are present within the experimentally determined peak widths. Regions I, II, III, and V have a matching factor of greater than 90% but less than 100% due to the expected peaks from the database that were not present in the experimental spectrum. In Region I, there are three Si I database emission lines at 212.12 nm, 212.30 nm and 212. 41 nm with strengths of $1.88*10^4$, of $2.18*10^6$, and of $6.12*10^7$ respectively. Silicon I 212.30 nm and 212.41 nm are database emission lines are present within the experimentally determined 212.41 nm peak that have high strengths greater than 2 orders of magnitude compared to the Si I 212.12 nm database line not present in the experimental spectrum resulting in a matching factor of 96.53%. This trend holds true for Si I for Regions II, III, and V.

Neutral carbon has two emission lines within the 210 nm to 224 nm region: 211.50 nm and 217.79 nm. Carbon I 211.50 nm emission line does not fall within Regions I and IV of interest. Regions I, II, and IV have no experimental spectral peak widths that contain the database emission of C I which results in a matching factor of 0%. Region II has one expected peak for C I at 217.79 nm. The one C I emission peak is found within the experimental spectrum which results in a matching factor of 100% for Region III.

The singly-ionized magnesium has a matching factor of 0% for Regions I, II, and III due to no database magnesium emissions occurring within those regions. Region IV and V have a

matching factor of 0.37% for Mg II. There are five expected Mg II emission peaks from the Kurucz database for Regions IV and V. Magnesium II has database emission lines at 220.268 nm, 220.268nm, 220.272 nm, 221.691 nm, and 221.701 nm. There are two emission lines of Mg II, 221.691 nm and 221.701 nm with small of strengths $2.39*10^{1}$ and $1.19*10^{1}$ respectively found within the experimental spectrum. The Mg II 220.268 nm, 220.268 nm, and 220.272 nm emission lines with large strengths of $3.40*10^{3}$, $1.71*10^{2}$, and $2.41*10^{3}$ respectively are not present within any of the peaks within Regions IV and V. The three Mg II database emission lines not present in experimentally determined peaks within Regions IV and V have strengths one and two orders of magnitude greater than the two emission lines that are present. which results in a small matching factor for Regions IV and V.

A matching factor of 0% was determined for neutral tin in Regions I, II, and III. There are no expected Kurucz emission lines for Sn I within Region I. Regions II and III have three expected Sn I database emission lines at 210.09 nm, 211.39 nm, and 214.87 nm which are not present in the experimental spectrum which results in a matching factor of 0%. There are five expected emissions from the Kurucz database for Sn I for Region IV. In region IV, there is one database Sn I line at 221.11 nm present within the experimental spectrum with a strength of $9.57*10^{5}$. The strength of the line present within Region IV for Sn I is very small compared to the other four emissions which results in a small matching factor of 6.05%. Region V has nine database emission lines for neutral tin. Tin I 221.11 nm is the only database emission line present in the experimental spectrum out of the nine for Region V. There are a larger number of theoretical

lines for Sn I for Region V that are not found within the experimental detected peaks' widths which results in a low matching factor of 4.12%

Neutral rhenium has five emission lines from the Kurucz database with in the 210 nm to 224 nm window. There are no expected emissions for Re I within regions I and II. Region III has three Kurucz emission lines at 215.67 nm, 216.79 nm, and 217.62 nm. Rhenium I 217.62 nm is present in the experimental spectrum while 215.67 nm and 216.79 nm are absent. The strength of 217.62 nm is $2.82 * 10^6$ which is relatively high compared to the strengths of 215.67 nm and 216.79 nm $2.58*10^6$ and $3.86*10^6$ respectively resulting in a 30.42% matching factor. Region V has a smaller matching factor than region III because there are more expected Kurucz database emission lines that are not present within the experimental spectrum.

Neutral vanadium shows the effect the spectral range used for evaluation has on the matching factor value. There are numerous transitions throughout all regions of the 210 nm to 224 nm spectral window. Many of the transitions from the Kurucz database for V I have low strength as seen in region IV and V. Due to the quantity of V I database emission lines, some of the lines will be present within the experimental peak widths. The main Kurucz emission lines for neutral vanadium are not present in the experimental spectral peak widths giving a small matching factor for all five regions.

The transition probability with the population of the upper energy level depends on the excitation temperature parameter. The excitation temperature affects the partition function value for the atom which affects the strength of an emitter's transition. It is not straightforward to measure excitation temperature with a commercial such as the Applied Spectra J200 LIBS in the laboratory. As a result, an estimation of the plasma temperature was necessary to calculate the SIF. The SIF is affected by the matching factor which is affected by the excitation temperature of the emitter's transition as shown in Figure 13.

For many emitters, the matching factor is minimally affected by the plasma temperature such as Ge II whose matching factor consistently stays between to 23.42% and 24.3%. Emitters such as Si I, Si II, Zn II, and Sn I have matching factors that are influenced by the excitation temperature. Neutral or singly-ionized silicon have the highest matching factor, independently of the excitation temperature. The high matching factor values for Si I and Si II are expected as the emission lines of silicon are similar and correlated. Silicon I has the highest matching factor for all plasma temperatures. Singly-ionized silicon has the second highest matching factor for 0.45 eV to 2.35 eV. The SIF calculation used 1.5eV as it was the optimal excitation temperature.

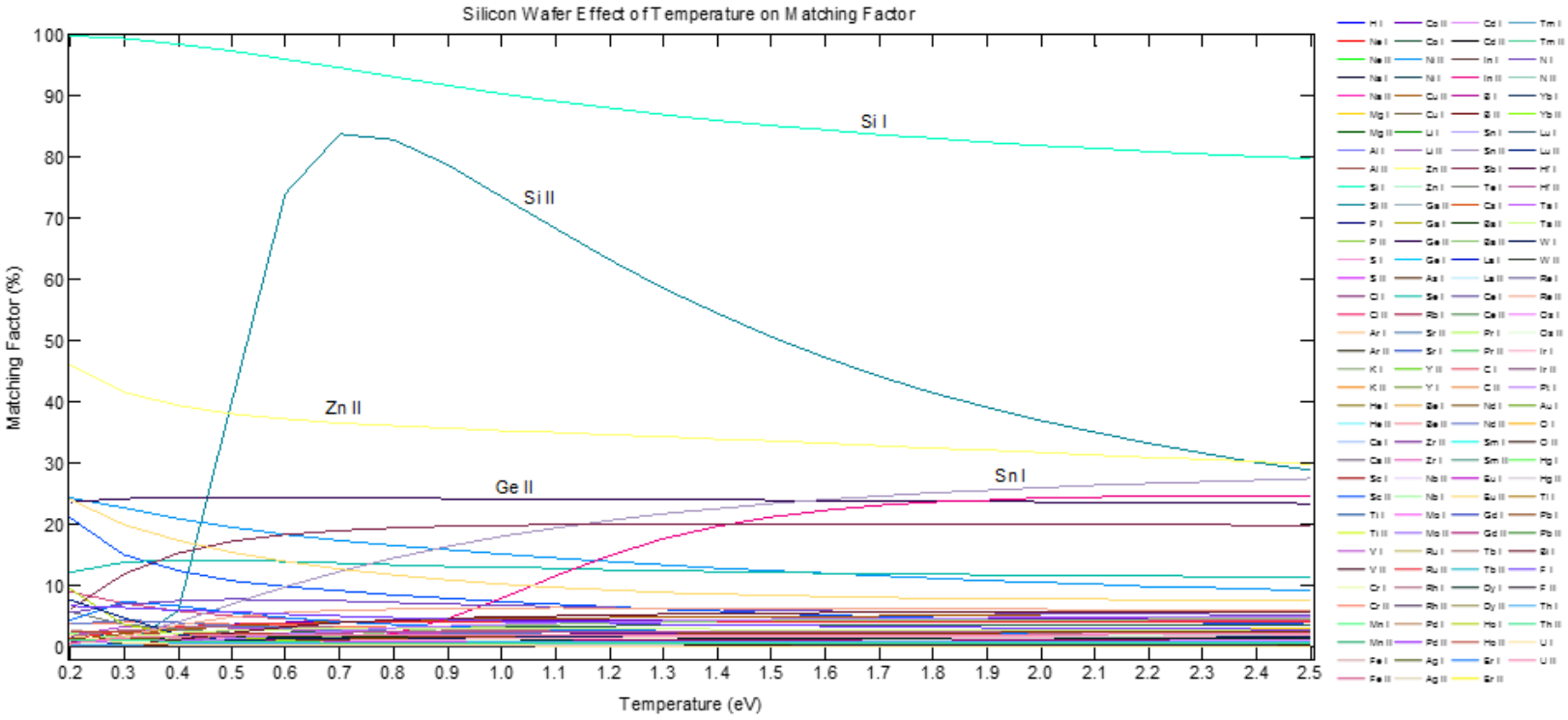

Figure 13: Effect of excitation temperature on the matching factor for the silicon sample. The excitation temperature chosen for analysis was 1.5eV[111].

Bayesian Inference

One method to quantify uncertainty is based on Bayesian Inference. Bayesian Inference can draw conclusions about experimental data that cannot be observed by other means. Uncertainty quantification by Bayesian Inference accounts for available data and provides a degree of uncertainty with the available evidence of data. The quantification of the degree of uncertainty is measured by probability. Bayesian Inference can be broken into three steps: creation of model, conditioning of model, and evaluation of model[110].

1. Creation of Model: The first step in Bayesian Inference is the creation of the probability model which contains all information known to a user about the scientific processes and data being evaluated.
2. Conditioning of Data: The second step of Bayesian Inference calculates the posterior distribution of the model and interprets the results obtained.
3. Evaluation of Model: The evaluation of the Bayesian Inference model asks questions about how well does the model fit the data. Do the results seem reasonable for the scientific process being evaluated? Do posterior distribution results change with the assumptions of the model created?

Model creation assumes joint probability distribution of the outcomes of the data. Joint probability distribution assigns probability to all combinations of random variables in the data and is used for answering questions about the model that arise. Probability statements are used to make conclusions about a variable or parameter from unobserved data. Joint probability is the

product of the prior distribution $p(\theta)$ or information known about the parameters and the data distribution $p(y|\theta)$ or likelihood to make probability statements about θ given y.

$$\boldsymbol{p(\theta, y) = p(\theta)p(y|\theta)} \quad \textbf{(60)}$$

The probability of the unobserved parameters to explain the observed data with prior knowledge of the scientific process is the posterior distribution of the model. The posterior distribution is given by the property of conditional probability also known as Bayes' rule. Bayes' rule is given by the following equation:

$$\boldsymbol{p(\theta|y) = \frac{p(\theta,y)}{p(y)} = \frac{p(\theta)p(y|\theta)}{p(y)}} \quad \textbf{(61)}$$

where $p(\theta, y)$ is the model, $p(y|\theta)$ the likelihood function, and $p(y)$ the probability distribution of the unknown but observable data.

$$\boldsymbol{p(y) = \sum p(\theta)p(y|\theta)} \quad \textbf{(62)}$$

Given observable data, two models that have the same likelihood function will have the same inference for θ. The evaluation of the created model for Bayesian Inference should be evaluated, revised, and re-evaluated until the user is satisfied with the model and results. Bayesian

Inference does have challenges when computing large and complex systems[111]. The computational challenge of large and complex data can be reduced by removing the number of models to fit the data. Reduction of the number of models of data leads to reduction in simulation time while being reasonably accurate. One of the biggest challenges to Bayesian Inference is the creation of the models needed to explain a specific system of experimental data. The variability that occurs in the output results of the model under the same repeated conditions lead to residual variability[112]. Residual variability leads to difficulty in setting up the model needed due to the random nature of the experimental setup. Bayesian Inference is flexible and a general process that can be applied to any scientific process.

The posterior distribution obtained from the model created from Bayesian Inference for quantification of spectral interference in optical emission spectroscopy will be analyzed for variance by the confidence interval and chi-square hypothesis test of variance.

Optimum Representation of the Experimental Spectrum

The individual SIF demonstrates the quantification of spectral interferences found within one experimental peak. Since, a LIBS spectrum is a multimodal distribution and emission lines of the same element should be correlated, the information for each peak is combined to explain the whole experimental spectrum by a Bayesian approach. The input for the Bayesian approach is the individual SIF for each emitter for each individual peak. The Bayesian approach of the combination of emitters includes any available prior knowledge of model parameters.

In this experimental silicon case, the focus was on the plasma composition as prior knowledge. The composition of the silicon sample is either known or not. When analyzing the silicon data with no knowledge of the silicon sample's composition, every emitter in the Kurucz database probability of emission is considered equally present. When the silicon sample's composition is known, a restriction is made to the emitters found within the sample's composition and the background gas for the LIBS analysis with an equal probability of emission given to each emitter. Knowledge of the sample's composition can be broken into two types of knowledge: qualitative and quantitative. Qualitative knowledge gives the emitters present in the sample the same probability of emission while absent emitters have no probability. Quantitative knowledge uses the concentration of the element present in the sample's composition as its probability of emission. The silicon wafer contained Si I and Si II. Knowledge of the background gas for the LIBS analysis is added to the knowledge of the sample composition because it can be excited and contribute to the emission spectrum. The background gas for the LIBS analyses was air so the following set of emitters were added to the prior knowledge of the sample composition {H I, N I, N II, O I, O II} because of air moisture.

Emitters found within the Kurucz database and their SIF for each individual peak are the known model parameters in this algorithm. Contribution from each atom to the entire experimental spectrum is not equally distributed. Based on the sum of their individual SIF for each peak, emitters are ordered in decreasing order of their contribution.

$$\boldsymbol{G = \sum_{n=1}^{N} \max({}^{p}SIF_{i\to j}^{e})} \quad \textbf{(63)}$$

A greedy search G of the largest sum of SIFs ${}^{p}SIF_{i\to j}^{e}$ for all peaks in the whole spectrum, orders first n, the emitter e with the highest contribution and the following emitters are ordered with the next highest likelihood until all emitters N are ordered[113]. The greedy search loops through each emitter and its likelihood is summed by the natural log of the individual SIF for all peaks. The atom with the maximum sum of the natural log of the individual SIF is ordered first. The process repeats until all emitters present in the Kurucz database for the experimental spectrum are ordered from highest to lowest likelihood.

A simple example of the greedy search ordering is given below where there are four possible emitters {A, B, C, D} for two peaks. The individual SIF values for the emitters and the two peaks are given in Table 6.

Table 6: Individual SIF of greedy search ordering example.

Emitter	Peak 1	Peak 2
A	0.1	0.4
B	0.8	0
C	0.1	0
D	0	0.6

To order the first emitter, the sum of the natural log of the individual SIF (likelihood, L) for each peak for each atom is calculated. Emitters B and C have no transitions within peak 2, and

emitter D has no transition within peak 1. The natural log of zero is undefined, which would create an issue with identifying and ordering the emitters with the highest SIF sum. To address this issue, any individual SIF that has no probability of emission is replaced with 0.00001. To find the first emitter, the likelihood for each individual emitter is calculated and shown below.

Table 7: Likelihood of one emitter for greedy search ordering example.

Equation	Value
$L_A = \ln(0.1) + \ln(0.4)$	-3.22
$L_B = \ln(0.8) + \ln(0.0001)$	-9.43
$L_C = \ln(0.1) + \ln(0.0001)$	-11.5
$L_D = \ln(0.0001) + \ln(0.6)$	-9.72

The maximum likelihood value is -3.22 which means that emitter A is ordered first. The next ordered atom is determined by the max individual SIF for each peak with the combination of emitter A and the next possible emitters.

Table 8: Likelihood of two emitters for greedy search ordering example.

Equation	Value
$L_{AB} = \ln(0.8) + \ln(0.4)$	-1.14
$L_{AC} = \ln(0.1) + \ln(0.4)$	-3.22
$L_{AD} = \ln(0.1) + \ln(0.6)$	-2.81

The next ordered emitter is B with a maximum likelihood of -1.14. The third ordered atom is determined to be emitter D with a maximum likelihood of -0.73 compared to emitter C which

has a likelihood of -1.14 (Table 9). Thus, the greedy search ordering of the four emitters for the two peaks is {A, B, D, C}.

Table 9: Likelihood for three emitters for greedy search ordering example.

Equation	**Value**
L_{ABC} = ln(0.8) + ln(0.4)	-1.14
L_{ABD} = ln(0.8) + ln(0.6)	-0.73

Bayesian Information Criterion

A Bayesian Information Criterion (BIC) is used to weigh all possible models that will be evaluated by the Bayesian approach for the combination of elements that create the elemental profile of a sample. The BIC is used to avoid unnecessary calculations of the combinations of elements of models that provide minimal information of the entire experimental spectrum. The selection of the emitters by the BIC determines which set of emitters should be chosen over another set to explain the combination of all peaks in the whole experimental spectrum. The BIC is calculated by:

$$\boldsymbol{BIC = -2 * ln(l) + K * \ln(n)} \quad \textbf{(64)}$$

where l is the maximum SIF estimate of each parameter, K is the number of emitters in the model and n is the number of observations in the data[114]. The set of emitters with the optimized

BIC is determined once all emitters are ordered. The optimized BIC determines the smallest number of emitters needed to explain the entire spectrum by which set of emitters have the lowest BIC value. The model selection of the BIC treats each atom separately resulting in a singly-ionized emitter possible being chosen for the optimal set of emitters without its neutral atom. The neutral atom of any chosen singly-ionized atom that is not present in the optimal set of emitters is added because the emission of a singly-ionized atom without its neutral is very rare in LIBS. The algorithm calculates the optimal number of emitters by the Bayesian Information Criterion to explain the whole spectrum, but more emitters could be added to the model. The addition of more emitters to the optimal model would increase computational times while providing little to no additional information about the SIF to the analysis.

Using the individual SIF of four emitters for two peaks from Table 6, the values for the parameters for the BIC equation are given in Table 10. Based on the lowest BIC value of 3.54, the optimal set of emitters to explain the simple example is {A, B, D} as seen in Figure 14. Emitter C could have been added to the analysis which would have increased the computation time to find the posterior SIF.

Table 10: Bayesian Information Criterion parameters for example.

Emitter	Likelihood	k	n	BIC
A	-3.22	1	2	7.13
A, B	-1.14	2	2	3.67
A, B, D	-0.73	3	2	3.54
A, B, D, C	-0.73	4	2	4.23

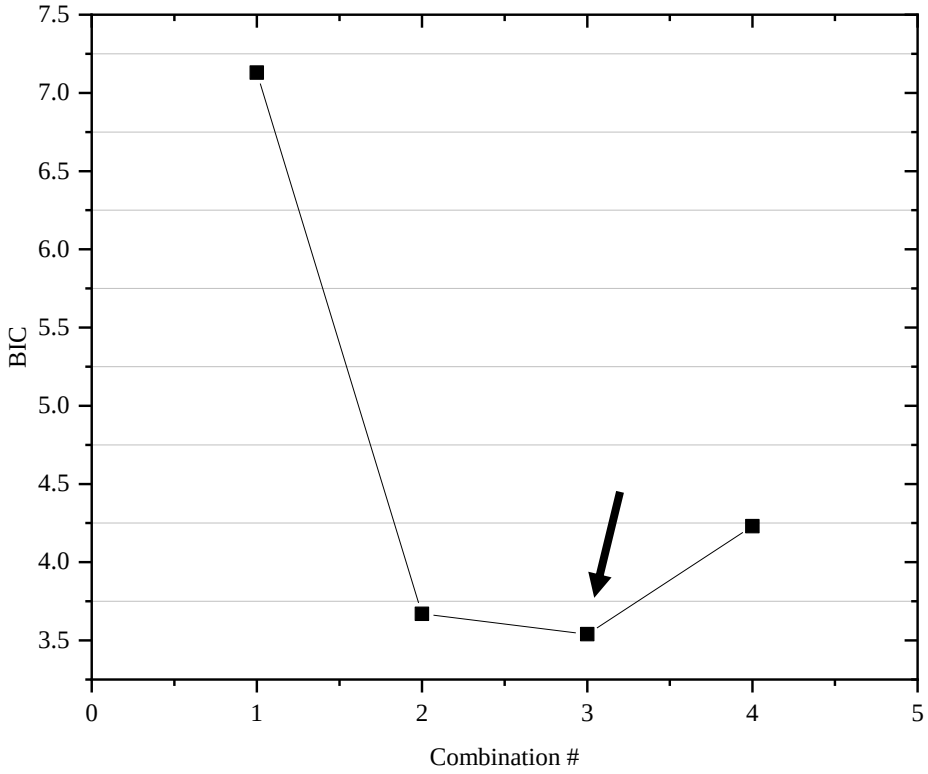

Figure 14: BIC graph example

The ordering of the emitters and their corresponding likelihood for the no prior knowledge and qualitative prior knowledge analyses of the experimental silicon spectrum are shown in Table 11. If emitters have an individual SIF for all peaks in the experimental spectrum, they are not considered in the ordering as they have no probability of being an emitter of the spectrum. There are twenty-four emitters that have at least one individual SIF value for the no prior knowledge analyses. Neutral silicon was ordered second and Si II was ordered eighth for the no prior knowledge analyses which is expected with a silicon experimental spectrum. With qualitative prior knowledge, only five emitters are possible emitters for the spectrum with Si I and Si II being ordered first and second, respectively. The higher an atom is ordered, the higher

the probability that that atom is present in the experimental spectrum. The reverse holds true also.

Table 11: Ordering of emitters in the no prior and qualitative prior analyses of silicon.

	No Prior		Qualitative Prior	
Order	**Emitter**	**Sum of log of SIF**	**Emitter**	**Sum of log of SIF**
1	Ni II	-3.61E+02	N I	-9.08E+02
2	Si I	-3.17E+02	N II	-6.86E+02
3	Cr I	-1.23E+02	O I	-6.29E+02
4	Fe I	-1.09E+02	Si I	-5.75E+02
5	N I	-9.55E+01	Si II	-5.51E+02
6	Na I	-8.93E+01		
7	Th I	-8.38E+01		
8	Si II	-7.92E+01		
9	Er I	-7.57E+01		
10	Fe II	-7.28E+01		
11	O I	-7.01E+01		
12	Re II	-6.81E+01		
13	Sc II	-6.63E+01		
14	Cu II	-6.46E+01		
15	Zn II	-6.30E+01		
16	Y I	-6.15E+01		
17	Gd II	-6.05E+01		
18	Sb I	-5.98E+01		
19	Pb I	-5.91E+01		
20	Rh I	-5.84E+01		
21	Eu I	-5.83E+01		
22	V I	-5.82E+01		
23	U II	-5.82E+01		
24	Be I	-5.82E+01		

Table 12 shows the top sixteen sets of ordered emitters and their corresponding BIC values for the experimental silicon spectrum with no prior knowledge. The determination of the BIC for

the first ordered atom, Ni II in the no prior knowledge sums the natural log of the individual SIF values for Ni II for the eighty-four experimental peaks. The first part of the BIC calculation is sum of the log of the individual SIF of each peak for Ni II which was -361.33 which was multiplied by negative two resulting in 722.66. The answer for part one is added to the product of the number of emitters in the set, one, and natural log of the number of peaks in the experimental data, eighty-four. Bayesian Information Criterion for Ni II for the no prior knowledge is 727.09. All of the set of emitters for the possible combinations BIC values are calculated and the lowest BIC value of 193.29 corresponds to the optimal set of emitters, twelve, needed to explain the silicon spectrum. When a singly-ionized emitter is missing its neutral atom, the neutral atom is added to the optimal set of emitters because it is rare for the emission of an emitter without its neutral emitter in LIBS. There are fourteen optimal ions for the no prior knowledge analysis with the expected Si I and Si II included.

Table 12: Bayesian Information Criterion for the no prior knowledge analysis of silicon.

Emitter	**BIC**
Ni II	727.09
Ni II, Si I	363.15
Ni II, Si I, Cr I	293.65
Ni II, Si I, Cr I, Fe I	264.03
Ni II, Si I, Cr I, Fe I, N I	239.23
Ni II, Si I, Cr I, Fe I, N I, Na I	217.55
Ni II, Si I, Cr I, Fe I, N I, Na I, Th I	209.68
Ni II, Si I, Cr I, Fe I, N I, Na I, Th I, Si II	203.10
Ni II, Si I, Cr I, Fe I, N I, Na I, Th I, Si II, Er I	198.24
Ni II, Si I, Cr I, Fe I, N I, Na I, Th I, Si II, Er I, Fe II	195.65
Ni II, Si I, Cr I, Fe I, N I, Na I, Th I, Si II, Er I, Fe II, O I	194.38
Ni II, Si I, Cr I, Fe I, N I, Na I, Th I, Si II, Er I, Fe II, O I, Re II	**193.29**
Ni II, Si I, Cr I, Fe I, N I, Na I, Th I, Si II, Er I, Fe II, O I, Re II, Sc II	193.73
Ni II, Si I, Cr I, Fe I, N I, Na I, Th I, Si II, Er I, Fe II, O I, Re II, Sc II, Cu II	194.62
Ni II, Si I, Cr I, Fe I, N I, Na I, Th I, Si II, Er I, Fe II, O I, Re II, Sc II, Cu II, Zn II	195.59
Ni II, Si I, Cr I, Fe I, N I, Na I, Th I, Si II, Er I, Fe II, O I, Re II, Sc II, Cu II, Zn II, Y I	196.90

Any prior information available about the sample is used once the optimal number of emitters to explain the complete spectrum is determined. Table 13 shows the top Bayesian Information Criterion values for the qualitative prior knowledge analysis. The optimal set of ions for the silicon sample for the qualitative prior knowledge analyses is five {N I, N II, O I, Si I, Si II}. Singly-ionized oxygen in the spectral region of interest does not contain any transitions even though it is a prior knowledge of the plasma composition in air.

Table 13: BIC for the qualitative prior knowledge analysis of silicon.

Emitter	**BIC**
Si I	854.21
Si I, Si II	704.44
Si I, Si II, N I	659.80
Si I, Si II, N I, O I	620.35
Si I, Si II, N I, O I, N II	608.58

The amount of prior knowledge required to evaluate spectral interferences for an unknown sample will be shown by the comparison of the two models of prior knowledge. Figure 15 shows the silicon spectrum's optimal set of emitters from the Bayesian Information Criterion.

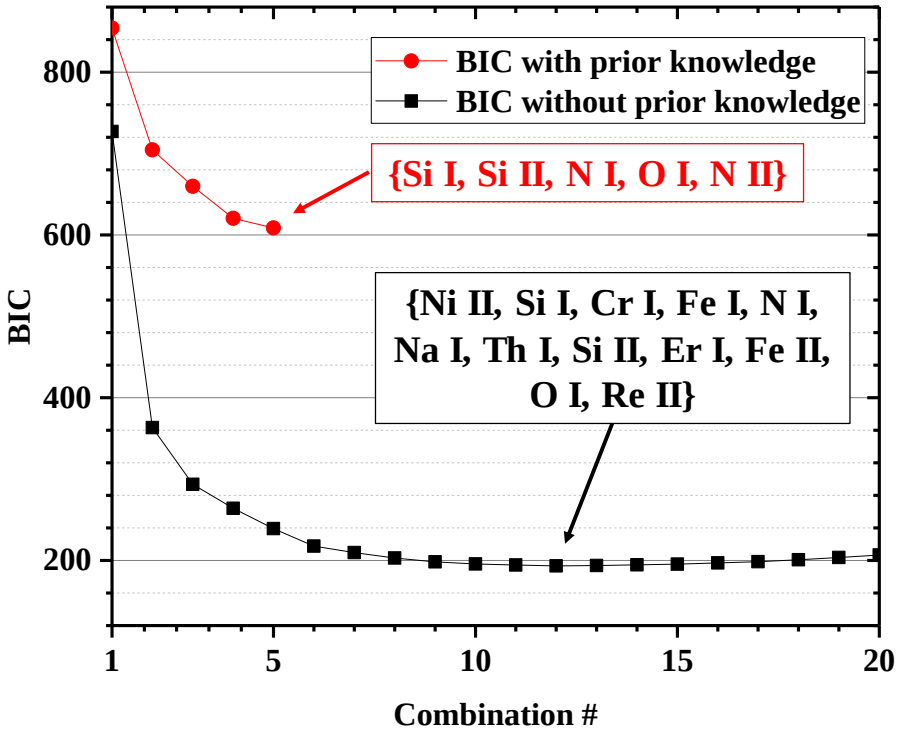

Figure 15: BIC graph for pure silicon[103].

The importance of prior information to optimize the set of emitters to explain the spectrum is shown in the two curves of Figure 15. The two cases of prior knowledge are represented. The red circles (symbol ●) represent the BIC with no prior knowledge of the sample's and plasma's composition. The black squares (symbol ■) represent the BIC with prior knowledge of the sample and plasma's composition. The optimum set of emitters was {N I, N II, O I, Si I, Si II} in the case of prior knowledge of silicon plasma in air. The number of emitters that contributed to the individual SIF at least once was considered for the case of no prior knowledge of the sample composition at all and the optimal number of emitters to explain the spectrum is large: {Cr I, Er I, Fe I, Fe II, N I, Na I, Ni I, Ni II, O I, Re I, Re II, Si I, Si II, Th I}. No prior

knowledge analyses contained neutral and singly-ionized silicon while the emitters with contribution to one line only was not removed. Four emitters are common to both prior knowledge analyses: {N I, O I, Si I, Si II}.

Bayesian calculation of the SIF for the combination of all of the detected peaks in the entire spectrum uses the individual peak SIF values from the optimal set of emitters determined by the Bayesian Information Criterion. The combination of emitters with individual SIFs are found and the best combination SIF for the experimental spectrum is determined by its Bayes likelihood. In the case of the no prior knowledge, the number of possible combinations for thirteen Emitters and eighty-four peaks is 6.03×10^{14}. In the case of prior knowledge, the number of possible combinations for five emitters and eighty-four peaks is 3.09×10^{7}. The threshold for the number of combinations in the algorithm is 1.0×10^{8}. Combinations greater in number than the threshold requires the allotment of large amounts of memory and power that are not feasible at this moment. For the silicon spectrum, it would be possible to run all of the combinations of emitters for the prior knowledge analysis but not the no prior knowledge combinations. Since, the combinations cannot be determined for the no prior knowledge silicon analysis, the process of determining combinations and their likelihood are applied to both knowledge analyses. To address the issue of memory and power, the spectral peaks are broken into subsections of ten peaks. The first subsection is comprised of peaks one through ten. Table 14 shows the possible emitters for each peak in the first subsection. The eighty-four peaks for the silicon sample was initially broken into nine subsections.

Table 14: Silicon subsection 1 possible emitters.

Peak 1	Peak 2	Peak 3	Peak 4	Peak 5	Peak 6	Peak 7	Peak 8	Peak 9	Peak 10
Ni II Si I	Fe II Ni I Ni II Si I	Cr I Fe II Ni I Ni II Si I	Fe II Si I	Fe II Ni II Si I	Fe I Fe II Ni II Si I	Cr I Fe II Ni II	Fe I Fe II Ni II Si I Si II	Fe I Fe II Ni I Ni II	Fe I Fe II

The number of possible combinations for subsection one is determined by the product of possible emitters for each peak within the subsection. Possible emitters for subsection one are {2,4,5,2,3,4,3,5,4,3} which results in 172,800 combinations. If there are more than twenty-eight emitters for the ten-peak subsection, the number of combinations is large, and that specific subsection is broken into two five peak sections. With the threshold value 1.0×10^8 combinations for determining the maximum number of combinations possible, each peak in the five-peak section can have up to one-hundred thirty-six possible emitters. The number of combinations for each subsection of the initial ten peaks is given in Table 15. There are no subsections that meet the threshold value for combinations too large thus the total number of subsections for the silicon data is nine.

Table 15: Number of combinations for each silicon subsection.

Subsection	# Combinations
1	1.73E+05
2	1.40E+06
3	1.04E+06
4	1.80E+06
5	4.06E+07
6	2.18E+06
7	3.24E+05
8	4.05E+06
9	4

For each subsection of five or ten peaks, all combinations of emitters are determined, and their sum of their individual SIFs calculated. The combinations are sorted from highest to lowest sum of SIFs. The top ten combinations are kept for each subsection and combined with the top ten combinations of the other subsections to produce the combination for the entire spectrum. If the total number of combinations is greater than one million and the number of experimental peaks less than four-hundred, the SIF algorithm keeps the top one million and discards the rest of the combinations due to memory and computation issues. The memory allotment for experimental data that have over four-hundred peaks does not allow for the determination of one-million combinations. Instead, the top one-hundred thousand combinations are obtained. The experimental silicon data had eighty-four peaks, thus, the top one-million combinations were found and sorted by their likelihood.

Combination of emitters are ranked according to their likelihood. The likelihood for each combination of emitters is determined by the following equation:

$$\textbf{Bayes Likelihood} = \exp\left[\sum \ln L + \ln\left(p(n)\right)\right] \quad \textbf{(65)}$$

where L is the SIF (likelihood) of the parameters and $p(n)$ is the probability of the number of peaks in the data[119]. For a simple example of the Bayes likelihood and the posterior likelihood of each peak's SIF is shown below for two emitters, A and B for two peaks. The individual SIF for emitter A and B are shown in Table 16.

Table 16: Individual SIF for Bayes likelihood example.

Emitter	Peak 1	Peak 2
A	0.3	1
B	0.7	0

The number of combinations for two emitters for two peaks is six shown in Table 17.

Table 17: Combinations for Bayes likelihood example.

Peak 1	Peak 2
A	A
A	B
B	A
B	B
A & B	A
A & B	B

With the six combinations, three of the combinations are not possible. The combinations with emitter B assigned to peak 2 cannot happen because emitter B does not have any transitions that could emit peak 2 thus the likelihood for these combinations is zero. The likelihood of the three possible combinations are shown below in Table 18.

Table 18: Bayes likelihood of each combination.

Equation	Value
$L_{(A,A)} = \exp(\ln(0.3) + \ln(1))$	0.30
$L_{(B,A)} = \exp(\ln(0.7) + \ln(1))$	0.70
$L_{(A\&B,A)} = \exp(\ln(0.7) + \ln(0.3) + \ln(1))$	0.21

Using the Bayes likelihood for each combination, the posterior SIF for each peak is individually calculated by the likelihood of each emitter for each peak and their corresponding probability. The probability of each emitter for combination for each peak is given in Table 19. The probability of emitter A producing the first peak is 0.3 and the second peak 1.0. The probability of emitter B producing the first peak is 0.7.

Table 19: Probability of each emitter for each combination

Probability	Value
$p(n)_{(A,A)}$	0.30
$p(n)_{(B,A)}$	0.70
$p(n)_{(A\&B,A)}$	0.30, 0.70

The likelihood that emitter A produces peak 1 is 19.37% and peak 2 is 100%. Peak 1 can also be produced from emitter B with a likelihood of 80.63%. The normalized posterior SIF likelihood is determined by product of the emitter's combination likelihood and probability as shown in Table 20.

Table 20: Posterior SIF calculation for peak 1 of Bayes likelihood example.

Equation	Norm. Posterior SIF (%)
$L_{(A)} = [L_{(A,A)} * p(n)_{(A,A)}] + [L_{(A\&B,A)} * p(n)_{(A\&B,A)}]$ $L_{(A)} = (0.3 * 0.3) + (0.21 * 0.3)$	19.37
$L_{(B)} = [L_{(B,A)} * p(n)_{(B,A)}] + [L_{(A\&B,A)} * p(n)_{(A\&B,A)}]$ $L_{(B)} = (0.7 * 0.7) + (0.21 * 0.7)$	80.63

The top combination for the experimental silicon spectrum of the qualitative prior knowledge analyses has five emitters. The probability of five emitters in the top combination for the experimental silicon spectrum is 0.0508 with the sum of the combination's natural logs of the SIFs for the peaks is -25.482. The Bayes likelihood for the combination is $4.357 * 10^{-13}$. The optimum combination of emitters chooses the combination with the largest likelihood value.

With the optimum combination chosen, a posterior SIF defines what each atom from the model contributes to each peak in the experimental spectrum.

Five intense peaks with their top ten emitters based on their individual SIF is listed in Table 21. Silicon I and Si II were expected to be the highest contributor to each peak. Neutral or singly-ionized silicon are not present within the top ten contributors of peak 206.57 nm because there is one database emission lines of silicon in the width of the peak. The individual SIF of Si I 206.55 nm transition within the experimental 206.57 nm is $3.94 \times 10^{-6}\ s^{-1}$. Peak 252.88 nm has neutral silicon as the second highest individual SIF because of the large interference from Sb I which is a well-known interference for the Si I 252.88 nm emission line[115]. For twenty-seven of the forty experimental peaks under 300 nm, Si I had the highest or second highest individual SIF. Singly-ionized silicon had the highest individual SIF for two peaks under 300 nm. Spectral interferences were found within the eleven other peaks

Table 21: Five peaks from the silicon spectrum with each peak's top emitters and individual SIF values[111].

Peak 206.57nm		**Peak 207.24nm**		**Peak 251.64nm**		**Peak 252.88nm**		**Peak 288.13nm**	
ION	**SIF**	**ION**	**SIF**	**ION**	**SIF**	**ION**	**SIF**	**ION**	**SIF**
Ni II	0.3714	Si II	0.4677	Si I	0.9584	Sb I	0.4666	Si I	0.9007
Ge I	0.2618	Ni II	0.1561	Fe I	0.0093	Si I	0.3744	Ni II	0.0271
Fe II	0.1198	Fe I	0.0792	Fe II	0.0074	Ni II	0.0850	Cu II	0.0144
Co II	0.1001	Fe II	0.0631	Co II	0.0049	Co II	0.0229	Fe I	0.0137
Cr II	0.0627	Sn I	0.0573	Th II	0.0034	Co I	0.0142	Fe II	0.0109
As I	0.0456	Cr II	0.0335	Cr II	0.0033	Fe I	0.0124	Th II	0.0071
Mn II	0.0342	Sc I	0.0245	Cr I	0.0020	Fe II	0.0102	Cr II	0.0056
W II	0.0019	V I	0.0237	Mn II	0.0019	Cr II	0.0027	Gd II	0.0047
Fe I	0.0011	Cr I	0.0213	Hf II	0.0019	Mn II	0.0019	Cr I	0.0035
V II	0.0009	Mn II	0.0183	V I	0.0016	Cr I	0.0017	Mn II	0.0032

Figure 16 shows the posterior SIF for the optimal set of emitters calculated from the 1,000,000 combinations for the forty experimental peaks for the silicon spectrum under 300 nm. The graph of the posterior SIF for the no prior knowledge and prior knowledge analyses are shown top and bottom respectively. Large spectral interferences occur when there is no emitter with an individual SIF greater than or equal to 90% in a peak. The peaks at 230.29 nm, 245.23 nm, and 297.04 nm exhibit large spectral interferences with no prior knowledge of the sample or plasma composition resulting in uncertainty in the elemental assignment of those peaks. The decision for accepting whether an emission line should be used or not is based on a SIF threshold that is user-defined.

When there is one emitter with a SIF greater than or equal to 90% and the rest of the interfering elements sum to 10% or less is considered a small interference as seen in peaks 207.24 nm and 208.25 nm of the no prior analysis. Silicon II contributions have small probabilities that their lines are interfered by other emitter emissions. The main contributor to peaks 217.68 nm and 225.99 nm is singly-ionized nickel with small interferences from neutral silicon. There is a total of twenty-three peaks in the under 300 nm spectral region of the silicon spectrum that were judged not to be interfered.

Prior knowledge of the sample and plasma composition was applied to the same forty peaks within the 185 nm to 300 nm spectral region. Thirty-five of the forty had 100% certainty in line assignment as they contained no spectral interferences.

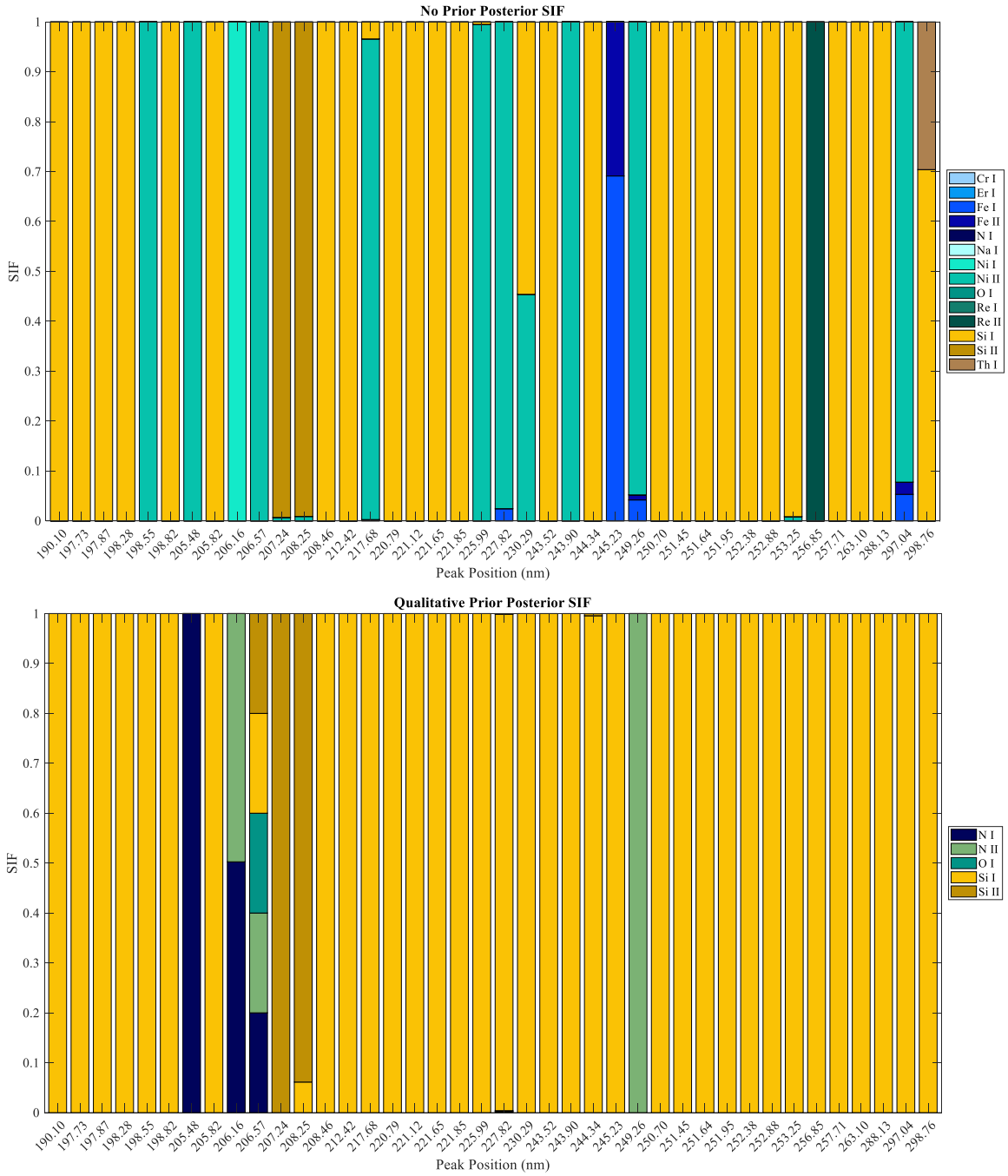

Figure 16: Posterior SIF for experimental silicon spectrum under 300 nm (top) no prior (bottom) qualitative prior[103].

Neutral and singly-ionized nitrogen have large interferences at peak 206.16 nm. Line assignment for peak 206.16 nm can be contributed to nitrogen since both N I and N II have equal probability of being the peak emitter. The five emitters needed to explain the silicon spectrum with prior knowledge have equiprobability of being the emitter of peak 206.57 nm. The 206.57 nm line is considered non-reliable for silicon analysis no matter whether the sample and plasma composition are known.

Comparison of the two knowledge analyses of the silicon spectral window 185 nm to 300 nm resulted in silicon being the main emitter of 60% of the spectral peaks. The no prior and prior knowledge analyses resulted in 67.5% of the peaks matching with the same largest emitter. The matching of the knowledge analyses was a result of the number and elements that make up the optimal set of ions which differ because of the optimization of the greedy search ordering of the emitters in the experimental spectrum. The main contributor (highest SIF) was Si I for twenty-two of the forty peaks and Si II for two peaks in the experimental silicon spectrum under 300nm. Some spectral lines in the experimental silicon spectrum can be used as silicon signals without spectral interferences even when the sample and plasma composition was unknown.

CHAPTER 6:
QUANTIFICATION OF SPECTRAL INTERFERENCES IN LIBS

LIBS Instrumentation

The LIBS instrument used in this research was a J200 LIBS system (Applied Spectra Inc., Fremont, CA). The J200 contains a Nd:YAG laser, 266nm with a 8 ns pulse width. NIST glass standards and a NIST nickel-cobalt-chromium alloy were collected with a laser output energy of 13 mJ, focused to a 100 µm diameter spot size. Five spectra of the NIST standards of twenty shots from five locations were averaged and analyzed for quantification of spectral interferences. Silicon wafer spectra were analyzed with a laser output energy of 21 mJ, focused to a 200 µm diameter spot size, and five spectra averaged of 10 shots from five locations. The J200 is equipped with a 6-channel spectrometer that encompasses the spectral window from 185 nm to 1040 nm. Each sample spectrum was collected with an acquisition delay of 1 µs for 1 ms acquisition duration assuming LTE.

NIST SRM 600 Glass Series

Samples of different elemental composition were evaluated to determine the statistical interference factor for each sample's detected peaks. The effect of spectral interferences by an element at various concentrations was evaluated for alumina pellets that were doped with varied nickel concentrations. More complex samples were analyzed from the NIST standards for a nickel-cobalt-chromium alloy, SRM 1243, and for the glass series: SRM 610, SRM 612, SRM 614, SRM 616. The variance in the posterior SIF of replicate SRM 616 was evaluated to show how reproducible the posterior SIF quantification of spectral interferences is.

NIST SRM 610 Glass

NIST SRM 610 glass sample contains sixty-one trace elements that have nominal mass fractions in the range of 100 mg/kg to 500 mg/kg[120]. The glass matrix for the SRM 600 series are composed of the same elements and nominal mass fractions. The mass fractions of the glass matrix are 72% SiO_2, 14% Na_2O, 12% CaO and 2 % Al_2O_3[116]. Of the sixty-one trace elements, there are twenty-four certified mass fraction values given in Table 22. The thirty-seven additional trace elements found within the NIST SRM 610 have no mass fraction value available.

Table 22: Mass fraction of elements in NIST SRM 610.

Element	**Ag**	**As**	**Au**	**B**	**Ba**	**Cd**	**Co**	**Cr**	**Cu**	**Fe**	**K**	**Li**
Mass Fraction (mg/kg)	268	340	25	351	453	244	390	415	444	458	461	488
Element	**Mn**	**Ni**	**Pb**	**Rb**	**Sb**	**Se**	**Sr**	**Th**	**Tl**	**Ti**	**U**	**Zn**
Mass Fraction (mg/kg)	457	458.7	426	425.7	415.3	115.2	515.5	457.2	61.8	437	461.5	433

Individual SIF

There were eight-hundred and forty-two detected peaks for the spectral range of 185 nm to 1050 nm for NIST SRM 610 glass sample. The matching factor for the experimental SRM 610 sample for the spectral range of interest is shown in Table 23. The total possible of neutral and singly-ionized elements for the Kurucz database for the 185 nm to 1050 nm is one-hundred forty-seven. There are four elements, Ag I, Be II, Ca II, and Na I with matching factors greater than 90%. For the SRM 610 sample, it is expected that the glass matrix elements of silicon,

aluminum, sodium, calcium, and oxygen have a high matching factor due to their large mass fraction values compared to the sixty-one trace elements with nominal mass fractions which is seen for calcium and sodium. Silicon and aluminum have matching factors less than 50% which results from expected theoretical Kurucz database peaks being absent from the experimental spectrum. There are fifteen elements with matching factors greater than 50%. It is expected that the emitters with higher mass fractions of elements present in the sample composition would have more theoretical peaks from the database that are found in the experimental spectrum resulting in a higher MF.

Strontium is one of the sixty-one trace elements with the highest mass fraction added to the glass matrix. The MF for Sr I is 42.87% and Sr II 62.36%. Neutral and singly-ionized strontium have numerous theoretical peaks and quite a few of those peaks occur in the experimental spectrum of SRM 610 yielding a high matching factor. One-hundred and thirty-two elements have matching factors less than 50% which means they have a small probability that the experimental spectrum peaks are produced from the element's database emission.

Table 23: NIST SRM 610 matching factor.

Element	MF (%)	Element	MF (%)	Element	MF (%)	Element	MF (%)	Element	MF (%)
Ag I	91.85	Cu I	54.66	Ir II	0	Os II	4.15	Sr II	62.36
Ag II	24.49	Cu II	11.84	K I	83.07	P I	1.00	Ta I	22.26
Al I	27.35	Dy I	24.76	K II	12.00	P II	7.98	Ta II	15.08
Al II	4.40	Dy II	20.75	La I	25.85	Pb I	36.47	Tb I	31.18
Ar I	29.47	Er I	36.75	La II	38.42	Pb II	0.13	Tb II	15.74
Ar II	19.89	Er II	17.73	Li I	6.03	Pd I	32.69	Te I	16.58
As I	6.66	Eu I	33.01	Li II	84.98	Pd II	0	Th I	23.81
Au I	37.03	Eu II	38.11	Lu I	40.07	Pr I	28.70	Th II	20.91
B I	18.86	F I	10.52	Lu II	22.81	Pr II	28.47	Ti I	34.14
B II	0	F II	13.13	Mg I	24.82	Pt I	15.72	Ti II	42.14
Ba I	51.21	Fe I	26.27	Mg II	59.62	Rb I	85.95	Tl I	0
Ba II	18.20	Fe II	14.09	Mn I	27.95	Re I	19.37	Tm I	35.50
Be I	4.81	Ga I	28.83	Mn II	9.56	Re II	3.65	Tm II	23.85
Be II	99.70	Ga II	0	Mo I	28.30	Rh I	26.70	U I	22.84
Bi I	16.82	Gd I	30.02	Mo II	6.69	Rh II	6.75	U II	18.34
C I	1.90	Gd II	27.54	N I	45.74	Ru I	16.94	V I	28.22
C II	11.27	Ge I	24.94	N II	26.02	Ru II	9.77	V II	25.83
Ca I	63.03	Ge II	0.34	Na I	95.18	S I	24.31	W I	15.37
Ca II	90.24	H I	2.03	Na II	38.06	S II	28.97	W II	22.06
Cd I	6.24	He I	5.03	Nb I	25.99	Sb I	32.66	Y I	42.24
Cd II	0	He II	13.04	Nb II	21.91	Sc I	44.44	Y II	44.06
Ce I	27.63	Hf I	17.30	Nd I	31.78	Sc II	65.91	Yb I	16.56
Ce II	19.79	Hf II	24.08	Nd II	23.45	Se I	0	Yb II	22.10
Cl I	6.60	Hg I	13.29	Ne I	13.68	Si I	3.84	Zn I	23.59
Cl II	28.19	Hg II	1.37	Ne II	20.05	Si II	38.56	Zn II	0
Co I	20.41	Ho I	49.97	Ni I	21.88	Sm I	25.25	Zr I	25.38
Co II	8.43	Ho II	44.22	Ni II	9.21	Sm II	24.64	Zr II	19.32
Cr I	28.47	In I	62.31	O I	47.68	Sn I	6.33		
Cr II	11.35	In II	21.16	O II	15.88	Sn II	23.33		
Cs I	61.30	Ir I	14.09	Os I	51.55	Sr I	42.87		

Calculation for the individual SIF for the eight-hundred and forty-two peaks were performed using the strength of each element's transition, the pseudo-Voigt integrated value, and the matching factor. The individual SIF for seven experimental peaks are shown in Table 24. It is expected that the top emitter for each peak be one of the elements present in the sample composition. Three of the peaks, 228.86 nm, 288.87 nm and 289.04 nm have an element with one of the highest individual SIF values that are not present within the sample composition. Peak 288.87 nm has Ce II and Nb II with very similar SIF values meaning that if no other information was available about the spectrum, it would be assigned to Ce II with large interferences. Prior knowledge of the sample composition does not have cerium or niobium in it which means Ti I and Fe II are the next best emitters to explain peak 288.87nm. Peak 227.75 nm has the highest SIF for Fe I and Fe II which would attribute the peak to iron for the individual SIF. Peak 228.86 nm has two emitters with very similar SIF values, Rh I and Sb I. Rhodium is not present in the sample composition, which means that Sb I would have the highest individual SIF for peak 228.86 nm with prior knowledge. Neutral and singly-ionized calcium have the highest individual SIF for peaks 393.40 nm and 527.00 nm. Peak 289.04 nm has Ta II as the second highest emitter and Dy II as the third highest contributor which are not possible as tantalum and dysprosium are not present in SRM 610.

The optimal set of emitters were identified for no prior knowledge of sample composition, qualitative prior knowledge and quantitative prior knowledge. This optimum set were used to determine the posterior SIF for each peak in the experimental spectrum.

Table 24: Seven peaks from NIST SRM 610 spectrum with each peak's top emitters and individual SIF values.

227.75 nm		228.86 nm		272.18 nm		288.87 nm		289.04 nm		393.40 nm		527.00 nm	
Elem	**SIF**	**Elem**	**SIF**	**Elem**	**SIF**	**Elem**	**SIF**	**Elem**	**SIF**	**Elem**	**SIF**	**Elem**	**SIF**
Fe I	0.5255	Rh I	0.1812	Th II	0.5079	Ce II	0.1880	Cu I	0.1311	Ca II	0.2269	Ca I	0.3077
Fe II	0.2819	Sb I	0.1808	Ag I	0.3829	Nb II	0.1803	Ta II	0.1305	Th I	0.1686	Ti I	0.1667
Co II	0.1688	Fe I	0.1467	Os I	0.0465	Ti I	0.1172	Dy II	0.1299	Gd I	0.0527	Cr I	0.1390
Hf II	0.0098	Ni I	0.1403	Nb II	0.0155	Fe II	0.1163	Fe I	0.0988	Gd II	0.0493	Ce I	0.1370
Ni II	0.0091	Mn I	0.1008	Ta I	0.0119	Rh I	0.0989	Cr I	0.0981	U I	0.0461	Fe I	0.1293
W I	0.0031	Fe II	0.0823	Ru I	0.0077	Cr II	0.0908	Mn I	0.0972	Rh I	0.0412	Fe II	0.0694
Ti I	0.0010	Sc II	0.0703	Er I	0.0064	Mn II	0.0787	Fe II	0.0530	Sm II	0.0409	Ni II	0.0453
Ti II	0.0002	Co I	0.0619	Co I	0.0063	Ti II	0.0763	Ni II	0.0416	Nd II	0.0385	Nd I	0.0045
Mn I	0.0002	Mn II	0.0346	Ni II	0.0028	Cr I	0.0167	Cr II	0.0391	Ce II	0.0310	Be II	0.0004
Mn II	0.0001	Co II	0.0008	Fe II	0.0028	Mo I	0.0162	Co II	0.0381	Mo I	0.0305	Nb I	0.0004
V I	0.0001	V I	0.0002	Ca I	0.0027	V II	0.0152	Mn II	0.0344	Nb I	0.0270	V I	0.0002
V II	0.0001	Cr II	0.0001	Mn II	0.0017	V I	0.0027	Ce II	0.0312	Cr I	0.0241	Nd II	0.0001
Cr II	6.15E-05	P II	3.12E-05	Cr I	0.0013	Fe I	0.0027	V II	0.0287	V I	0.0239	Co I	9.37E-07
S II	1.07E-07	Ar II	1.98E-05	Sc II	0.0010	Mn I	0.0001	Tm II	0.0278	Sc II	0.0233	Sc I	1.31E-07
Ne II	2.44E-11	V II	5.76E-07	Nb I	0.0009	Co I	7.14E-05	Os I	0.0203	Fe I	0.0229	Si II	1.25E-07

Optimal Set of Emitters

All elements in the Kurucz database for the spectral range of interest from 185 nm to 1050 nm are ordered by their sum of their individual SIF for the experimental SRM 610 peaks. The BIC value is obtained for each set of ordered emitters for the no prior, qualitative prior, and quantitative prior knowledge and shown in Figure 17. The no prior knowledge analysis needs 59 emitters to explain the experimental SRM S610 sample. The large list of emitters is quite large for the no prior knowledge analysis, since many emitters have transitions that contribute to the individual SIF for each peak. The lowest BIC value is 2224.13 which results in the optimum set, {Ag I, Al I, Ba I, C I, Ca I, Ca II, Ce I, Co I, Cr I, Cs I, Cu I, Er I, Eu I, Eu II, Fe I, Fe II, Ga I, Gd I, Gd II, Ge I, Hf I, Ho I, In I, K I, La I, Mg I, Mn I, Mo I, Na I, Nd I, Ni I, Os I, Pb I, Pd I, Rb I, Re I, Rh I, Ru I, S I, Sb I, Sc I, Sc II, Sm I, Sm II, Sn I, Sn II, Sr I, Ta I, Ta II, Th I, Th II, Ti I, U I, U II, V I, Y I, Y II, Yb I, Zr I}. The qualitative prior knowledge analysis has the smallest BIC for 29 emitters. The optimal set of emitters to explain the qualitative prior knowledge analyses is {Ag I, Al I, Ba I, Ba II, Ca I, Ca II, Co I, Cr I, Cu I, Fe I, Fe II, K I, Mn I, Na I, Ni I, O I, Pb I, Rb I, Sb I, Si I, Sr I, Th I, Th II, Ti I, Ti II, U I, U II, Zn I}. The optimal set of emitters to explain the spectrum with quantitative knowledge is twenty-nine with the BIC value of -9479.87. There are twenty-three emitters common to all three knowledge analyses {Ag I, Al I, Ba I, Ca I, Ca II, Co I, Cr I, Cu I, Fe I, Fe II, K I, Mn I, Na I, Ni I, Pb I, Rb I, Sb I, Sr I, Th I, Th II, Ti I, U I, U II}. The glass matrix components, Al I, Ca I, Ca II, and Na I are part of this list. Neutral or singly-ionized silicon are missing from the emitters common to all prior knowledge analyses because Si I was ordered eighty-first in the no prior knowledge analysis. The qualitative and quantitative prior knowledge analyses have twenty-six emitters in common,

{Ag I, Al I, Ba I, Ca I, Ca II, Co I, Cr I, Cu I, Fe I, Fe II, K I, Mn I, Na I, Ni I, O I, Pb I, Rb I, Sb I, Si I, Sr I, Th I, Th II, Ti I, Ti II, U I, U II}. Neutral zinc is found in the qualitative prior knowledge but not in the quantitative and singly-ionized oxygen is found in reverse. The mass fraction of zinc much lower than the mass fraction of oxygen which is why O II is added to the quantitative prior knowledge. The quantity of emitters that are common to the qualitative and quantitative prior knowledge compared to all prior knowledge is expected as the emitters are restricted to what is present in the SRM 610 sample composition. The BIC of the set of emitters containing Si I with the no prior knowledge analysis is 2274.70 which is higher than the optimum 2274.13 and based on the lowest positive BIC value, it is considered an additional atom that could provide little more information about the experimental spectrum.

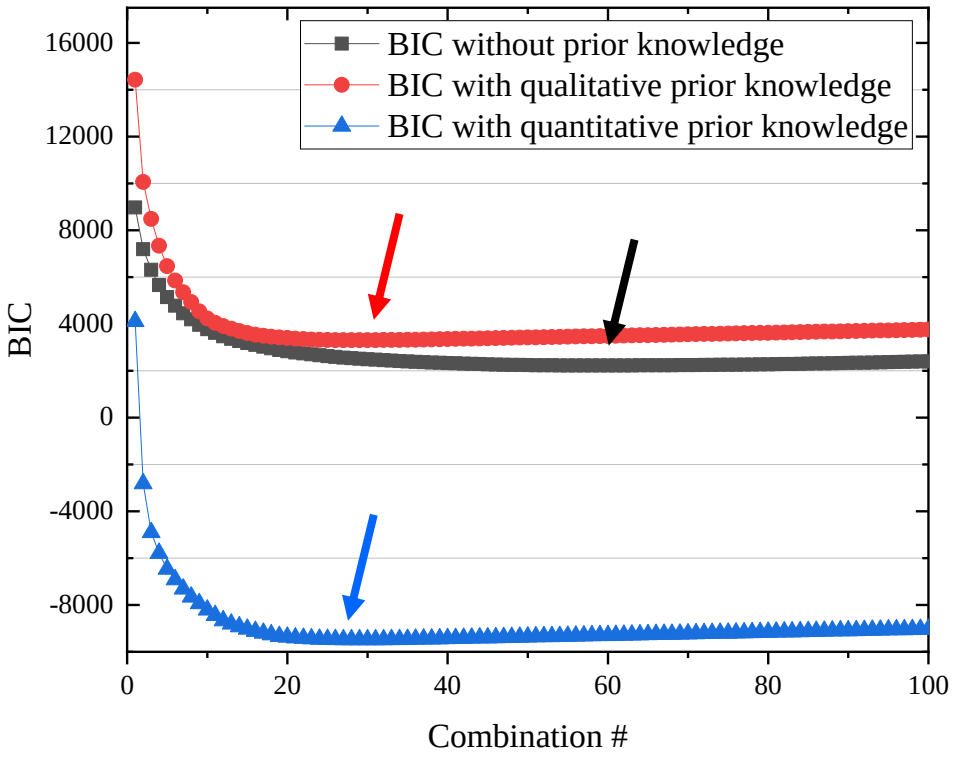

Figure 17: BIC graph for NIST SRM 610.

Posterior SIF

With the optimal set of emitters to explain the experimental spectrum for each prior knowledge analyses, the posterior SIF was calculated for each peak. Figures 18-20 show twenty experimental peaks for the no prior knowledge , qualitative prior knowledge , and quantitative prior knowledge that are representative of the eight-hundred and forty-two peaks. Six of the peaks showed a single emitter for all knowledge analyses. Peaks 267.9 nm, 268.70 nm, and 270.08 nm have Th II as the only contributor. Singly-ionized calcium is the sole emitter for peak 393.4 nm. Peaks 231.90 nm and 396.14 nm have Al I as the sole emitter for the no prior,

qualitative prior, and quantitative knowledge analyses. Peaks of calcium, silicon, and thorium are expected in the experimental SRM 610 glass spectrum because calcium and aluminum make up the glass matrix and thorium is one of the trace elements added to the matrix. The other fourteen peaks in Figures 18-20 show spectral interferences and line assignment based on the input of prior knowledge. Peaks 261.42 nm, 281.55 nm, and 324.79 nm have a sole contribution from neutral osmium. Input of the prior knowledge, changes the line assignment of the qualitative and quantitative analyses because osmium was not one of the trace elements added to the SRM 610 sample composition. Peaks 261.42 nm, 281.55 nm, and 324.79 nm have a sole emitter of Pb I, U II, and Cu I respectively. The elemental profile of peaks 261.42 nm, 281.55 nm, and 324.79 nm occur from strong emission lines of Pb I, U II, and Cu I respectively along with prior knowledge occur in individual SIF values greater than 98% for each of the peaks. Peak 777.41 nm has a sole contribution from neutral rhodium for the no prior knowledge analysis. Neutral rhodium and oxygen are the only possible emitters for peak 777.41 nm. Once prior knowledge was added, the emission profile for peak 777.41 nm changed as rhodium is not present in SRM 610 composition to O I. Peaks 535.70 nm, 680.14 nm, 887.42 nm, and 922.86 nm have no spectral interferences for the no prior, multiple interferences for the qualitative prior, and large interferences in the quantitative prior knowledge analyses. Peaks 887.42 nm and 922.86 nm are assigned S I as the sole contributor for the no prior knowledge analysis.

Peaks 535.70 nm and 680.14 nm for the no prior knowledge are assigned Ga I and Eu I respectively as the only emitter. Gallium, europium, and sulfur were not present in the SRM 610 glass sample. The qualitative prior knowledge of the peaks 535.70 nm, 680.14 nm, 887.42 nm,

and 922.86 nm have multiple spectral interferences of ten emitters with equiprobability. This equiprobability results from the ten emitters having the same individual SIF value of $1.0*10^{-12}$ for peaks 535.70 nm, 680.14 nm, and 877.42 nm and $3.4*10^{-2}$ for peak 922.86 nm. Quantitative prior knowledge of these peaks results in a large interference between O I and O II. Oxygen is found in higher mass fractions than the ten emitters of the qualitative prior for the peaks thus the individual SIF for oxygen increases while the individual SIF for the ten emitters decreases. The assignment of peaks 535.70 nm, 680.14 nm, 887.42 nm, and 922.86 nm can be contributed to oxygen as both O I and O II have the same probability of being the peak emitter. With the difference in spectral interferences and line assignment of peaks 535.70 nm, 680.14 nm, 887.42 nm, and 922.86 nm, these peaks were judged to be non-reliable for spectral line assignment. The peaks at 228.86 nm and 289.04 nm have spectral interferences in the no prior knowledge. The input of prior knowledge at peaks 228.86 nm and 289.04 nm result in the line assignment of a single emitter with no spectral interferences in the qualitative and quantitative knowledge analyses. Peak 228.86 nm has a main contributor of Rh I with a large spectral interference from Sb I. Rhodium is not present in the sample composition which results in a line assignment of Sb I for the qualitative and quantitative prior knowledge analyses. Peak 289.04 nm has a main emitter of Cu I with a large interference from Mg I. Like rhodium, magnesium is not present in the sample composition which results in qualitative and quantitative prior knowledge analyses that have Cu I as the sole contributor of peak 289.04 nm. Peak 289.04 nm has other emitters with individual SIFs present such as Cr I and Fe I but with finding the best combination of emitters to explain the entire experiment spectrum it is explained by Cu I.

Peaks 288.87 nm and 311.07 nm have spectral interferences in the no prior and quantitative prior knowledge analyses. There are two emitters, Fe I and Ti I with high individual SIF values for peak 288.87 nm. Based on no prior knowledge, peak 288.87 nm has main contribution from Ti I with a large interference of Fe I based on the top 100,000 combinations. Qualitative prior knowledge results in the assignment of peak 288.87 nm solely to Ti I. The mass fraction of iron and titanium in the SRM 610 sample are very close with 458 mg/kg and 437 mg/kg respectively. The matching factor for the neutral and singly-ionized titanium are higher than the iron which means that there are more theoretical titanium peaks found in the experimental spectrum. The individual SIF for Fe I and Fe II is increased in the quantitative prior knowledge because iron is found in a slightly higher mass fraction whereas Ti I and Ti II individual SIFs are reduced because they have a smaller mass fraction than iron. Based on the mass fraction, matching factor, and the optimal set of emitters, the quantitative prior knowledge analyses combination of emitters for the entire spectrum results in the main assignment of Fe I to peak 288.87 nm with a very small interference from Ti I. Peak 288.87 nm is judged to be unreliable for peak assignment because spectral interferences are present and line assignment changes depending on the prior knowledge. Peak 311.07 nm has a main contribution of Mn I with a small interference of Th II in the no prior and quantitative prior knowledge analyses. The top 100,000 combinations of emitters to explain the experimental spectrum result in 94,464 combinations with Mn I and 5,536 with Th II. Qualitative prior knowledge of peak 311.07 nm has a sole contribution of Mn I because all 100,000 combinations of emitters for the entire spectrum need only Mn I to explain peak 311.07 nm. Peak 272.18 nm shows that singly-ionized thorium is the only contributor when no prior and qualitative prior knowledge is known. The addition of the

concentration of the elements present in the sample composition results in spectral interference of peak 272.18 nm. Peak 272.18 nm has six possible emitters including Ag I, Ca I and Th II. Singly-ionized thorium has the highest individual SIF with Ag I second and Ca I third. Based on the individual SIF and the top 100,000 combinations, Th II is the only emitter for the no prior and qualitative knowledge analyses. The mass fraction of calcium with 12% is greater than Th II and Ag I. Input of the quantitative prior results in a main contribution from Ca I with a large interference from Th II because Ca I is found in higher concentrations than Th II and the combinations with the top likelihoods need Ca I more often than Th II. Quantitative knowledge of the sample composition results in a different line assignment for no prior and qualitative prior knowledge of peak 396.85 nm. Unlike peak 272.18 nm, the top 100,000 combinations of emitters for the spectrum for peak 396.85nm only need Ca I with quantitative knowledge of its higher mass fraction content in the sample composition. The posterior SIF depends on the individual SIF and optimal set of emitters which find the top combinations of emitters for each peak in the experimental spectrum.

From the optimal set of emitters, there were thirty-six emitters needed to explain the spectrum which were not present in the SRM 610 sample composition. The no prior knowledge analysis for the entire spectrum had three-hundred forty-three peaks with an SIF of 100% where the emitters were not found in the SRM 610 sample composition. There was a total of fifty interfered peaks for the no prior knowledge analysis. The qualitative prior knowledge analysis had four interfered peaks while the quantitative had fifty-six interfered peaks. The highest SIF being attributed to the same atom for the no prior and qualitative prior occurred 55.94%. The no

prior and quantitative prior knowledge had 40.02% peaks with the same atom having the highest SIF. Knowledge of the sample composition resulted in 66.27% of the peaks between the qualitative and quantitative prior having the highest SIF for the same emitter. There were 40.02% peaks that were common to all three prior knowledge analyses that had the same main emitter. The common analysis between all three prior knowledge analyses is a resultant of the number of emitters common to all analyses.

Figure 18: Posterior SIF of NIST SRM 610 -- No Prior.

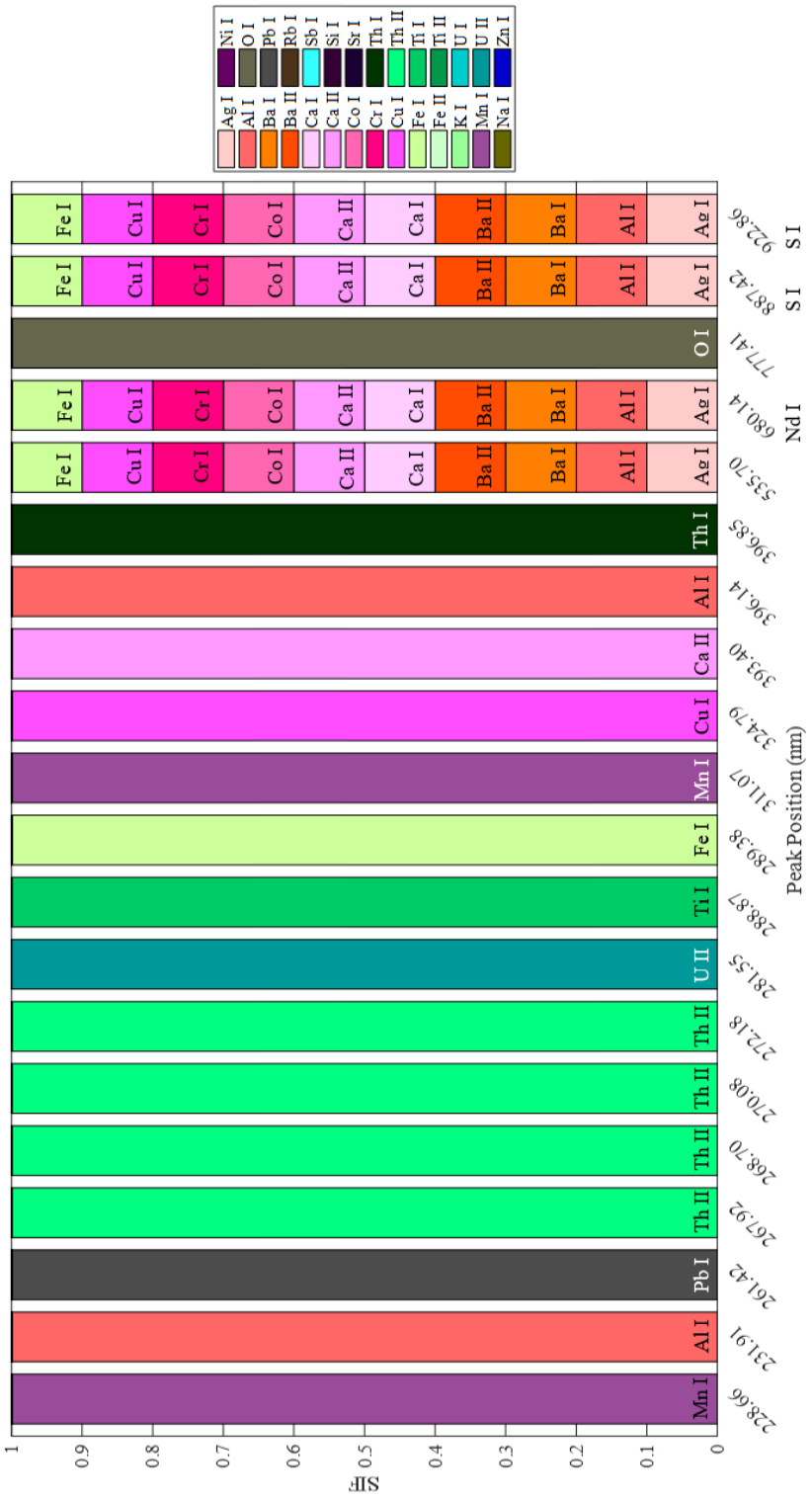

Figure 19: Posterior SIF of NIST SRM 610 – Qualitative Prior.

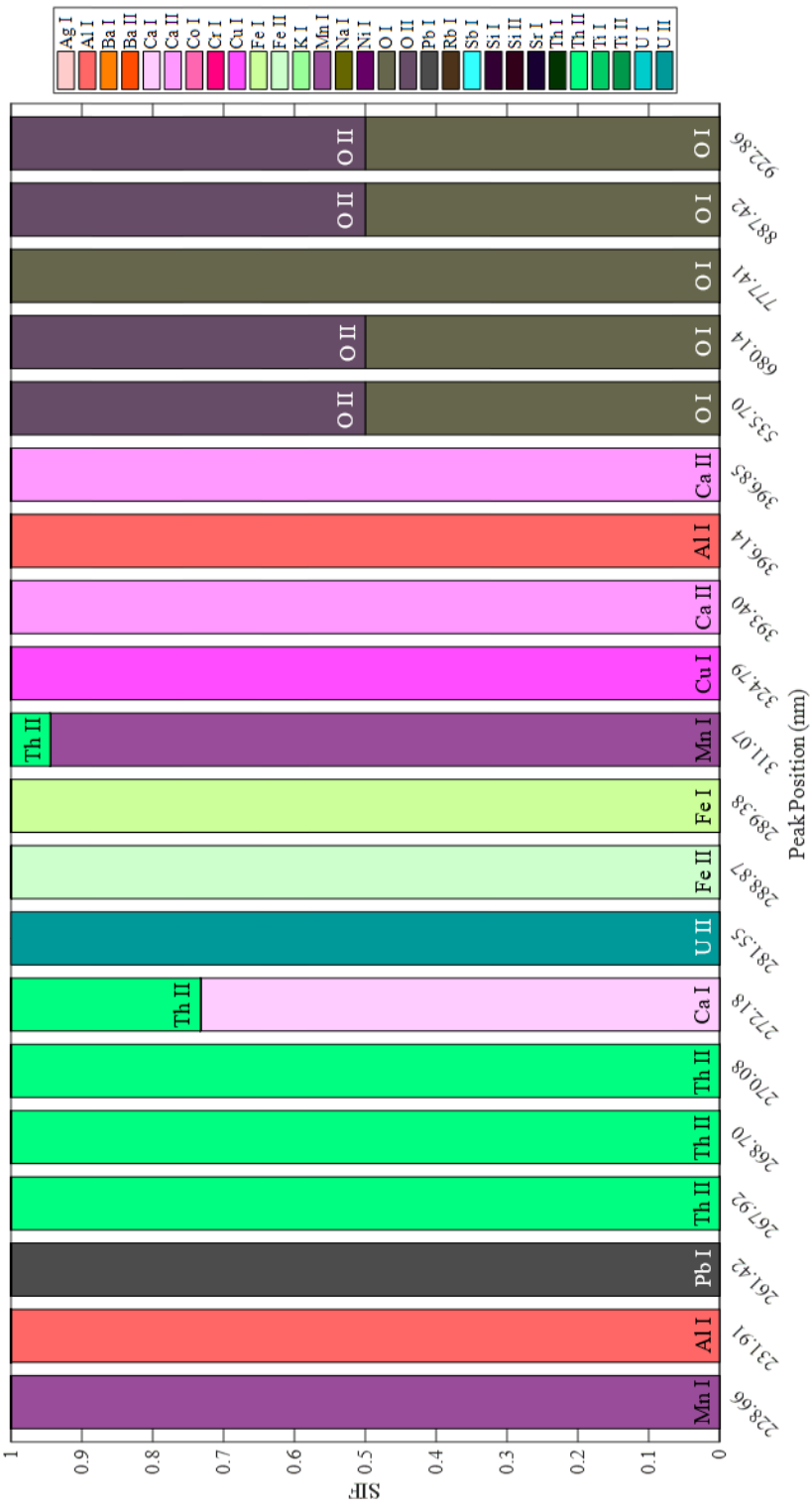

Figure 20: Posterior SIF of NIST SRM 610 - Quantitative Prior.

NIST SRM 612 Glass

The NIST SRM 612 sample is a glass matrix with sixty-one elements in the range of 10 mg/kg to 80 mg/kg[117]. Table 25 shows the thirty-two trace elements and their certified mass fraction values. There are twenty-nine trace elements added to the NIST SRM 612 sample that have no certified mass fractions.

Table 25: Mass fraction of NIST SRM 612.

Element	**Ag**	**As**	**Au**	**B**	**Ba**	**Cd**	**Ce**	**Co**	**Cr**	**Cu**	**Dy**
Mass Fraction (mg/kg)	22	37.4	5	32	38.6	29.9	39	35.5	35	37.7	35
Element	**Er**	**Eu**	**Fe**	**Gd**	**K**	**La**	**Li**	**Mn**	**Nd**	**Ni**	**Pb**
Mass Fraction (mg/kg)	39	36	51	39	64	36	40	37.7	36	38.8	38.57
Element	**Rb**	**Sa**	**Sb**	**Se**	**Sr**	**Th**	**Ti**	**Tl**	**U**	**Yb**	
Mass Fraction (mg/kg)	31.4	39	34.9	16.1	78.4	37.79	50.1	15.7	37.38	42	

Individual SIF

The experimental spectrum of SRM 612 had five-hundred and thirty-one detected peaks within the spectral region of interest of 185 nm to 1050 nm. The matching factor for each neutral and singly-ionized element present in the Kurucz database for the spectral region of interest is shown in Table 26. The highest matching factor of 89.73 % belongs to Ca II and Ca I has a MF of 70.98%. These high matching factors are expected as calcium is a part of the sample matrix. Neutral would be expected to have a high matching factor which did not occur because there

were numerous theoretical lines that were not found within the experimental spectrum resulting in a low MF of 23.42% for Si I. Singly-ionized silicon had a MF of 56.07% which is on the higher scale meaning that there was a higher probability of Si II lines than Si I in the experimental spectrum. Neutral rubidium had a high matching factor of 87.39% which is expected because rubidium is one of the trace elements added to the glass matrix for SRM 612.

The individual SIF for each experimental peak was determined using the matching factor, an emitter's transition, and the integral value from the pseudo-Voigt fit. Table 27 shows seven experimental peaks and their corresponding individual SIF emitters and values. Six of the seven peaks have a top emitter that is present in the sample composition. Peak 245.17 nm has the top emitters, W I, Os I, W II and Nb. Tungsten, osmium, and niobium are not present in SRM 612 which means that these emitters will be removed when prior knowledge of the sample composition is added. With prior knowledge, peak 245.17 nm will have Fe I as the top emitter. Peak 253.21 nm has a top emitter of Mg II which is not in the sample composition while the second highest emitter Si I is present in the glass matrix.

Table 26: NIST SRM 612 matching factor.

Element	MF (%)	Element	MF (%)	Element	MF (%)	Element	MF (%)	Element	MF (%)
Ag I	50.81	Cu I	40.43	Ir II	0	Os II	12.89	Sr II	63.31
Ag II	23.55	Cu II	3.65	K I	80.58	P I	0.32	Ta I	8.84
Al I	31.08	Dy I	22.55	K II	8.99	P II	3.62	Ta II	15.11
Al II	3.87	Dy II	12.85	La I	18.95	Pb I	32.79	Tb I	31.18
Ar I	8.33	Er I	23.40	La II	24.23	Pb II	0.05	Tb II	8.56
Ar II	16.38	Er II	14.65	Li I	35.83	Pd I	22.35	Te I	0
As I	6.86	Eu I	26.32	Li II	22.05	Pd II	0	Th I	23.58
Au I	41.19	Eu II	23.97	Lu I	17.02	Pr I	12.75	Th II	12.08
B I	18.90	F I	22.29	Lu II	13.62	Pr II	19.98	Ti I	22.66
B II	1.25	F II	4.65	Mg I	53.51	Pt I	11.17	Ti II	24.85
Ba I	25.89	Fe I	14.58	Mg II	10.09	Rb I	87.39	Tl I	8.00
Ba II	18.01	Fe II	8.41	Mn I	26.12	Re I	12.88	Tm I	18.80
Be I	4.01	Ga I	42.23	Mn II	13.55	Re II	12.37	Tm II	12.63
Be II	66.35	Ga II	0	Mo I	16.49	Rh I	14.73	U I	11.02
Bi I	1.25	Gd I	13.97	Mo II	6.55	Rh II	2.21	U II	10.82
C I	1.84	Gd II	15.34	N I	25.66	Ru I	12.25	V I	17.16
C II	17.65	Ge I	22.88	N II	15.58	Ru II	14.07	V II	9.81
Ca I	70.98	Ge II	23.93	Na I	36.51	S I	1.83	W I	9.27
Ca II	89.73	H I	0.58	Na II	27.39	S II	9.53	W II	9.44
Cd I	4.83	He I	3.21	Nb I	22.38	Sb I	1.45	Y I	30.66
Cd II	38.91	He II	1.99	Nb II	12.73	Sc I	32.79	Y II	27.70
Ce I	25.93	Hf I	11.93	Nd I	16.10	Sc II	50.64	Yb I	20.93
Ce II	16.01	Hf II	12.34	Nd II	16.85	Se I	0	Yb II	15.46
Cl I	4.35	Hg I	6.31	Ne I	13.65	Si I	23.42	Zn I	17.76
Cl II	6.90	Hg II	0.18	Ne II	29.51	Si II	56.07	Zn II	0
Co I	16.05	Ho I	10.56	Ni I	15.95	Sm I	24.72	Zr I	20.61
Co II	9.57	Ho II	2.76	Ni II	7.91	Sm II	16.13	Zr II	18.16
Cr I	21.02	In I	52.25	O I	42.55	Sn I	7.36		
Cr II	8.28	In II	21.16	O II	24.96	Sn II	0		
Cs I	22.87	Ir I	11.85	Os I	50.53	Sr I	34.74		

Table 27: Seven peaks from NIST SRM 612 spectrum with each peak's top emitters and individual SIF values.

245.17 nm		253.21 nm		272.80 nm		300.68 nm		489.10 nm		818.32 nm		824.80 nm	
Elem	**SIF**	**Elem**	**SIF**	**Elem**	**SIF**	**Elem**	**SIF**	**Elem**	**SIF**	**Elem**	**SIF**	**Elem**	**SIF**
W I	0.6285	Mg I	0.2043	Si I	0.8390	Ca I	0.4209	Ni II	0.136	Na I	0.9999	Ca I	0.5864
Os I	0.1682	Si I	0.1840	Th II	0.0788	Th II	0.1418	Nd I	0.136	N I	2.99E-05	Ni II	0.1086
W II	0.0836	Th II	0.1585	Gd II	0.0117	V I	0.0723	Fe I	0.111	Er I	2.29E-05	Fe I	0.0880
Nb II	0.0556	Ta II	0.0922	Ce iI	0.0102	Ti I	0.0668	Sc I	0.105	Ni II	1.10E-05	La I	0.0872
Fe I	0.0331	Ni II	0.0616	Zr II	0.0089	Ni II	0.0636	V I	0.104	Ca I	8.97E-06	V I	0.0645
Co I	0.0185	V I	0.0596	Ni II	0.0088	Cr I	0.0579	Ti I	0.097	Cu II	6.61E-06	Fe II	0.0388
Fe II	0.0067	Cr I	0.0484	Cr I	0.0064	Fe I	0.0517	Cr I	0.085	Nd II	6.22E-06	Cr II	0.0257
V I	0.0021	Co I	0.0329	Co I	0.0058	Mn I	0.0344	W I	0.084	Sc II	2.03E-06	Ti I	0.0006
Cr II	0.0015	Mn I	0.0322	Ru II	0.0048	V II	0.0280	Mn I	0.052	Cr I	9.98E-07	H I	0.0001
Mn II	0.0014	Co II	0.0247	Mn I	0.0045	Fe II	0.0228	Fe II	0.049	Fe II	9.47E-07	Mn II	6.52E-07
Ti II	0.0004	V II	0.0234	Rh I	0.0042	Cr II	0.0195	Cr II	0.029	Cr II	6.24E-07	He I	2.26E-08
Sc I	0.0003	Fe II	0.0220	Fe II	0.0030	Mn II	0.0100	Nb I	0.006	Ni II	2.20E-07	He II	2.47E-17
Co II	2.50E-05	Cr II	0.0164	Cr II	0.0025	Re I	0.0063	Nd II	0.004	C I	1.97E-07		
P I	3.17E-07	Al II	0.0116	Cd I	0.0020	Ru I	0.0034	Mo I	0.002	Mn I	2.34E-08		
Ni II	1.08E-07	Mn II	0.0097	V I	0.0018	Tm II	0.0005	Ca I	2.28E-05	Cl II	1.28E-08		

Optimal Set of Emitters

Figure 21 shows the BIC value for the optimal set of emitters obtained for the no prior, qualitative prior, and quantitative prior knowledge. The prior knowledge analysis needs an optimum number of forty-five emitters to explain the experimental SRM S612 for the spectral range of 185 nm to 1050 nm. The number of emitters with transitions that have individual SIFs for each individual peak is numerous providing a large list of emitters for the no prior knowledge. The optimum set of emitters is {Ag I, Al I, Ba I, Ba II, Ca I, Ca II, Ce I, Ce II, Cr I, Cu I, Dy I, Er I, Eu I, F I, Fe I, Ga I, Gd I, Ir I, K I, La I, Mg I, Mg II, Mo I, Na I, Nd I, Ni I, Ni II, O I, Pr I, Pr II, Re I, S I, Sb I, Sc I, Sc II, Si I, Sr I, Th I, Th II, U I, U II, V I, W I, Y I, Zr I}. The optimal set of emitters for the qualitative analysis is similar to the no prior with forty-four emitters needed to explain the spectrum with {Ag I, Al I, As I, Ba I, Ba II, Ca I, Ca II, Ce I, Ce II, Co I, Cr I, Cu I, Cu II, Dy I, Dy II, Er I, Eu I, Eu II, Fe I, Fe II, Gd I, K I, La I, Mn I, Na I, Nd I, Ni I, Ni II, O I, Sb I, Si I, Sm I, Sm II, Sr I, Th I, Th II, Ti I, Ti II, U I, U II}. The qualitative prior knowledge set removes the elements in the no prior knowledge, {F I, Ga I, Ir I, Mg I, Mg II, Mo I, Pr I, Pr II, Re I, S I, Sc I, Sc II, V I, W I, Y I, Zr I}, that are not present in the sample composition. The quantitative prior knowledge analysis needs thirty-nine emitters to explain the experimental spectrum. The optimum set of emitters is {Al I, Al II, Ba I, Ba II, Ca I, Ca II, Ce I, Ce II, Co I, Cu I, Cu II, Dy I, Er I, Er II, Eu I, Eu II, Fe I, Fe II, Gd I, K I, Mn I, Na I, Nd I, Ni I, Ni II, O I, Si I, Si II, Sm I, Sm II, Sr I, Sr II, Th I, Th II, Ti I, Ti II, U I, U II}. Twenty-five emitters are common to all three analyses {Al I, Ba I, Ba II, Ca I, Ca II, Ce I, Ce II, Cr I, Cu I, Dy I, Er I, Eu I, Fe I, Gd I, K I, Na I, Nd I, Ni I, Ni II, O I, Si I, Th I, Th II, U I, U II}. The common emitters include the glass matrix components plus elements that are present in the SRM

612 such as K I and Fe I. After the glass matrix elements, iron and potassium have second and third highest mass fractions. The qualitative and quantitative prior knowledge optimum set of emitters have thirty-three emitters in common with differences of {Ag I, As I, Dy II, Er II, La I, Sb I, Si II, Sr II}. These differences arise from the mass fraction of an emitter plus the individual SIF that is used to order the elements. Singly-ionized strontium is found in the quantitative and not in the qualitative because of the ordering of the optimal emitters.

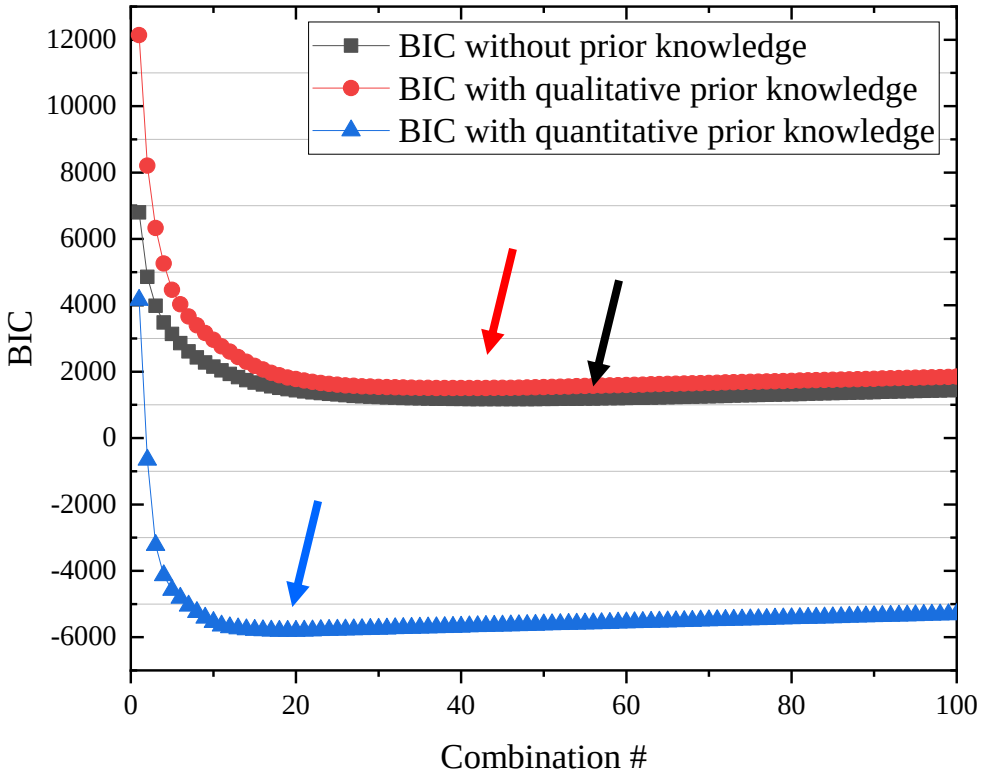

Figure 21: BIC graph for NIST SRM 612.

Posterior SIF

Figures 22-24 show the posterior SIF for a subset of twenty peaks calculated from the optimal set of emitters for the different prior knowledge analyses. Five of the spectral peaks have no spectral interferences between the no prior, qualitative, and quantitative prior knowledge. Peak 288.18 nm, 308.21 nm, and 818.32 nm have a sole emitter of Si I, Al I, and Na I respectively. Peaks 854.21 nm and 866.22 nm are produced from the emission of singly-ionized calcium. Aluminum, calcium, sodium, and silicon are expected to be common to all prior knowledge analyses because they make up the glass matrix and have the highest mass fractions of the elements within the SRM 612 composition. Peaks 360.20 nm, 373.06 nm, and 489.10 nm have spectral interferences within all three knowledge analyses. Peak 360.20 nm has a main emitter of Cu I with a small interference from U I for the no prior knowledge analysis and qualitative prior knowledge analyses. Input of the quantitative prior knowledge of the sample composition results in a main contributor of Cu I with a large interference of U I. This large interference in the quantitative assignment of peak 360.20 nm arises from the optimal set of emitters needed to explain the spectrum. The quantitative needs nineteen emitters while the qualitative prior needs forty. The optimal set of emitters give the combination of emitters to explain the spectrum. Removal of emitters results in quantitative prior knowledge top 100,000 combinations that mainly need Cu I for peak 360.20 nm while some of the combinations need U I.

Large interferences are seen for peak 489.10 nm for the no prior and qualitative prior knowledge. Singly-ionized nickel is the contributor with a higher SIF with large interference from Nd I. The individual SIF for peak 489.10 nm has seven possible emitters. The emitters with the top

individual SIF values are Ni II, Nd I, and Fe I. Iron is found in higher concentration than nickel and neodymium. Addition of the quantitative prior knowledge increases the probability of iron while decreasing nickel and neodymium creating interferences in the posterior SIF assignment. Peak 489.10 nm is judged to be interfered for all knowledge analyses and should not be used for spectral line assignment. Peak 373.06 nm has a main contribution from Th I with interference from Th II for all three prior knowledge analyses. Assignment of peak 373.06 nm can be attributed to thorium because the interference is between the singly-ionized and neutral thorium emitters. Peaks 245.11 nm, 253.21 nm, 265.26 nm, 280.26 nm, 330.28 nm, 742.38 nm, and 760.59 nm show how prior knowledge of the sample composition leads to line assignment of a peak with no interferences. Peak 253.21 nm has a main contributor of Mo I for no prior knowledge with a small interference from Si I. Molybdenum is not present in the sample composition, which results in a qualitative and quantitative assignment of Si I with no spectral interferences for peak 253.21 nm. Neutral antimony is the main emitter for peak 265.26 nm with a small interference from Al I with the no prior analysis and qualitative prior knowledge analysis. Antimony has a mass fraction of 34.9 mg/kg which is smaller than aluminum which has 2% that results in peak 253.21 nm having a sole emitter of Al I with no interference from Sb I. Peak 742.38 nm has a main emitter of Ca I with a small interference from K I while peak 760.59 nm has a main contribution from Si I with a small interference from Ca I for the no prior and qualitative prior knowledge analyses. Quantitative prior knowledge of the sample composition results in the small interferences being removed and peak 742.38 nm and 760.59 nm being attributed to Si I and Ca I respectively. Neutral yttrium is the only emitter for peak 245.11 nm for the no prior analysis. Yttrium is not present in SRM 612 which leads to a different

emission profile for the peak for the prior knowledge analyses. Peak 245.11 nm has only three possible emitters, Fe I, Mg I, and Mg II. Qualitative and quantitative line assignment of peak 245.11 nm result in 100% SIF of Fe I. Peak 330.29 nm has a main contribution from Na I for no prior knowledge analysis with a small interference form Mo I. No prior knowledge analysis of peak 484.66 nm has a sole emitter of Mo I. Input of the prior knowledge, results in the removal of Mo I from assignment leading to peak 330.29 nm and 484.66 nm having a sole emitter of Na I and Ca I respectively. Peak 280.26 nm has only one emitter for the no prior knowledge analysis, Mg II, which is not present in the sample composition. The qualitative and quantitative prior knowledge analyses of peak 280.26 nm results in the assignment of U II as the only emitter because it has the second highest individual SIF after Mg II. Peak 420.83 nm has a main emitter of Gd I with a small interference from Cu I for the no prior and qualitative prior knowledge. Quantitative prior input results in Ca I being the sole contributor to peak 420.83 nm. There are eight emitters with individual SIFs present in peak 420.83 nm. The concentration of calcium compared to seven other emitters including Cu I and Gd I is greater which results in the top 100,000 combinations having the sole emitter of Ca I for peak 420.83 nm. Peak 420.83 nm is considered non-reliable as there are disagreements between the no prior and quantitative prior knowledge analyses.

Peaks 369.13 nm, 483.58 nm, and 510.24 nm show how prior knowledge results in interferences of line assignment. Neutral nickel has the highest individual SIF value for peak 369.13 nm. With the optimal set of emitters, the no prior knowledge and qualitative prior knowledge analyses assign Ni I to peak 369.13 nm. Quantitative prior knowledge analysis for peak 369.13

nm has a main contributor of Ni I with a large interference from Fe I. Neutral iron has the second highest individual SIF for peak 369.13 nm and is found in higher concentrations than nickel which leads to a posterior SIF with spectral interferences. Peaks 483.58 nm and 510.24 nm have a sole emitter of Mo I and Nd I respectively for the no prior knowledge analysis. Molybdenum is not present in the sample composition which leads to the main emitter of peak 483.58 nm being Fe I for both qualitative and quantitative prior knowledge. The qualitative prior knowledge has a large interference from Ni II for peak 483.58 nm while the quantitative prior knowledge has a small interference. The reduction in interference is due to iron the higher concentration of iron along with the top combinations of emitters with Fe I for peak 483.58 nm have a higher likelihood than Ni II. No prior knowledge analysis of peak 510.24 nm results in the sole emitter Nd I. Neutral neodymium has the highest individual SIF for peak 510.24 nm and Ti II the second highest. Titanium is present in higher concentrations of neodymium which results in the qualitative prior knowledge analysis having a main contribution from Nd I and a large interference from Ti II. Input of the prior knowledge along with the smaller optimal set of emitters for the quantitative analysis results in the main assignment of peak 510.24 nm with a small interference from Nd I.

The no prior knowledge optimal set of emitters has sixteen emitters not present within SRM 612 sample composition. There were seventy-five peaks that had 100% SIF line assignment with the sixteen emitters not in the sample. Four-hundred and seven peaks had a sole emitter and forty-nine peaks were interfered for the no prior knowledge analysis. The qualitative prior knowledge analysis had thirty-four interfered peaks while the quantitative prior had fifty. There were more

spectral interferences with the quantitative than qualitative with most of these being small interferences less than a SIF of 0.10%. The highest SIF for a main emitter for the no prior knowledge and qualitative prior occur 94.54. This high occurrence results from having twenty-nine emitters in common to both analyses. The no prior and quantitative prior knowledge had 35.22% occurrence of the same emitter producing the highest posterior SIF for the same peaks. The qualitative and quantitative prior knowledge had 40.30% of the same peaks with the same highest SIF emitter. All three prior knowledge analyses had 36.91% peaks that had the same emitter with the highest posterior SIF. The smaller number of peaks that had the same main emitter for the peaks between the no prior and quantitative and the qualitative and quantitative prior knowledge analyses result from the large number of emitters that contribute to the experimental peaks creating differences in the top 100,000 combinations of the spectrum.

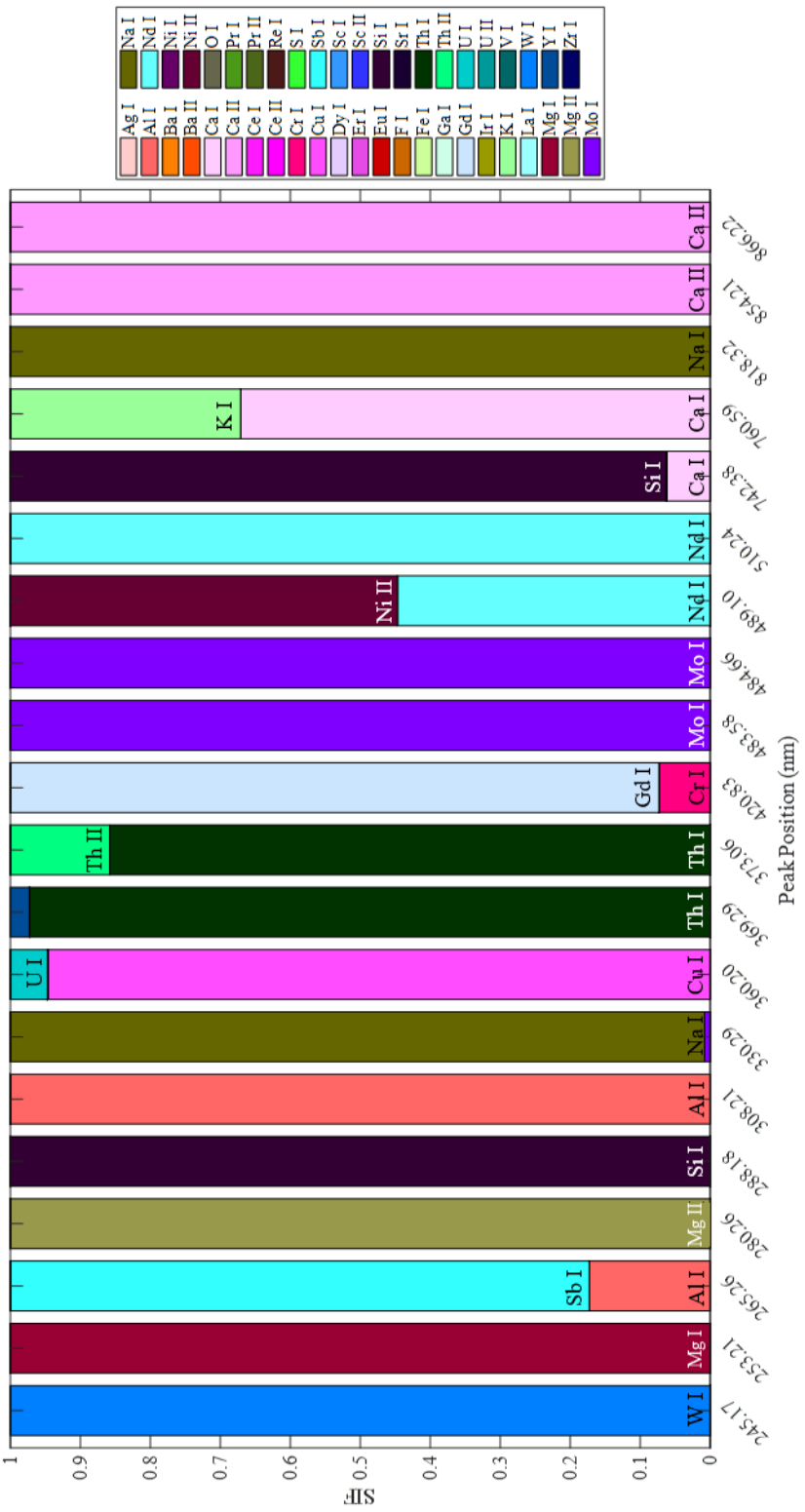

Figure 22: Posterior SIF of NIST SRM 612 – No Prior.

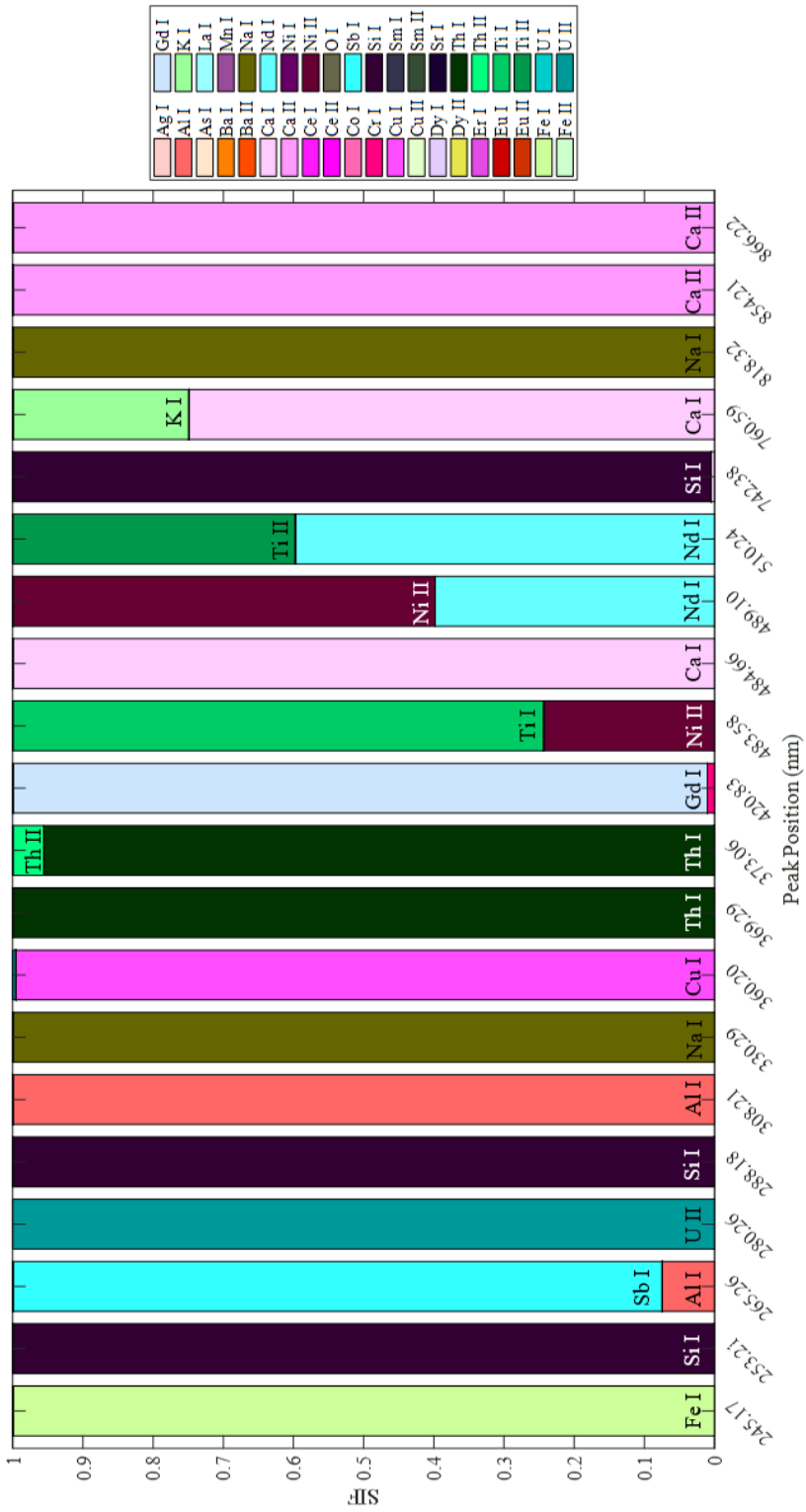

Figure 23: Posterior SIF of NIST SRM 612 - Qualitative Prior.

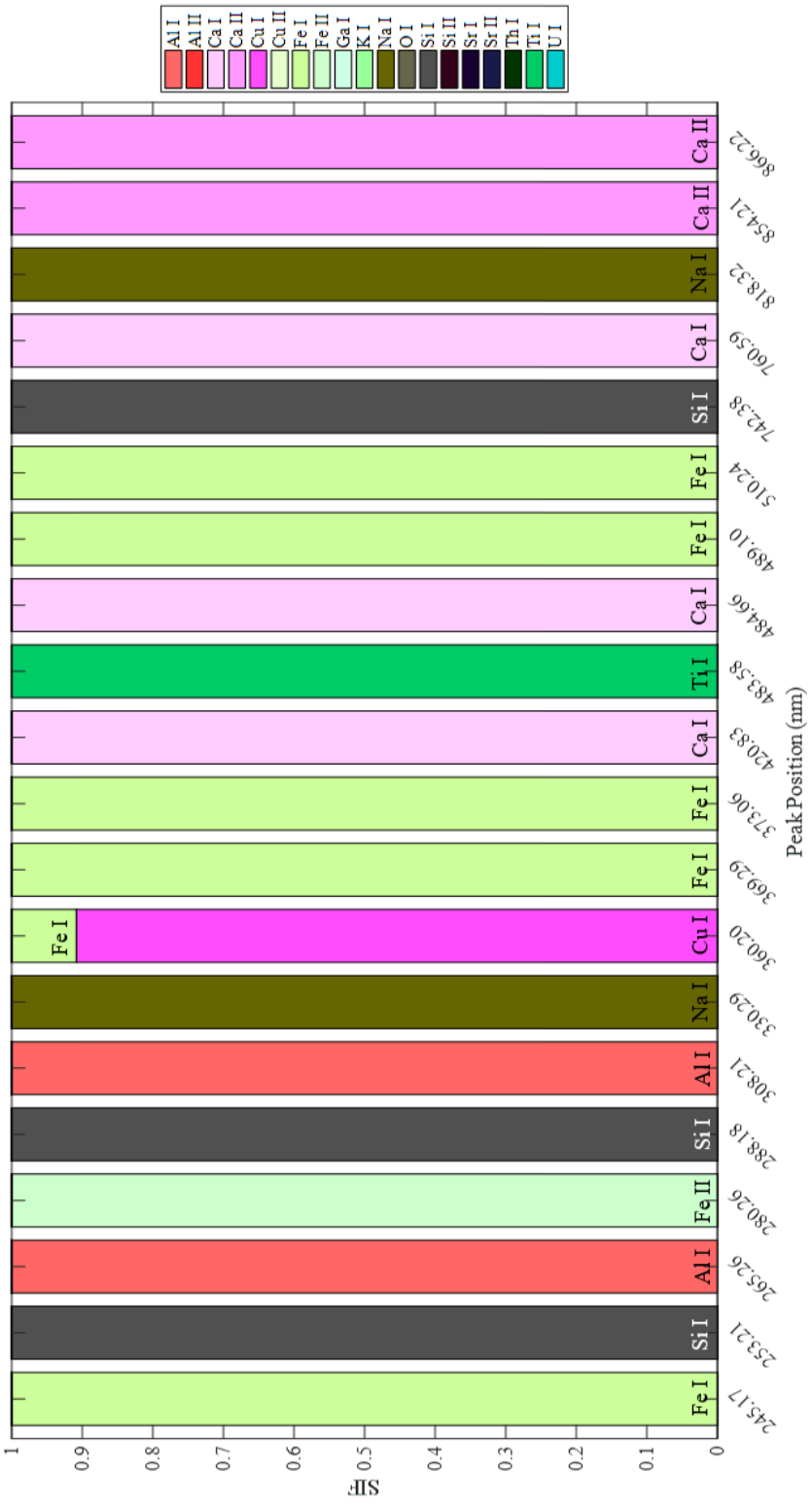

Figure 24: Posterior SIF of NIST SRM 612 - Quantitative Prior.

NIST SRM 614 Glass

The sixty-one trace elements in NIST SRM 614 have nominal mass fractions in the range of 0.5 mg/kg to 50 mg/kg[118]. Table 28 gives the twenty trace elements with certified mass fractions in SRM 614. Forty-one additional trace elements are added to the SRM 614 but have no certified mass fraction.

Table 28: Mass fraction of NIST SRM 614.

Element	**Ag**	**Au**	**B**	**Cd**	**Co**	**Cu**	**Eu**	**Fe**	**K**	**La**
Mass Fraction (mg/kg)	0.42	0.5	1.3	0.55	0.73	1.37	0.99	13.3	30	0.83
Element	**Ni**	**Pb**	**Rb**	**Sb**	**Sc**	**Sr**	**Th**	**Ti**	**Tl**	**U**
Mass Fraction (mg/kg)	0.95	2.32	0.855	1.06	0.59	45.8	0.748	3.1	0.269	0.823

Individual SIF

There were a total of six-hundred and five detected peaks for NIST SRM 614 within the 185 nm to 1050 nm spectral range. The matching factor for SRM 614 for the wavelength range of interest is shown in Table 29. The highest matching factors for SRM 614 belong to Ca I, Ca II, K I, Li I, Mg II, and Si I. Calcium, potassium, lithium, and silicon are present within the sample while magnesium was not one of the trace elements added to the sample. Thallium was one of the certified mass fraction elements added to the SRM 614 sample. There were no theoretical Tl I emission lines present within any of the experimental peak widths resulting in a MF of 0%.

Table 29: NIST SRM 614 matching factor.

Element	MF (%)	Element	MF (%)	Element	MF (%)	Element	MF (%)	Element	MF (%)
Ag I	10.93	Cu I	17.16	Ir II	8.84	Os II	16.40	Sr II	49.00
Ag II	48.05	Cu II	10.63	K I	79.60	P I	6.77	Ta I	6.14
Al I	39.06	Dy I	11.21	K II	6.66	P II	1.36	Ta II	10.30
Al II	4.19	Dy II	11.88	La I	10.70	Pb I	0.66	Tb I	31.18
Ar I	3.59	Er I	15.18	La II	17.90	Pb II	0	Tb II	5.84
Ar II	8.28	Er II	10.52	Li I	98.38	Pd I	6.45	Te I	0
As I	7.07	Eu I	23.36	Li II	18.89	Pd II	53.24	Th I	13.98
Au I	3.06	Eu II	18.25	Lu I	10.79	Pr I	11.97	Th II	9.50
B I	18.90	F I	6.81	Lu II	10.25	Pr II	14.03	Ti I	17.23
B II	0	F II	7.10	Mg I	46.80	Pt I	13.39	Ti II	18.90
Ba I	14.83	Fe I	17.77	Mg II	82.21	Rb I	1.89	Tl I	0
Ba II	8.62	Fe II	10.73	Mn I	14.75	Re I	13.41	Tm I	8.61
Be I	0.01	Ga I	26.78	Mn II	5.41	Re II	19.00	Tm II	14.41
Be II	33.15	Ga II	0	Mo I	11.94	Rh I	11.76	U I	16.98
Bi I	0.88	Gd I	11.76	Mo II	2.55	Rh II	11.19	U II	10.36
C I	4.37	Gd II	13.15	N I	47.48	Ru I	9.80	V I	12.96
C II	11.85	Ge I	21.04	N II	10.56	Ru II	13.87	V II	11.61
Ca I	75.29	Ge II	26.50	Na I	37.05	S I	23.66	W I	8.97
Ca II	90.20	H I	0.44	Na II	36.04	S II	12.99	W II	16.29
Cd I	1.38	He I	0.66	Nb I	13.39	Sb I	21.88	Y I	23.50
Cd II	38.28	He II	2.12	Nb II	11.34	Sc I	17.33	Y II	11.14
Ce I	18.77	Hf I	12.08	Nd I	18.56	Sc II	12.48	Yb I	6.48
Ce II	12.49	Hf II	9.98	Nd II	15.46	Se I	0	Yb II	7.79
Cl I	4.97	Hg I	13.61	Ne I	15.89	Si I	75.04	Zn I	18.36
Cl II	6.33	Hg II	0.89	Ne II	18.74	Si II	61.15	Zn II	0.64
Co I	9.48	Ho I	24.69	Ni I	6.62	Sm I	18.61	Zr I	10.59
Co II	9.16	Ho II	15.60	Ni II	16.80	Sm II	11.82	Zr II	9.37
Cr I	12.48	In I	0.10	O I	54.76	Sn I	15.48		
Cr II	5.67	In II	0	O II	13.12	Sn II	23.47		
Cs I	7.32	Ir I	9.05	Os I	9.04	Sr I	25.27		

Table 30 shows the individual SIF for seven peaks of the SRM 614 spectrum. Peaks 348.85 nm, 396.14 nm, and 818.32 nm have an emitter with an individual SIF value greater than 92% which means that these peaks can be attributed with very little spectral interference to these emitters. Peaks 252.84 nm and 285.20 nm have neutral magnesium as one of the top contributors. Prior knowledge of the sample would remove magnesium because it is not present in the sample even though it has theoretical emission lines within those peaks.

Table 30: Seven peaks from the NIST SRM 614 spectrum with each peak's top emitters and individual SIF values.

252.84 nm		285.20 nm		288.12 nm		348.85 nm		396.14 nm		459.47 nm		818.32 nm	
Elem	**SIF**	**Elem**	**SIF**	**Elem**	**SIF**	**Elem**	**SIF**	**Elem**	**SIF**	**Elem**	**SIF**	**Elem**	**SIF**
Si I	0.6569	Mg I	0.3019	Si I	0.7933	U I	0.9234	Al I	0.9895	Eu I	0.7787	Na I	0.9999
Mg I	0.0693	Fe I	0.1150	Th II	0.0690	Er I	0.0186	Er I	0.0028	Th I	0.0656	N I	6.11E-05
Sn I	0.0466	Ti I	0.1111	Ce II	0.0278	Fe I	0.0095	Ce II	0.0015	Ni II	0.0367	Er I	1.89E-05
Mn I	0.0293	Mn I	0.0953	Fe I	0.0148	Cu II	0.0064	Ni II	0.0015	Sm II	0.0271	Ni II	1.62E-05
Ti II	0.0289	V I	0.0837	Ni II	0.0143	Fe II	0.0057	Mo I	0.0012	Co I	0.0207	Cu II	1.02E-05
Fe II	0.0216	Cr I	0.0806	Mn I	0.0118	Co I	0.0057	Ni II	0.0006	Fe I	0.0192	Ca I	8.26E-06
Pt I	0.0216	Fe II	0.0694	Cu II	0.0091	Co II	0.0055	Fe I	0.0004	Os I	0.0152	Nd II	6.85E-06
Cr I	0.0209	Cu II	0.0688	Fe iI	0.0091	Mn I	0.0042	Os I	0.0004	V I	0.0137	Fe II	2.48E-06
V I	0.0202	Cr iI	0.0366	CO I	0.0081	Cr I	0.0034	Cr I	0.0003	Cr I	0.0133	Sc II	2.18E-06
V II	0.0195	Mn II	0.0349	Cr I	0.0078	Mn II	0.0029	Fe II	0.0003	Cr II	0.0060	C I	1.78E-06
Co II	0.0192	Th II	0.0014	La II	0.0067	Ni I	0.0026	Co I	0.0002	Ti I	0.0022	Cr I	1.14E-06
Fe II	0.0129	Ta II	0.0008	Mn II	0.0044	V I	0.0026	Sm I	0.0002	Sc I	0.0007	Cr II	9.96E-07
W I	0.0110	Nb I	0.0005	Cr II	0.0044	Cu I	0.0022	Nb I	0.0002	Mo I	0.0007	Ni II	2.61E-07
Mn II	0.0109	Zr II	0.0002	Gd II	0.0034	Ce II	0.0016	Nd II	0.0001	Nd II	0.0002	Mn I	5.31E-08
Cr II	0.0098	Yb II	9.05E-06	Cd I	0.0029	Cr II	0.0015	Re I	0.0001	Ca I	1.83E-05	Cl II	9.75E-09
Bi I	0.0012	V II	2.29E-06	Dy II	0.0022	Ti I	0.0015	Cr II	0.0001	Mn I	5.53E-06	Mn II	9.71E-10
Ni I	0.0003	Ti II	1.20E-06	Sc I	0.0020	Sc I	0.0015	Pr II	0.0001	Ni II	2.28E-06	Al II	8.30E-10
Ni II	1.46E-06	Sc I	2.56E-07	V I	0.0018	Dy II	0.0006	Mn II	0.0001	F I	2.87E-07	Ar I	2.14E-10
N II	1.07E-08	Ni II	4.75E-08	V II	0.0016	Nb II	0.0006	Sm II	6.29E-05	Cu II	1.43E-07	Ne II	2.84E-12

Optimal Set of Emitters

The elements for the SRM 614 are ordered by their likelihood of individual SIF for the spectral range of interest from 185 nm to 1050 nm. Three prior knowledge analyses were performed: no prior knowledge, qualitative prior knowledge, and quantitative prior knowledge of the sample composition for the optimal set of emitters shown in Figure 25. For no prior knowledge of the sample composition, the number of optimal set of emitters is fifty-three with a BIC of 1547.05. The optimum set of emitters for the no prior knowledge analysis is large with many emitters contributing to at least one peak, {Ag I, Al I, B I, Ba I, Be II, Ca I, Ca II, Cd I, Cd II, Ce I, Co I, Cr I, Cu I, Cu II, Eu I, Fe I, Fe II, Ga I, Ge I, Ge II, Ho I, K I, La I, Li I, Mg I, Mg II, Mo I, N I, Na I, Nd I, Ni I, Ni II, O I, Os I, Os II, Re I, Re II, Rh I, S I, Sb I, Sc I, Sc II, Si I, Sm I, Sn I, Sr I, Th I, Th II, Ti I, U I, U II, Y I, Zr I}. Qualitative prior knowledge of the SRM 614 sample results in the optimum set of {Ag I, Al I, B I, Ca I, Ca II, Cd I, Cd II, Co I, Cu I, Cu II, Eu I, Fe I, Fe II, Ga I, K I, la I, na I, Ni I, Ni II, Sb I, Sc I, Sc II, Si I, Sr I, Th I, Th II, Ti I, U I, U II}. The quantitative prior knowledge analysis needs twenty-six emitters with a BIC of 5354.70. The set of optimal emitters for the quantitative prior knowledge are {Al I, Al II, B I, Ca I, Ca II, Cd I, Cd II, Cu I, Cu II, Eu I, Fe I, Fe II, Ga I, K I, Na I, Ni I, Ni II, Sc I, Sc II, Si I, Si II, Sr I, Sr II, Th I, Ti I, U I}. There are twenty-three emitters in common to all three prior knowledge analyses, {Al I, B I, Ca I, Ca II, Cd I, Cd II, Cu I, Cu II, Fe I, Fe II, Ga I, K I, Na I, Ni I, Ni II, Sc I, Sc II, Si I, Sr I, Sr II, Th I, Ti I, U I}. The glass matrix components, Al I, Ca I, Ca II, Na I, and Si I are present in this list. Oxygen is missing from this list because it is not in the optimal set of emitters for the qualitative prior knowledge analysis. Within the no prior knowledge optimal set of emitters, there are twenty-three emitters included that are not present within the sample

composition, {Ba I, Be II, Ce I, Cr I, Ge I, Ge II, Ho I, Li I, Mg I, Mg II, Mo I, N I, Nd I, Os I, Os II, Re I, Re II, Rh I, S I, Sm I, Sn I, Y I, Zr I}. The qualitative and quantitative prior knowledge optimal set of emitters have twenty-two emitters in common, {AL I, B I, Ca I, Ca II, Cd I, Cd II, Cu I, Cu II, Fe I, Fe II, Ga I, K I, Na I, Ni I, Ni II, Sc I, Sc II, Si I, Sr I, Th I, Ti I, U I}. The only atom not in common between the qualitative and quantitative prior knowledge analyses is O I because its BIC is larger than the optimal BIC value. Using the optimal BIC value, O I is excluded from the posterior SIF analysis but could be added to the analysis.

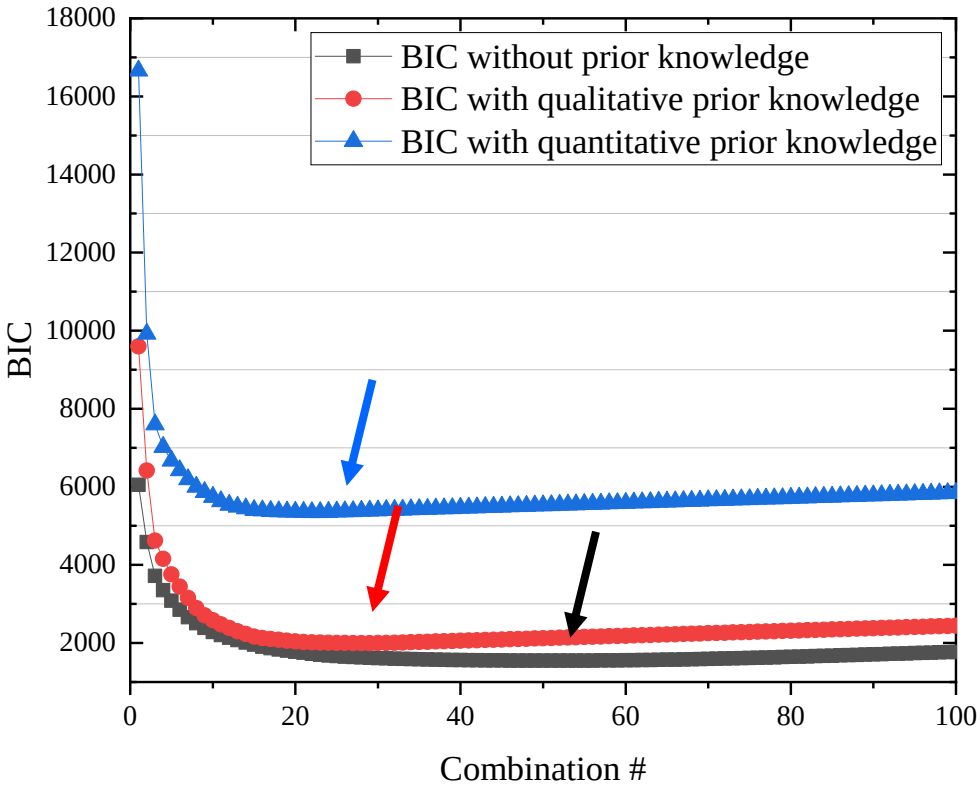

Figure 25: BIC graph of NIST SRM 614.

Posterior SIF

Given the optimal set of emitters and their individual SIF data for the no prior, qualitative prior, and quantitative prior knowledge analyses, the posterior SIF was determined. Figures 26-28 show a twenty-peak subset representative of the whole experimental SRM 614 spectrum for the three knowledge analyses. Five of the twenty peaks show no spectral interferences within all three prior knowledge analyses. Peak 250.02 nm, 288.18 nm, 396.14 nm, 766.54 nm and 818.32 nm have one emitter, Ga I, Si I, Al I, K I and Na I respectively. Singly-ionized calcium has the main contribution for peak 299.69 nm for the no prior and qualitative prior knowledge analyses. The quantitative prior knowledge analysis of peak 299.69 nm results in a main contribution from Ca II with a small interference from Ca I. Peak 299.69 nm can be judged reliable for calcium line assignment because the interferences are from the neutral and singly-ionized calcium for the quantitative analysis while the no prior and qualitative prior knowledge analyses Ca II had a posterior SIF of 100%. Prior knowledge of the sample composition for peaks 348.85 nm, 361.53 nm, 369.87 nm, 387.95 nm, 410.32 nm, and 459.47 nm show how the line assignment in the no prior knowledge has interferences as quantitative knowledge is introduced. Europium is the sole emitter for the no prior and qualitative prior knowledge analyses of peak 459.47 nm. The addition of the quantitative prior knowledge creates a large interference in peak 459.47 nm from Fe I. Iron is found in higher concentrations than europium in SRM 614 which increases its individual SIF for the quantitative prior knowledge analysis while decreasing europium's SIF. Although many combinations need Fe I to explain the spectral peak 459.47 nm it is less than europium.

Peaks 348.85 nm and 410.32 nm have a sole emitter of U I for the no prior and qualitative prior knowledge analyses. The individual SIF for U I for the no prior and qualitative prior knowledge analyses is the highest value and Fe I has the second highest. The mass fraction of iron is 13.3 mg/kg compared to uranium at 0.823 mg/kg. The input of quantitative prior knowledge results in quantitative individual SIF values within 0.01 of each other. The top 100,000 combinations of all emitters for the quantitative prior knowledge analyses result in U I being the main emitter of peak 348.85 nm and 410.32 nm with a small interference from Fe I. Peaks 361.53 nm, 369.87 nm, and 387.95 nm have a sole emitter of Th II in the no prior and qualitative prior knowledge analyses. Singly-ionized thorium is not found within the quantitative prior knowledge optimal set of emitters. Input of the prior knowledge and the optimal set of emitters, attributes the main emitter of peaks 361.53 nm, 369.87 nm, and 387.95 nm as Fe I with a large interference from Th I. The individual SIF with the prior knowledge added results in Fe I with the highest value and Th I second. Using the optimal set of emitters and their individual SIF, the top 100,000 likelihoods have combinations with line assignment of these peaks of Fe I with a few thousand attributing the peaks to Th I. The peaks 361.53 nm, 369.87 nm, and 387.95 nm are considered to be non-reliable for thorium assignment.

Peaks 198.25 nm, 252.84 nm, and 456.95 nm have different line assignments in the quantitative prior knowledge analyses. Peak 198.25 nm is attributed to Co I for the no prior and qualitative prior knowledge analyses. Given the quantitative prior knowledge optimal set of emitters, the possible number of emitters for peak 198.25nm becomes one, Si I. Neutral lanthanum is the sole emitter for peak 456.95 nm for the qualitative and no prior knowledge analyses. Peak 252.84 nm

is attributed to Sb I for the no prior knowledge and qualitative prior knowledge analyses. The peaks at 252.84 nm and 456.95 nm are assigned differently for their quantitative prior knowledge analyses due to the optimal set of emitters to explain the spectrum. Peak 252.84 nm has the sole emitter of Si I and 456.95 nm Ca I because they are the only possible emitters to explain those peaks in the quantitative prior knowledge analyses. Peaks 665.96 nm and 922.86 nm have line assignment of Mo I and Mg II for the no prior knowledge analyses respectively. Input of the prior knowledge, changes the elemental profile of these two peaks because their emitters are not present in SRM 614. The qualitative prior knowledge of peak 665.96 and 922.86 nm have multiple spectral interferences with ten emitters with equiprobability. Quantitative prior knowledge results in spectral interferences between O I and O II equally. Peaks 665.96 nm and 922.86 nm are considered non-reliable for line assignment as the emitter for the peak changes between all three prior knowledge analyses. Peaks 279.50 nm and 285.20 nm are attributed to Mg II for no prior knowledge analyses. Magnesium is not present in sample composition which results in Fe I being the sole emitter for the prior knowledge analyses. Neutral iron has the highest individual SIF for the two peaks compared to Ni II which had the second highest. Iron has a higher concentration than nickel which results in line assignment of peaks 279.50 nm and 285.20 nm as Fe I with no spectral interferences. Peak 320.04 nm has a main emitter of Re I with a large spectral interference from Fe I. Rhenium is not one of the trace elements added to the SRM 614 glass matrix. The line assignment for the qualitative and quantitative prior knowledge for peak 320.04 nm is only Fe I as Re I was not a possible emitter for the peak.

Twenty-three emitters were determined for the optimal set of emitters that were contained in the SRM 612 sample which lead to one-hundred twenty-nine peaks for the entire spectrum with a

100% SIF of emitters not possible when the composition was known. Forty-eight of the six-hundred and five peaks had spectral interferences with thirty-four being small interferences that arise from Fe I. There were only nine peaks that had spectral interferences with the qualitative prior knowledge. Quantitative prior knowledge had five-hundred and sixty-six peaks that had one emitter. The emitter with the highest SIF for the no prior and qualitative prior occurred 76.86% because of the twenty-eight common emitters between the optimal set of emitters. The quantitative and no prior knowledge analyses had the same main emitter for 34.38% due to the optimal set of emitters determined by the knowledge individual SIF for each emitter. Prior knowledge of the had 42.31% peaks with the same main emitter. This value is lower than expected because of the optimal set of emitters where the quantitative doesn't need some of the emitters that are found in the sample composition. Singly-ionized thorium is present in many peaks for the qualitative prior knowledge analyses but is not needed for the quantitative which leads to different combinations that determine the posterior SIF. The main emitter for all experimental peaks occurred 34.38% for all three prior knowledge analyses. This occurrence for all three prior is the same as the no prior and quantitative prior because the experimental peak emitters for the qualitative prior knowledge had many peaks with sole emitters different from the other knowledge analyses.

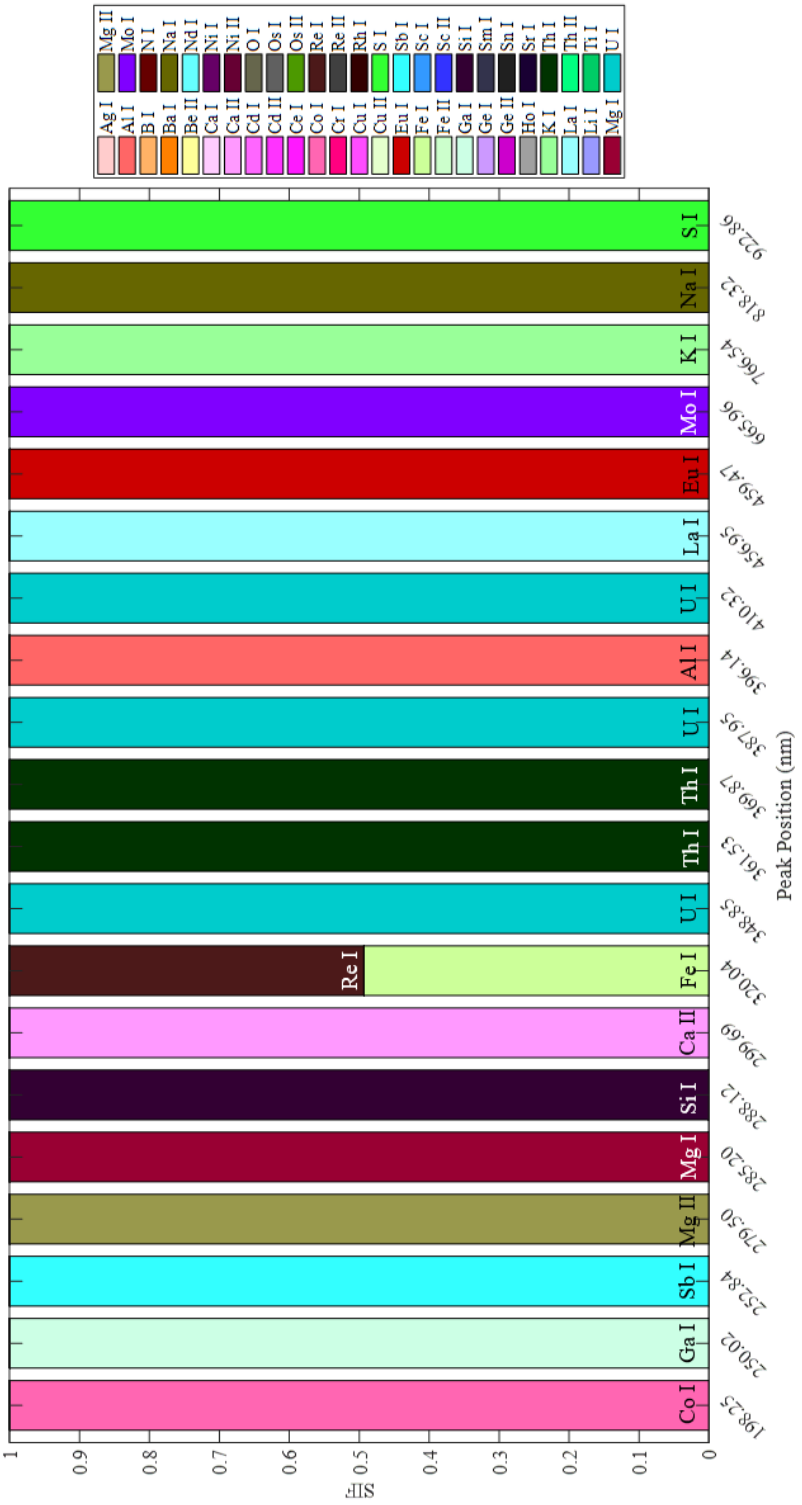

Figure 26: Posterior SIF of NIST SRM 614 - No Prior.

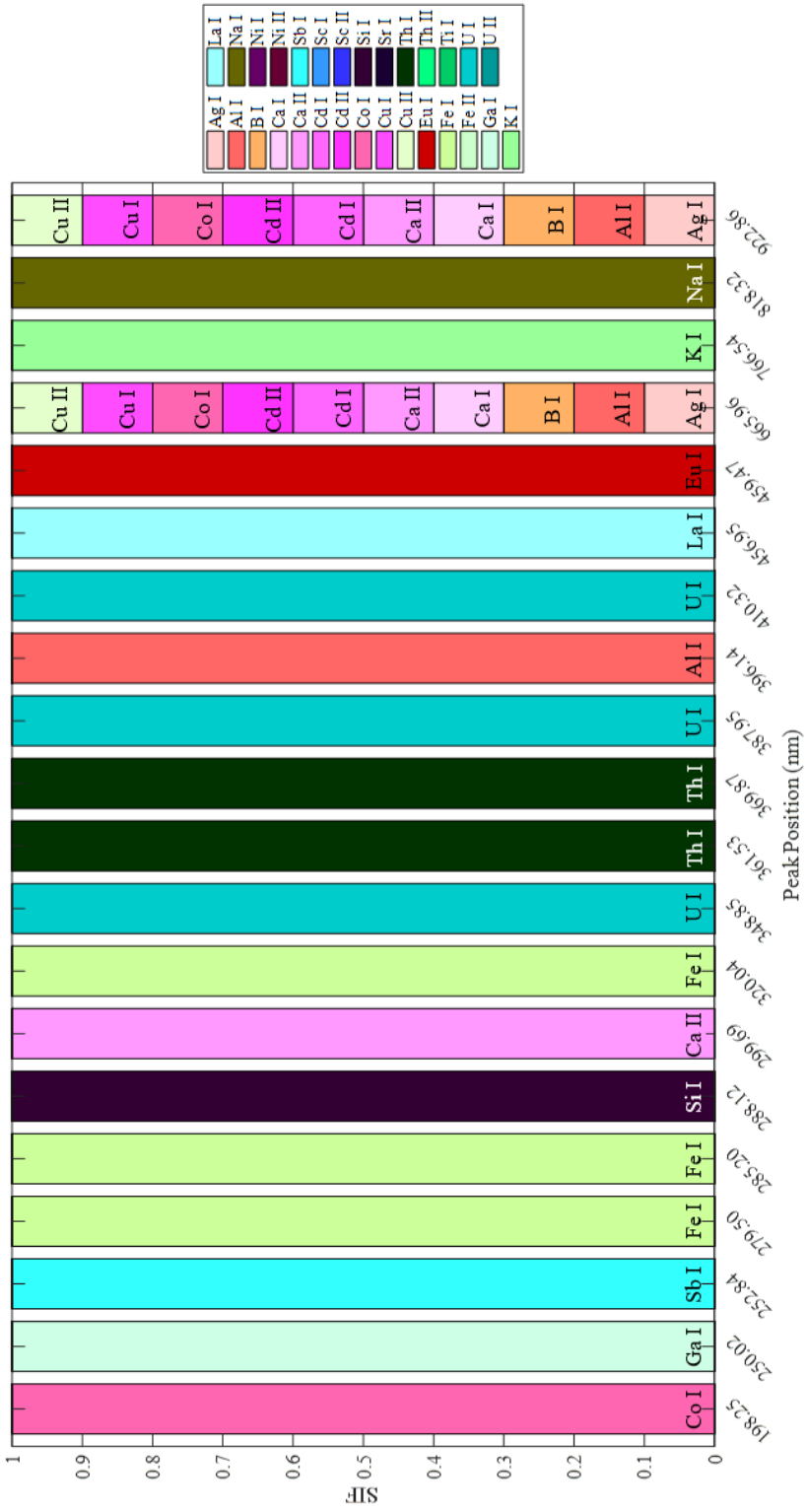

Figure 27: Posterior SIF of NIST SRM 614 - Qualitative Prior.

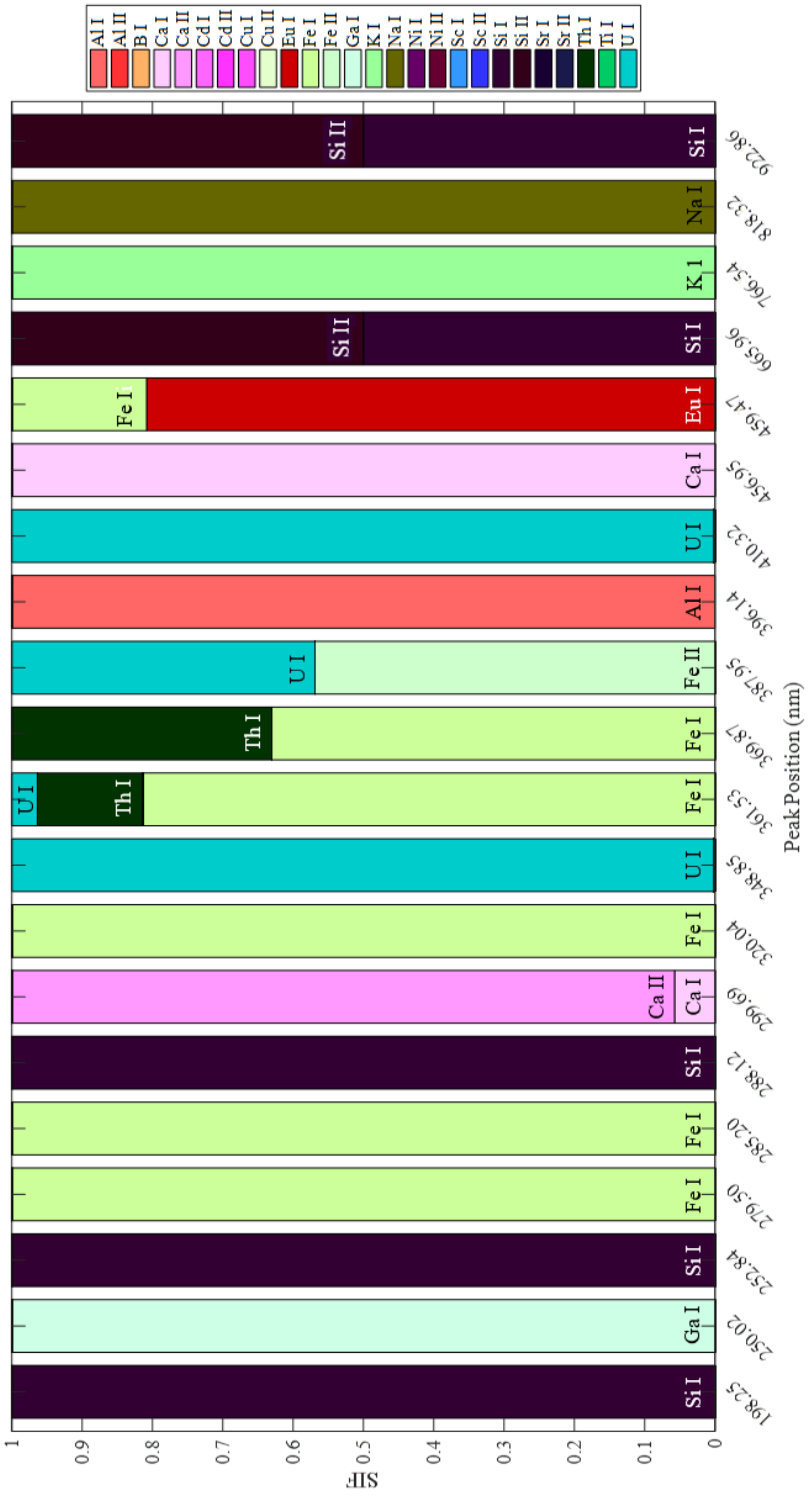

Figure 28: Posterior SIF of NIST SRM 614 - Quantitative Prior.

NIST SRM 616 Glass

There are sixty-one trace elements in the range of 0.008 mg/kg to 30 mg/kg in NIST SRM 616[119]. The fourteen elements with certified mass fractions are given in Table 31 and forty-seven additional elements have no reference values.

Table 31: Mass fraction of NIST SRM 616.

Element	**Au**	**B**	**Cu**	**Fe**	**Ga**	**K**	**Pb**	**Rb**	**Sb**
Mass Fraction (mg/kg)	0.18	0.2	0.8	11	0.23	29	1.85	0.1	0.078
Element	**Sr**	**Th**	**Ti**	**Tl**	**U**				
Mass Fraction (mg/kg)	41.72	0.0252	2.5	0.0082	0.0721				

Individual SIF

The experimental SRM 616 spectral data had four-hundred and seventy detected peaks in the spectral range of 185 nm to 1050 nm. The matching factor was determined and provided a semi-quantitative statistic of how many emitters' theoretical peaks were present in the experimental spectrum. The highest matching factor is Li I with 97.67% which has many theoretical lines present in the experimental spectrum but it is not one of the trace elements added to the glass matrix of SRM 616. Neutral and singly-ionized calcium have the third and fourth highest matching factors which is expected as calcium is a part of the glass matrix which has higher concentrations and more emission lines that are present in the experimental spectrum. The other

glass matrix elements, aluminum, sodium and silicon have low matching factors which means that many expected theoretical peaks are not present within the sample. Of the fourteen elements with certified mass fractions that were added to the SRM 616 glass matrix, boron had the smallest matching factors for both the neutral and singly-ionized emitters. There were no theoretical lines of B II which were present within the experimental spectrum and two theoretical lines of B I were present.

The individual SIF for each experimental detected peak is found and Table 33 shows seven peaks and their SIF. Of the seven peaks, peaks 205.84 nm, 243.84 nm, and 484.96 nm have an emitter with the highest individual SIF that is not present in the sample composition. Neutral silicon has a high individual SIF for peak 288.18 nm thus the peak can be attributed to silicon with small probabilities of interferences. Peak 844.65 nm has only seven possible emitters. Neutral oxygen has the highest SIF with .9871 compared to the other six emitters which makes peak 844.65 nm reliable for oxygen emission.

Table 32: NIST SRM 616 matching factor.

Element	MF (%)	Element	MF (%)	Element	MF (%)	Element	MF (%)	Element	MF (%)
Ag I	0.29	Cu I	0.52	Ir II	0	Os II	4.45	Sr II	47.89
Ag II	23.55	Cu II	2.59	K I	79.49	P I	0.22	Ta I	2.11
Al I	33.00	Dy I	9.25	K II	8.56	P II	1.14	Ta II	3.71
Al II	4.84	Dy II	4.67	La I	7.28	Pb I	0	Tb I	31.18
Ar I	1.37	Er I	9.57	La II	13.42	Pb II	0	Tb II	1.42
Ar II	10.51	Er II	5.07	Li I	97.67	Pd I	9.75	Te I	0
As I	0.64	Eu I	11.38	Li II	17.30	Pd II	0	Th I	7.92
Au I	1.69	Eu II	6.38	Lu I	13.80	Pr I	3.29	Th II	4.90
B I	0.01	F I	3.94	Lu II	2.02	Pr II	10.34	Ti I	7.55
B II	0	F II	7.95	Mg I	35.94	Pt I	4.36	Ti II	9.04
Ba I	19.20	Fe I	4.84	Mg II	82.14	Rb I	1.78	Tl I	0
Ba II	6.71	Fe II	3.71	Mn I	4.70	Re I	7.74	Tm I	5.89
Be I	0.01	Ga I	9.81	Mn II	1.90	Re II	2.08	Tm II	2.81
Be II	0.03	Ga II	0	Mo I	6.62	Rh I	6.50	U I	5.02
Bi I	0.36	Gd I	6.76	Mo II	2.35	Rh II	2.76	U II	4.52
C I	0.37	Gd II	5.75	N I	10.96	Ru I	4.30	V I	5.68
C II	4.07	Ge I	0.86	N II	11.56	Ru II	4.86	V II	6.91
Ca I	80.31	Ge II	0.55	Na I	36.41	S I	0.74	W I	3.87
Ca II	90.78	H I	0.01	Na II	19.80	S II	6.47	W II	4.01
Cd I	1.28	He I	0.07	Nb I	6.30	Sb I	22.45	Y I	15.50
Cd II	0	He II	0.29	Nb II	2.23	Sc I	7.63	Y II	5.13
Ce I	11.28	Hf I	2.88	Nd I	11.80	Sc II	9.47	Yb I	5.84
Ce II	5.84	Hf II	5.32	Nd II	7.51	Se I	0	Yb II	3.25
Cl I	2.03	Hg I	0	Ne I	7.26	Si I	45.72	Zn I	8.84
Cl II	3.11	Hg II	0	Ne II	7.69	Si II	16.04	Zn II	0
Co I	5.21	Ho I	2.40	Ni I	3.89	Sm I	10.93	Zr I	8.09
Co II	4.03	Ho II	1.73	Ni II	8.50	Sm II	5.53	Zr II	4.29
Cr I	8.29	In I	0	O I	28.69	Sn I	6.88		
Cr II	1.59	In II	0	O II	4.77	Sn II	0		
Cs I	1.74	Ir I	3.21	Os I	1.81	Sr I	16.20		

Table 33: Seven peaks from NIST SRM 616 spectrum with each peak's top emitters and individual SIF values.

205.84 nm		243.84 nm		288.18 nm		365.09 nm		484.96 nm		643.91 nm		844.65 nm	
Elem	**SIF**	**Elem**	**SIF**	**Elem**	**SIF**	**Elem**	**SIF**	**Elem**	**SIF**	**Elem**	**SIF**	**Elem**	**SIF**
Ni II	0.2021	Ag II	0.6302	Si I	0.8461	Th II	0.8160	Eu I	0.6261	Ca I	0.7318	O I	0.9871
Sc II	0.1760	Re I	0.1276	Th II	0.0701	Gd II	0.0824	K I	0.3388	Ni II	0.0775	Fe I	0.0122
Cr I	0.1540	Ta II	0.1066	Ni II	0.0122	W I	0.0315	Ce I	0.0245	Ti I	0.0689	Sc I	0.0005
Ca I	0.1215	Sc I	0.0460	Gd II	0.0106	Nb I	0.0182	V I	0.0050	Fe I	0.0441	Ca I	0.0001
Mn I	0.1116	Ni II	0.0242	Cr I	0.0093	Ce II	0.0179	Cr I	0.0022	Mn I	0.0428	Ni I	7.03E-05
V II	0.1110	Co I	0.0137	Co I	0.0075	Nb II	0.0106	Mo I	0.0017	Fe II	0.0338	Co I	2.09E-05
Fe II	0.0881	Co II	0.0115	Zr II	0.0063	Zr II	0.0064	Co I	0.0015	Cd I	0.0010	Fe II	6.56E-08
Cr II	0.0341	Ca I	0.0110	Mn I	0.0063	Sm II	0.0062	Fe I	0.0001	Ti II	1.01E-05		
Fe II	0.0014	Fe II	0.0097	Ru II	0.0061	Au I	0.0031	N I	2.06E-06	Cr I	2.03E-06		
Co II	0.0002	Mn I	0.0056	Rh I	0.0059	Mo II	0.0018	Fe II	1.16E-06	Ni II	4.89E-07		
Sc II	6.36E-05	Mn II	0.0049	Fe II	0.0050	Co I	0.0015	Ni II	6.95E-07	V II	2.13E-07		
Mn II	4.06E-05	Cr I	0.0033	V II	0.0027	Fe I	0.0014	Ne I	2.12E-07	V I	8.42E-08		
Cu II	2.62E-05	Fe II	0.0032	Mn II	0.0025	Fe II	0.0011	Mn II	1.77E-07	Co II	2.12E-08		
F II	4.18E-07	Cr II	0.0016	Cr II	0.0021	Cu I	0.0008	Cr II	3.50E-08	Cr II	1.13E-08		
He II	4.54E-16	Ti I	0.0010	Ta II	0.0018	Cr I	0.0003			Co I	1.72E-09		

Optimal Set of Emitters

The no prior knowledge analysis for the optimal set of emitters takes the ordered elements found by the max sum of the individual SIF for all four-hundred and seventy peaks in the spectral range of interest. The BIC value for each set of emitters is shown in Figure 29. The optimum set of emitters to explain the experimental SRM 616 is fifty-seven, {Al I, Ba I, Ca I, Ca II, Ce I, Ce Ii, Co I, Co II, Cr I, Cr II, Dy I, Dy II, Er I, Eu I, F I, Fe I ,Fe II, Ga I, Gd I, Ho I, K I, La I, Mg I, Mg II, Mn I, Mn II, Mo I, N I, N II, Na I, Nd I, Ni I, Ni II, O I, Os I, Pd I, Rh I, Sc I, Sc II, Si I, Sm I, Sr I, Sr II, Ta I, Ta II, Th I, Th II, Ti I, Ti II, U I, U II, V I, W I, Y I, Y II, Yb I, Zr I}. There are thirty-eight emitters present in the no prior knowledge optimum set of emitters that are not present in the SRM 616 sample composition, {Ce I, Ce II, Co I, Co II, Cr I, Cr II, Dy I, Dy II, Er I, Eu I, F I, Gd I, Ho I, La I, Mg I, Mg II, Mn I, Mn II, Mo I, N I, N II, Nd I, Ni I, Ni II, Os I, Pd I, Rh I, Sc I, Sc II, Sm I, Ta I, Ta II, V I, W I, Y I, Y II, Yb I, Zr I}. Knowing the presence of elements in the SRM 616 sample, the qualitative prior knowledge analysis needs twenty emitters to explain the spectrum. The qualitative prior optimum set of emitters is {Al I, Al II, Ca I, Ca II, Fe I, Fe II, Ga I, K I, Na I, o I, Si I, Si II, Sr I, Sr II, Th I, Th II, Ti I, Ti II, U I, U II}. For the quantitative prior knowledge of the sample composition, the optimal set of emitters to explain the experimental spectrum is twenty with a BIC of -3191.08 and contains the exact set of emitters as the qualitative prior knowledge analysis. The optimum list of emitters for the quantitative prior knowledge is {Al I, Al II, Ca I, Ca II, Fe I, Fe II, Ga I, K I, Na I, O I, Si I, Si II, Sr I, Sr II, Th I, Th II, Ti I, Ti II, U I, U II}. There are no additional emitters that can be added to the qualitative and quantitative prior optimal set of emitters because every element not present in the sample's optimal set of emitters is not found within the sample's composition. There are

eighteen emitters common to all three knowledge analyses, they are {Al I, Ca I, Ca II, Fe I, Fe II, Ga I, K I, Na I, O I, Si I, Sr I, Sr II, Th I, Th II, Ti I, Ti II, U I, U II}. The large number of elements common to all prior knowledge analyses means that no matter the prior knowledge the elements found within the sample's composition can be identified and evaluated.

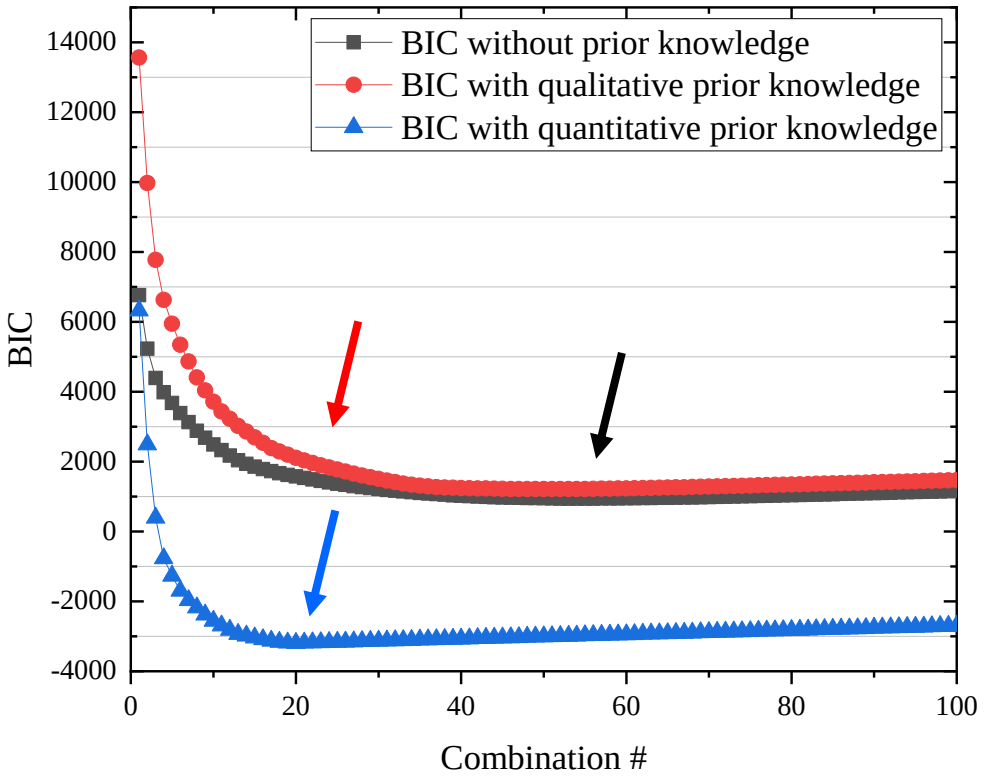

Figure 29: BIC graph of NIST SRM 616.

Posterior SIF

Figures 30-32 show a subset of twenty peaks representative of the entire spectrum for conciseness and clarity of all three knowledge prior analyses. Seven of the twenty peaks had the same emitter with no spectral interferences for five peaks. Peak 288.18 nm, 257.49 nm, 327.50 nm, 388.19 nm, 393.32 nm, 643.91 nm, and 844.65 nm had spectral line assignments of Si I, Al I, Th II, Ti I, Ca I, Ca II, and O I respectively. Titanium is found in small mass fractions compared to silicon, aluminum, calcium, and oxygen for SRM 616. The assignment of peak 388.19 nm for no prior, qualitative prior and quantitative prior shows that trace elements added to the glass matrix need to be included no matter the prior knowledge because no other combination of emitters provide information about that specific peak. The lines of 288.18 nm, 257.49 nm, 388.19 nm, 643.91 nm, and 844.65 nm are considered reliable for peak assignment. Peak 327.50 nm and 393.32 nm have no spectral interferences with complete assignment to the singly-ionized thorium and calcium respectively. These peaks are judged reliable for line assignment when considered spectral interferences. Consideration of the absence of the neutral atom for peaks 327.50 nm and 393.32 nm judges these lines reliable if there are no other possible emitters that can contribute to the peaks. The individual SIF for the qualitative and quantitative prior knowledge only have Th II as a contributor to peak 327.50 nm and two contributors, Ca I and Ca II for peak 393.32 nm. Peak 327.50nm is considered reliable for line assignment while peak 393.32 nm is not. Peaks 244.29 nm and 348.85 nm have spectral interferences in the no prior and quantitative prior knowledge but not in the qualitative prior. Neutral cobalt is the main emitter of peak 348.85 nm with a small interference of Fe I. Input of the prior knowledge results in assignment of Fe I for the qualitative knowledge analysis because Co I is not present within

the SRM 616 sample composition. The quantitative prior knowledge analysis has a main emitter of Fe I also with a small interference of Fe II but this peak can be attributed to iron because both the neutral and singly-ionized emitters of iron are the only spectral interferences. Neutral and singly-ionized chromium have spectral interferences for peak 244.29 nm for the no prior knowledge analysis. Removal of chromium because it is not in the sample results in assignment of peak 244.29 nm for Fe I with no spectral interferences for qualitative and Fe I with a small interference for quantitative prior knowledge analysis. Prior knowledge of the sample composition results in interferences for peaks 883.28 nm and 884.90 nm whereas no prior has one sole emitter, Cr II and Ho I respectively. Holmium and chromium are not present in the sample which means it is removed from optimal set of emitters for the qualitative and quantitative prior knowledge analyses. Qualitative prior knowledge has ten emitters that have equiprobability of producing peaks 884.90 nm and 883.28 nm because the individual SIF for these ten are equal with oxygen having the eleventh individual SIF, neutral silicon the twelfth, and singly-ionized silicon the thirteenth. The quantitative prior knowledge assigns the main emitter of peaks 883.28 nm and 884.90 nm to O I with small interferences from Si I and Si II. The optimal set of emitters between the qualitative and quantitative prior knowledge have the same emitters which means that the concentration of the emitters affects the assignment of a peak for the top 100,000 combinations because O I and Si I have the highest concentrations.

Peaks 205.84 nm, 227.49 nm, 243.84 nm, and 484.96 nm have a different assignment between the no prior and the prior knowledge analyses. No prior knowledge of peak 205.84 nm has a main emitter of Ni II and a small interference Sc II and Ni II the sole emitter for peak 227.49 nm.

Nickel and scandium are not present within the sample composition which results in a different element profile for the qualitative and quantitative prior knowledge analyses. Peak 205.84 nm has a sole emitter of Ca I and peak 227.49 nm has a sole emitter of Fe II for the qualitative and a main emitter of Fe II with a small interference of Fe I for the quantitative prior knowledge analyses. There are interferences between Fe I and Fe II for the quantitative prior knowledge analyses because the best combinations of the entire spectrum have Fe II for more of the top combinations than Fe I. Peak 227.49 nm can be attributed to iron for prior knowledge of the sample. Peaks 243.84 nm and 484.96 nm have sole emitters of Ta II and Eu I respectively. Input of prior knowledge, results in the assignment of peaks 243.84 nm and 484.96 nm to Ca I and K I respectively for both the qualitative and quantitative prior knowledge analyses. Peak 316.67 nm has a main emitter of Ca I with a large interference of Os I for the no prior knowledge where osmium is not present in the sample. Neutral calcium becomes the sole emitter for the qualitative and quantitative prior knowledge analyses of peak 316.67 nm removing the osmium interference. The concentration of iron is greater than thorium in the SRM 616 which gives it a higher individual SIF for peak 316.67 nm. This higher individual SIF is seen in other peaks such as 365.09 nm that have only thorium and iron which results in a combination of that needs mostly thorium for these peaks, but many top combinations need Fe I and Fe II. Peak 356.52 nm has a sole emitter of U I for the no prior and qualitative prior knowledge analyses. The quantitative prior knowledge of the sample and the optimal set of emitters increases the individual SIF of Ca I for peak 356.52 nm from 0.02% to 90% which results in the complete assignment of Ca I. Peak 360.70 nm and 365.84 nm have different main emitters for all three prior knowledge analyses. No prior knowledge of peak 360.70 nm and 365.84 nm attribute the

peaks to Er I and Mo I respectively. The addition of prior knowledge of the sample composition changes the elemental profile of these peaks because molybdenum and erbium are not one of the trace elements added to the glass matrix of SRM 616. Qualitative prior knowledge of peaks 360.70 nm and 365.84 nm have a sole emitter of Ti I. Iron is found in concentrations of four times that of titanium which results in the assignment of Fe I as the main peak emitter for the quantitative analyses. Peak 365.84 nm has a small interference from Ti I due to the top 100,000 combinations of the top likelihoods which have several combinations with Ti I for the peak. No prior knowledge analyses have four-hundred and twenty-two peaks with one emitter. Of that four-hundred and twenty-two peaks, one-hundred and eight-three peaks have an emitter not present in the sample composition. Forty-eighty of the peaks for the no prior knowledge analysis have spectral interferences with thirty-small interferences. Qualitative prior knowledge analysis had five peaks that were interfered with multiple emitters and four-hundred and sixty-five peaks that have one contributor. The emitter with the highest SIF for the no prior and qualitative prior knowledge analyses occurred 23.62%. Quantitative prior knowledge has one-hundred and two peaks that have small interferences that result from emitters many of which are Fe I which have a higher concentration than Th I and Ti I that were the sole peak emitter in the qualitative prior knowledge analysis. No prior and quantitative prior knowledge had the same main emitter 39.79% while qualitative and quantitative had 30.00%. Between all three knowledge the highest posterior SIF for the same emitter occurred 21.91%. This small match results from differences in the optimal set of emitters for the no prior and prior knowledge along with the prior knowledge of the concentration that increases the probability of an emitter that was smaller for the no prior and qualitative prior.

Figure 30: Posterior SIF of NIST SRM 616 - No Prior.

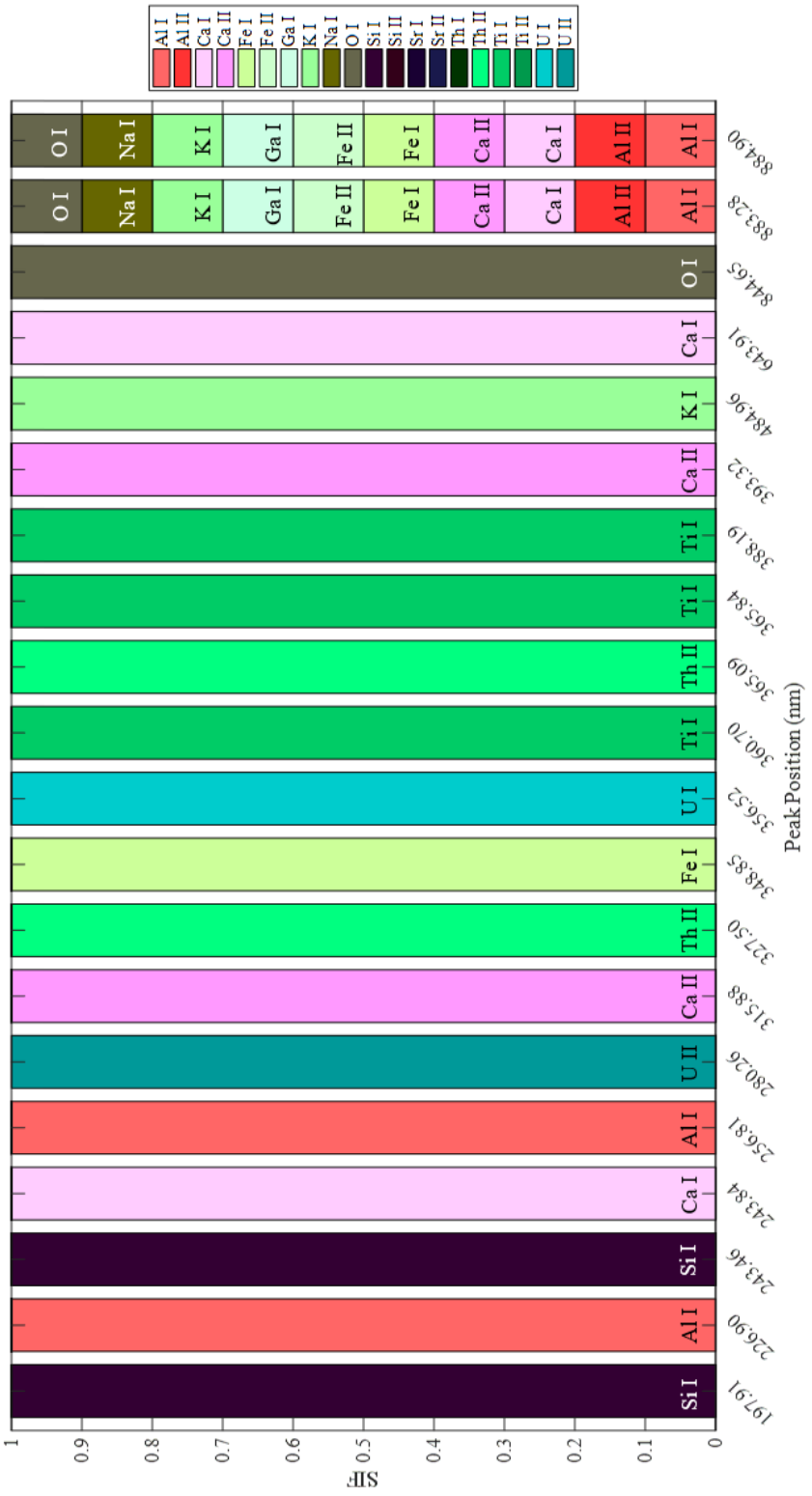

Figure 31: Posterior SIF of NIST SRM 616 - Qualitative Prior.

Figure 32: Posterior SIF of NIST SRM 616 - Quantitative Prior.

Comparison of Major, Minor, and Trace Elements in SRM 600 Glass Series

Comparison of the posterior SIF for the NIST glass 600 series shows that the major elements present in the samples such as the matrix elements of aluminum, calcium, sodium, and silicon are almost always needed in the optimal set of emitters. These elements have numerous transitions that fall within the detected peak widths' which is used to order the elements and orders these elements higher than other minor or trace elements. The posterior SIF is calculated by finding the combination of optimal emitters with the highest likelihood. Major elements have a higher individual SIF therefore combinations with more major elements will have higher likelihoods than other combinations. Minor and trace elements are very dependent on the greedy search ordering and the optimal set of emitters needed to explain the spectrum to influence the posterior SIF. For instance, SRM 610 sample composition has minor concentrations of cadmium. Neutral cadmium shows up in only a few experimental peaks with small individual SIF values that it is ordered ninety-ninth out of the one-hundred and forty-seven possible emitters for the no prior knowledge. Cadmium is not found in the posterior SIF because it isn't even found in the optimal set of emitters. Lead is a minor element of SRM 610 and found in all three knowledge analyses' optimal set of emitters because lead has a high individual SIF value for peak 261.42 nm with 0.8763 which means that this peak is assigned to lead in combination of emitters with the highest likelihood. Peaks 283.3 nm and 405.7 nm are standard lines for Pb I that are highly interfered by the major element Ca I and minor elements Cr I and Fe I. In the case of the NIST 600 glasses, the spectral line 261.4 nm is a great analytical line for Pb I. SRM 614 has several minor elements that are needed to explain the entire experimental spectrum such as nickel. Both neutral and singly-ionized nickel are present in all three prior knowledge analyses

because nickel has many peaks with individual SIF values. Potassium is a common minor element to all SRM 600 glass samples and is needed to explain several peaks including 766.54 nm because although there are several possible other emitters their combinations have very low likelihoods in comparison. When a minor or trace element is highly probable for an individual peak, it is needed as an emitter to explain the experimental spectrum. For instance, in SRM 616, peak 250.02 nm can only be explained by neutral gallium no matter the knowledge of the sample composition because it has the highest individual SIF and other emitters have the lowest probability of being the peak emitter. The major elements of the SRM 600 glass samples predominate over the minor and trace elements as they are found in more experimental peaks with higher individual SIF values that influence the combination of emitters with the highest likelihoods. Minor and trace elements will be present in the posterior SIF for a sample if it is the highest contributor to a peak with very little probability of another emitter. If minor and trace elements are found in few peaks or have lower individual SIF values, they will not be in the optimal set of emitters and will not have a posterior SIF assignment.

NIST SRM 1243 Nickel Chromium Cobalt Alloy

There are fourteen elements with certified mass fraction, four elements with reference mass fractions and one element with mass fraction information for the SRM 1243 nickel-chromium-cobalt alloy[120]. The mass fractions for the components of SRM 1243 are given in Table 34.

Table 34: Mass fraction of NIST SRM 1243.

Element	Al	B	C	Co	Cr	Cu	Fe	Mn	Mo	Nb
Mass Fraction (%)	1.23	49.4*	0.024	12.39	19.05	63*	0.776	73*	4.226	0.0286
Element	**Ni**	**P**	**S**	**Si**	**Ta**	**Ti**	**V**	**W**	**Zr**	
Mass Fraction (%)	58.782	31.7*	21.7*	0.0192	0.0003	3.054	0.1043	0.0139	0.053	

Individual SIF

The NIST SRM 1243 experimental spectrum in the spectral range of 185 nm to 1050 nm had nineteen-hundred and twenty-seven detected peaks. Table 35 shows the matching factor for the spectral region of interest. The elements with the highest mass fractions are nickel, cobalt, chromium, molybdenum, aluminum, and titanium. The matching factors for nickel, cobalt, and chromium are about 50% for the neutral atom and 15% for the singly-ionized atom which is a little lower than expected due to the large number of theoretical emission lines that were not present in the experimental spectrum. Molybdenum and titanium have larger matching factors than nickel, cobalt, and chromium because their theoretical lines were found within more experimental peak widths. There are three elements, Ca II, He II, Tb I which have matching factors greater than 70%. These elements have a large number of theoretical database peaks that are present within the sample but are not present within the SRM 1243 sample composition.

The individual SIF of seven peaks for SRM 1243 are shown in Table 36. Peaks 217.88 nm, 224.08 nm, 650.73 nm, and 808.75 nm show the only possible emitters otherwise the top fourteen emitters' and their individual SIF. The emitters present in the sample composition

should be one of the top individual SIF emitters for each peak. Peak 568.11 nm has Lu I and Eu I as the top emitters but these elements are not present in the sample which means that the next top emitter would be Mo I. Neutral oxygen is the main emitter of peak 808.75 nm. There was no oxygen in the sample SRM 1243 but the samples were ran in air. Only elements with certified mass fractions were added to the prior knowledge of the sample which is why C I is the emitter of peak 808.75 nm with oxygen removed.

Table 35: NIST SRM 1243 matching factor.

Element	MF (%)	Element	MF (%)	Element	MF (%)	Element	MF (%)	Element	MF (%)
Ag I	0.29	Cu I	17.24	Ir II	31.68	Os II	43.02	Sr II	39.05
Ag II	24.49	Cu II	5.35	K I	1.09	P I	2.35	Ta I	32.64
Al I	31.57	Dy I	20.73	K II	48.69	P II	15.03	Ta II	26.27
Al II	22.98	Dy II	31.05	La I	24.76	Pb I	28.32	Tb I	75.21
Ar I	5.45	Er I	36.22	La II	33.69	Pb II	5.20	Tb II	26.01
Ar II	24.32	Er II	29.41	Li I	49.21	Pd I	59.60	Te I	41.66
As I	30.04	Eu I	23.15	Li II	11.02	Pd II	53.24	Th I	31.81
Au I	22.14	Eu II	19.20	Lu I	29.78	Pr I	39.76	Th II	32.82
B I	0	F I	15.87	Lu II	45.60	Pr II	32.90	Ti I	57.03
B II	18.35	F II	37.73	Mg I	18.18	Pt I	24.23	Ti II	63.86
Ba I	16.42	Fe I	31.33	Mg II	2.82	Rb I	6.46	Tl I	61.86
Ba II	1.26	Fe II	21.04	Mn I	31.64	Re I	27.33	Tm I	42.35
Be I	4.90	Ga I	50.18	Mn II	20.60	Re II	28.59	Tm II	30.38
Be II	0.08	Ga II	0	Mo I	46.20	Rh I	20.93	U I	32.99
Bi I	35.42	Gd I	28.54	Mo II	58.00	Rh II	19.69	U II	33.72
C I	3.31	Gd II	30.53	N I	14.95	Ru I	22.21	V I	36.33
C II	9.56	Ge I	3.44	N II	19.24	Ru II	24.53	V II	37.56
Ca I	35.95	Ge II	0	Na I	29.59	S I	12.11	W I	28.59
Ca II	74.81	H I	9.96	Na II	40.39	S II	39.64	W II	21.17
Cd I	19.03	He I	20.24	Nb I	28.51	Sb I	42.14	Y I	26.11
Cd II	0	He II	73.56	Nb II	28.64	Sc I	20.68	Y II	25.68
Ce I	28.81	Hf I	32.17	Nd I	26.82	Sc II	34.46	Yb I	39.94
Ce II	27.34	Hf II	29.44	Nd II	27.34	Se I	0	Yb II	34.90
Cl I	7.50	Hg I	38.92	Ne I	4.58	Si I	32.63	Zn I	8.99
Cl II	26.32	Hg II	1.49	Ne II	53.62	Si II	11.84	Zn II	0.64
Co I	44.92	Ho I	30.14	Ni I	50.14	Sm I	27.51	Zr I	26.48
Co II	16.52	Ho II	33.10	Ni II	14.22	Sm II	26.55	Zr II	32.52
Cr I	57.03	In I	12.41	O I	32.59	Sn I	27.44		
Cr II	53.90	In II	5.04	O II	32.72	Sn II	0.32		
Cs I	3.33	Ir I	31.67	Os I	59.43	Sr I	35.95		

Table 36: Seven peaks from NIST SRM 1243 spectrum with each peak's top emitters and individual SIF values.

217.88 nm		224.08 nm		349.27 nm		549.00 nm		586.11 nm		650.73 nm		808.75 nm	
Elem	**SIF**	**Elem**	**SIF**	**Elem**	**SIF**	**Elem**	**SIF**	**Elem**	**SIF**	**Elem**	**SIF**	**Elem**	**SIF**
Cu I	0.9814	Co I	0.5120	Ni I	0.3375	Cr I	0.2730	Lu I	0.8238	Cr II	0.3377	O I	0.6264
Fe I	0.0183	Ti I	0.3954	Th II	0.2422	Cr II	0.2588	Eu I	0.1528	Ne II	0.3358	C I	0.3667
Cr II	0.0003	Fe I	0.0665	U II	0.2359	V I	0.1707	Mo I	0.0096	Li I	0.3082	Ca I	0.0066
Mn II	1.91E-05	Si I	0.0222	Mo I	0.0478	Ti I	0.1579	Sm I	0.0086	Ce II	0.0179	Mn II	0.0003
V II	7.15E-06	Cr II	0.0021	Co I	0.0378	Ni II	0.0683	Gd II	0.0018	Fe I	0.0002	He I	4.85E-07
Fe II	1.78E-06	Fe II	0.0014	Mn I	0.0169	Co I	0.0549	Ca I	0.0015	V I	0.0002	O II	3.52E-09
		V II	0.0002	Fe I	0.0168	Mo I	0.0152	Cr I	0.0009	Ar II	3.67E-07		
		V II	5.00E-05	Co II	0.0139	Ca I	0.0008	Ti I	0.0005				
		Sc II	2.63E-05	Ni II	0.0120	Fe I	0.0005	Fe I	0.0002				
		C II	2.45E-08	Fe II	0.0114	Ar I	1.82E-06	Ti II	7.47E-05				
				Tm II	0.0083	V II	1.72E-06	V I	3.47E-05				
				Ti II	0.0065	Mn II	3.90E-07	Fe II	2.51E-05				
				Gd II	0.0035	Fe II	3.28E-07	Sc II	7.26E-06				
				Er II	0.0026	P I	2.02E-07	Ni II	7.29E-09				

Optimal Set of Emitters

The number of emitters that have contribute to the individual SIF for the experimental spectrum of SRM 1243 is numerous which results in a large number of emitters in the no prior knowledge analyses. There are one-hundred and forty-seven emitters in the Kurucz database found within the spectral region of interest. The no prior knowledge optimal set of emitters needs ninety emitters, {Al I, Ar I, Ar II, As I, Ba I, Bi I, C I, Ca I, Ce I, Ce II, Cl I, Co I, Co II, Cr I, Cr II, Cu I, Cu II, Dy I, Dy II, Er I, Eu I, Fe I, Fe I, Fe II, Ga I, Gd I, Gd II, He I, Hf I, Hg I, Ho I, In I, Ir I, K I, La I, La II, Mg I, Mn I, Mn II, Mo I, N I, N II, Na I, Nb I, Nd I, Nd II, Ne I, Ne II, Ni I, Ni II, O I, Os I, Os II, P I, Pb I, Pd I, Pr I, Pr II, Pt I, Re I, Re II, Rh I, Ru I, Ru II, S I, Sb I, Sc I, Sc II, Si I, Sm I, Sm II, Sn I, Sr I, Ta I, Ta II, Te I, Th I, Th II, Ti I, Ti II, Tl I, U I, U II, V I, V II, W I, Y I, Yb I, Yb II, Zr I}. There are nineteen elements in the SRM 1243 sample composition which amounts to thirty-eight total emitters of neutral and singly-ionized, thus seventy of the no prior knowledge optimal emitters are not needed when the sample composition is known. Given the sample composition of SRM 1243, the qualitative prior knowledge analysis needs thirty emitters to explain the spectrum. The optimal set of emitters for the qualitative prior knowledge is {Al I, Al II, C I, Co I, Co II, Cr I, Cu I, Cu II, Fe I, Fe II, Mn I, Mn II, Mo I, Mo II, Nb I, Ni I, Ni II, P I, S I, Si I, Ta I, Ta II, Ti I, Ti II, V I, V II, W I, Zr I, Zr II}. The quantitative prior knowledge optimal set of emitters is {Al I, Al II, C I, Co I, Co II, Cr I, Cr II, Cu I, Cu II, Fe I, Fe II, Mn I, Mn II, Mo I, Nb I, Ni I, Ni II, P I, P II, S I, Si I, Ti I, Ti II, V I, V II, W I, Zr I}. The quantitative set of emitters different than the qualitative are the absence of {Mo II, Ta I, Ta II, Zr II} and the presence of P II.

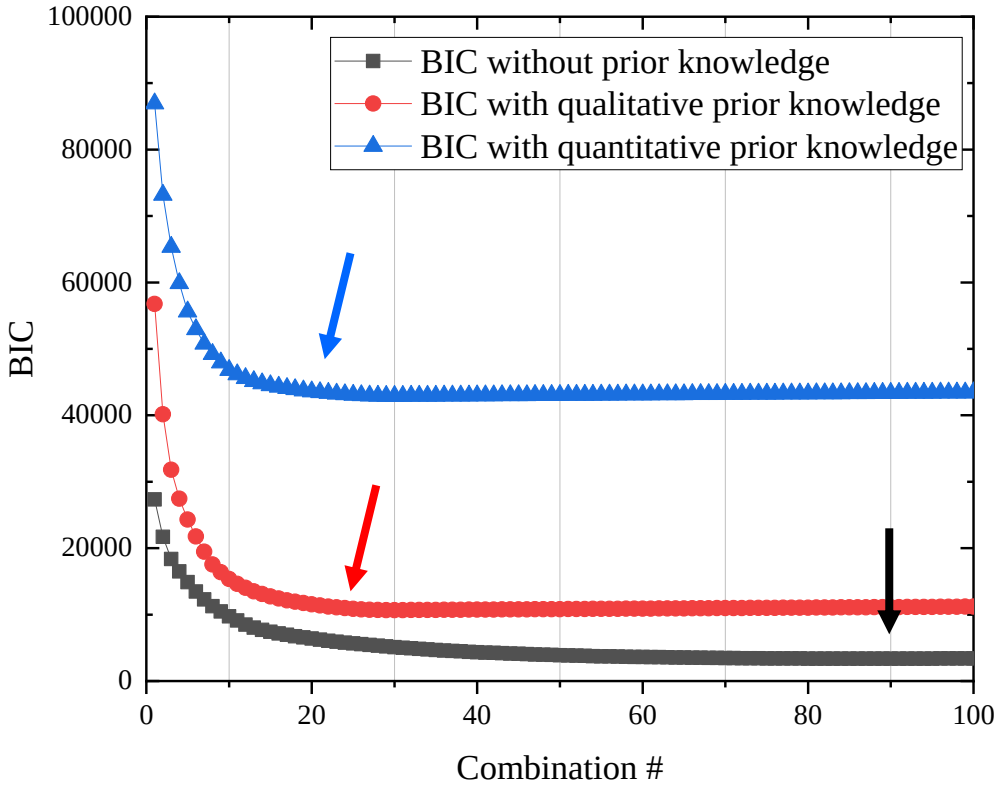

Figure 33: BIC graph of NIST SRM 1243.

Posterior SIF

Each prior knowledge analyses with their optimal set of emitters calculated the posterior SIF for every experimental peak. NIST SRM 1243 has many peaks thus a small subset of twenty peaks are shown in Figures 34-36 representative of the entire spectrum. Four of the twenty peaks, showed no spectral interferences and the same sole emitter for all three knowledge analyses. Peaks 212.42 nm, 217.88 nm, 224.08 nm, 341.44 nm, and 349.27 nm are produced from the sole emitters of Si I, Cu I, Co I, Ni I, and Ni I, respectively. These peaks are judged reliable for line

assignment because no matter the prior knowledge, these peaks are assigned the same with no spectral interferences. Peaks 205.51 nm, 212.82 nm, and 549.00 nm have different elemental profiles in the quantitative prior knowledge compared to the no prior and qualitative prior. Singly-ionized copper is the sole emitter for peak 205.51 nm in the no prior and qualitative prior. Copper is found in SRM 1243 in lower concentrations than chromium which decrease the quantitative individual SIF of Cu II and increases Cr I. Based on the quantitative prior knowledge combination of the optimal set of emitters, peak 205.51 nm has a higher likelihood with Cr I than Cu II. Peak 212.82 nm is has V II as the sole emitter but with quantitative prior knowledge that peak is attributed to Cr I. Nickel is found in higher mass fraction than chromium which results in the assignment of peak 549.00 nm as Ni I in the quantitative prior knowledge whereas it was attributed to Cr I for no prior and qualitative prior knowledge analyses.

Input of the prior knowledge of the sample results in a same elemental profile of peaks 211.28 nm, 417.18 nm, 595.64 nm, and 747.32 nm. The no prior knowledge analysis had the sole emitter of Ir I, Ga I, Pr II, and O I respectively. Based on the prior knowledge of the sample composition and the optimal set of emitters, these peaks are attributed to Ni I, Ga I, W I, and C I respectively. Addition of the prior knowledge can reduce the spectral interferences in the posterior SIF. Peaks 448.14 nm and 650.73 nm had a main emitter of Cr I with large interferences from Ti I. The quantitative prior knowledge and the combinations of the optimal set of emitters result in complete assignment of peaks 448.14 nm and 650.73 nm to Cr I with no interference from Ti I. Quantitative prior knowledge analysis of peaks 441.72 nm, 573.96 nm, and 638.53 nm result in different assignment than the no prior and qualitative prior. Peaks

441.72 nm and 573.96 nm have a main emitter of Cr I with a small interference from Ti I for the no prior and qualitative prior knowledge analyses. These peaks have multiple possible emitters which include Cr I, Ti I, and Ni I that have individual SIF values close together. The combination of the optimal set of emitters for the quantitative knowledge results in assignment of peaks 441.72 nm and 573.96 nm as Ni II instead of Cr I or Ti I because nickel is found in the SRM 1243 sample with the highest concentration. Peak 638.53 nm has a main emitter of Cr II with a small interference from Nd II which is not present in the sample composition. Qualitative prior knowledge assigns Cr I to be the sole emitter of peak 638.53 nm while quantitative prior knowledge Ni II.

Peaks 271.40 nm, 586.11 nm, and 808.75 nm have different elemental profiles for all knowledge analyses. The no prior knowledge analysis of peaks 271.40 nm, 586.11 nm, and 808.75 nm have a sole emitter of La I, Eu I, and Sc II respectively. These elements are not present in the sample composition which is why the prior knowledge analyses have different emitters for these peaks. Qualitative prior knowledge of peaks 271.40 nm, 586.11 nm, and 808.75 nm have one emitter of Zr II, Mo I, and P I respectively. The quantitative prior knowledge analysis of these peaks results in the sole contribution of Ti II, Cr I, and Cr I respectively. The concentration plays a major role in line assignment for the prior knowledge. Peaks 271.40 nm, 586.11 nm, and 808.75 nm qualitative prior knowledge analysis combinations use the emitter found in the sample with the highest individual SIF for each peak which defines their elemental profile. Addition of the concentration to the individual SIF affects an emitter's value which is used by the combination of the optimal emitters to determine the peak assignment with the highest likelihood.

The same main emitter for the qualitative and no prior knowledge analyses occurred 46.81% because they have a number of optimal set of emitters in common. No prior and quantitative prior knowledge have the same emitter with the highest SIF for 23.09%. The qualitative and quantitative prior knowledge analyses had 44.47% experimental peaks that had the occurrence of the same main emitter. All prior knowledge analyses had the same main contributor 23.14%. This low percentage is attributed to the fact that no prior knowledge analysis optimal set of emitters was so large because there were so many emitters with at least one contribution to the experimental spectrum

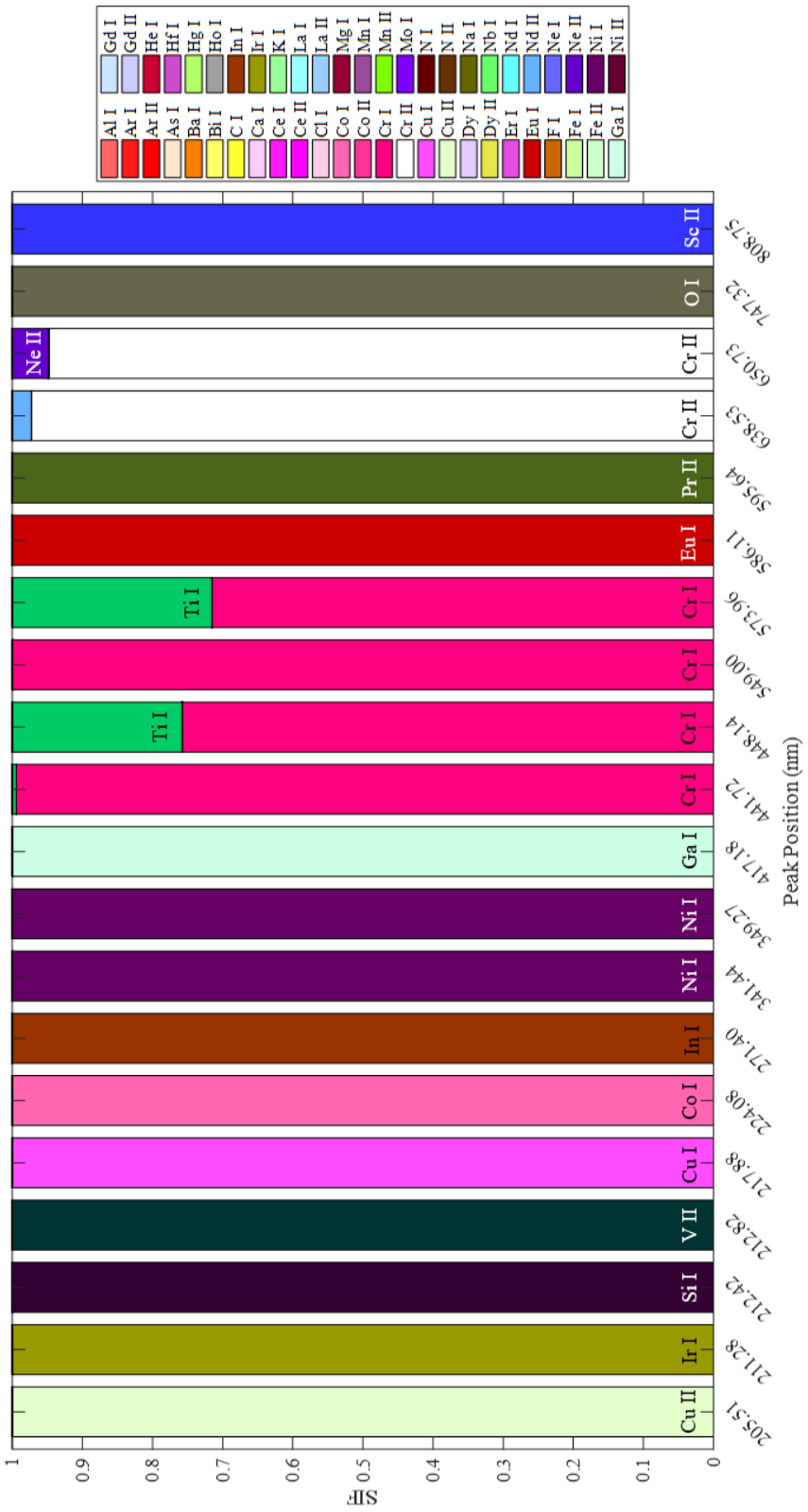

Figure 34: Posterior SIF of NIST SRM 1243 – No Prior.

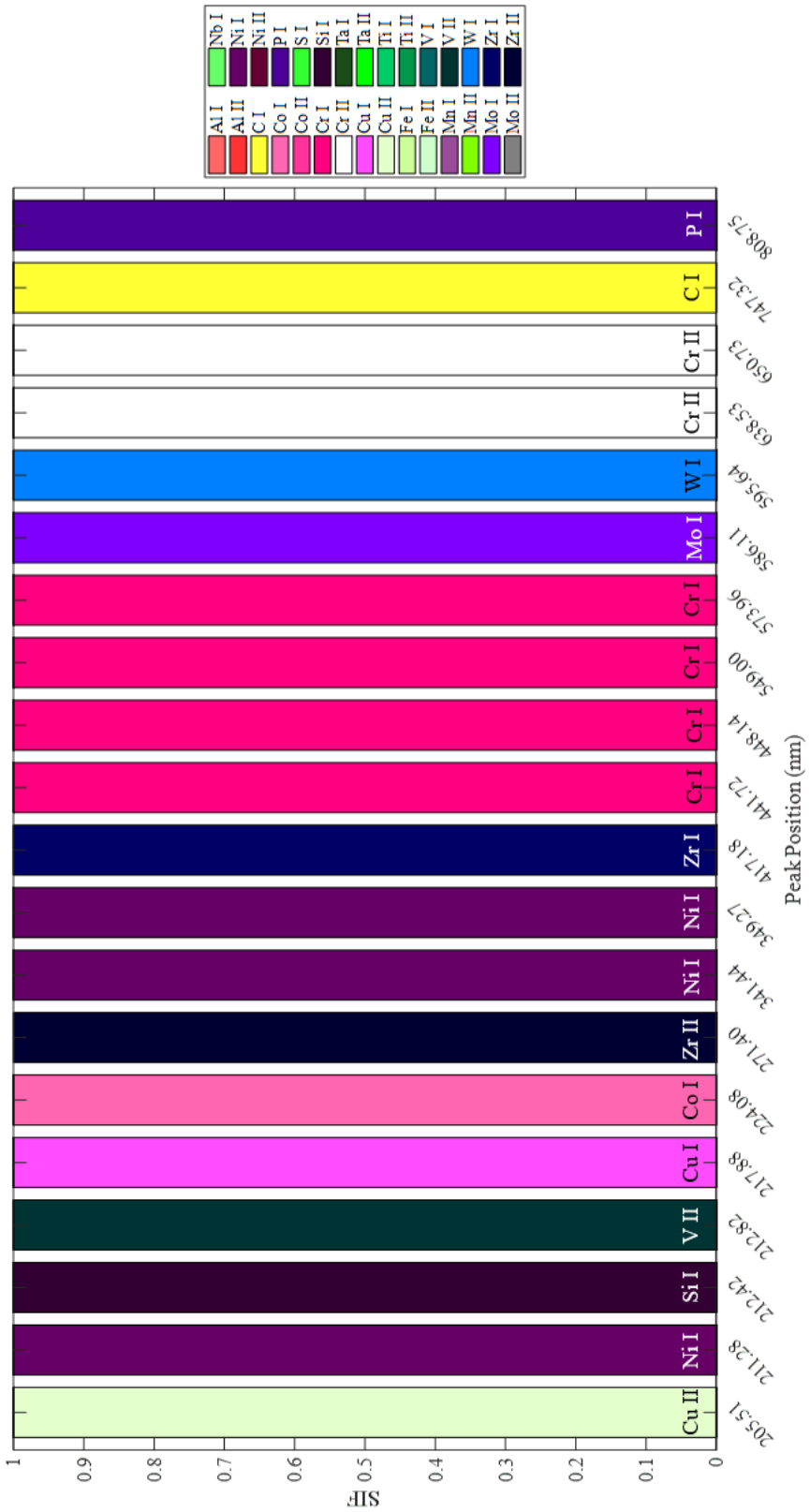

Figure 35: Posterior SIF of NIST SRM 1243 - Qualitative Prior.

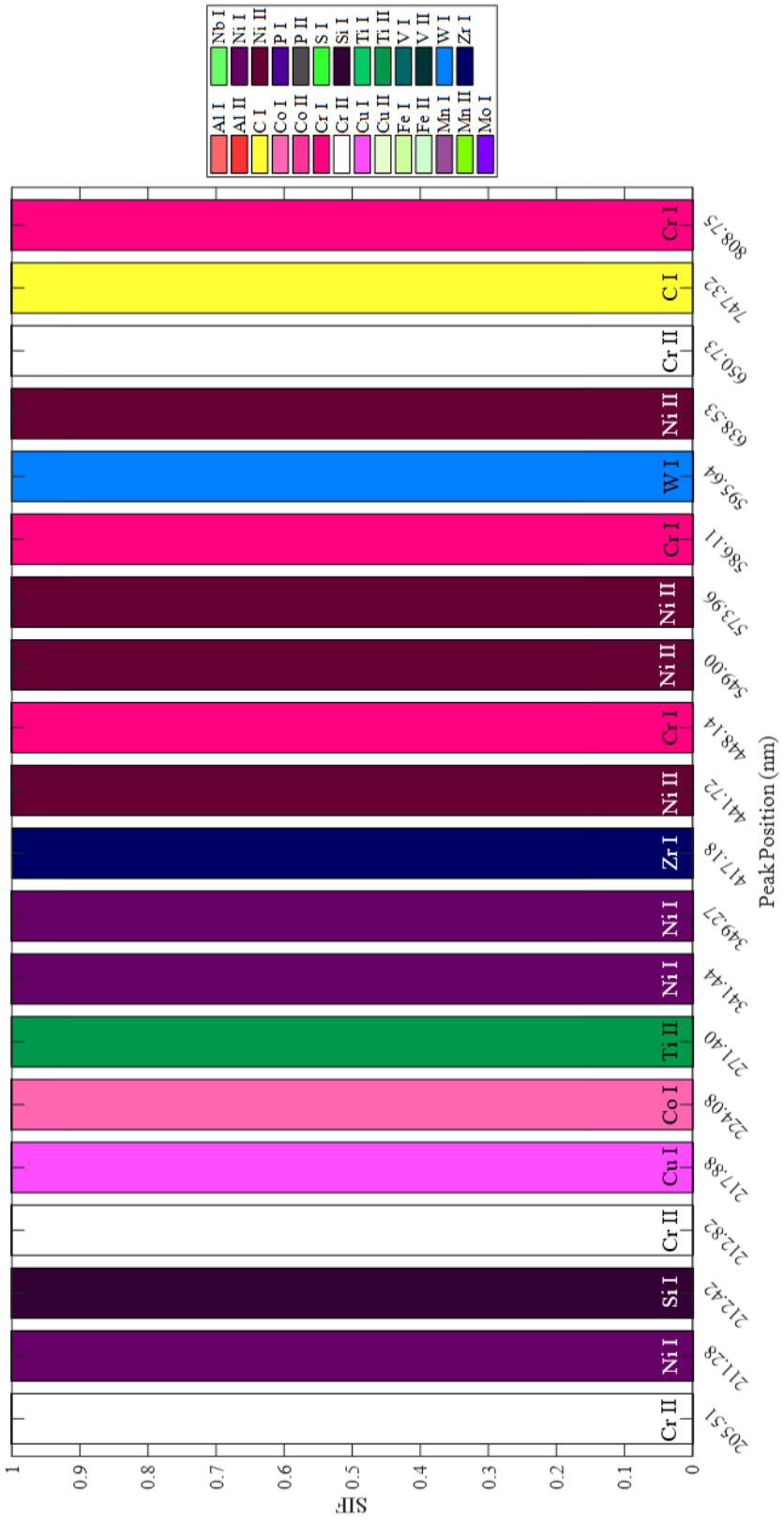

Figure 36: Posterior SIF of NIST SRM 1243 - Quantitative Prior.

Nickel Spiked Alumina

In order to evaluate the SIF for spectral lines interfered by an element at different concentrations, we prepared pellets of pure alumina (Al_2O_3) samples with varied nickel doping concentrations (0, 1000, and 2000 ppm wt). The procedure for their preparation and acquisition of LIBS data is found in Pandey article[121]. The wavelength region of interest was from 300 nm to 307 nm. The molar concentration of the elements present in the nickel doped alumina are shown in Table 37 that were used for the prior knowledge of the sample's composition.

Table 37: Molar concentration of Ni-spiked alumina powder pellets.

	0 ppm (%wt)	**1000 ppm (%wt)**	**2000 ppm (%wt)**
Element	**Molar Concen. (M)**	**Molar Concen. (M)**	**Molar Concen. (M)**
Al I	0.0156	11.96	5.98
Al II	0.0156	11.96	5.98
Cl I	0	0.0838	0.0847
Cl II	0	0.0838	0.0847
Ni I	0	0.0419	0.0423
Ni II	0	0.0419	0.0423
O I	0.0139	4.49	2.24
O II	0.0139	4.49	2.24

There were eight detected peaks from the blank nickel spiked alumina spectrum in Figure 37 (black): 302.55 nm, 304.24 nm, 305.02 nm, 305.47 nm, 305.72 nm, 305.87 nm, 306.44 nm, and 306.60 nm. The 1000 ppm and 2000 ppm nickel doped alumina had thirteen detected peaks which included the eight peaks present in the 0 ppm. In Figure 37, the experimental peaks not present in the blank, but the 1000 ppm (red) and 2000 ppm (blue) include 301.20 nm, 301.91 nm,

302.45 nm, 303.47 nm, and 303.79 nm. There are a total of one-hundred and ninety-eight nickel and aluminum transitions that are found in the Kurucz database for the wavelength region of 300 nm to 307 nm. The probability of emission for seventeen transitions of aluminum and nickel are shown in Figure 37 by the drop-down lines with aluminum in brown and nickel in green. The peaks at 301.20 nm, 301. 87 nm, and 303. 79 nm are clearly assigned to nickel because they increase in intensity with the increase in the concentration of the nickel doping the alumina and their absence in the blank alumina sample.

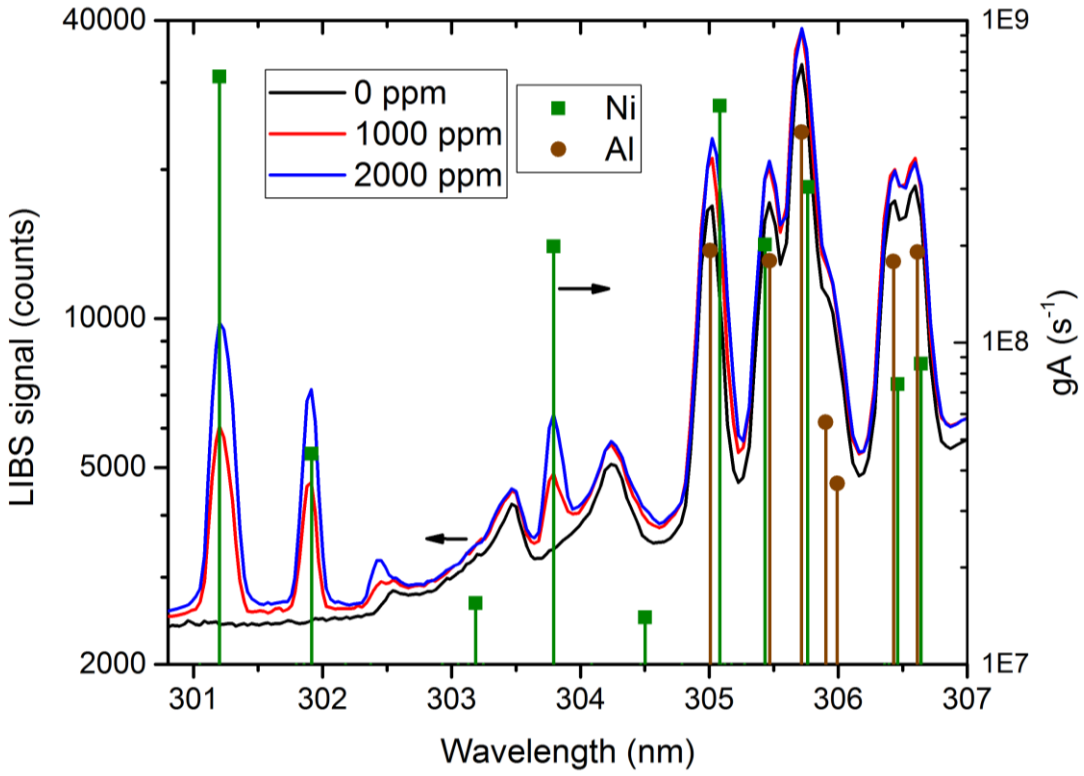

Figure 37: LIBS spectra of Ni-spiked alumina powder pellets[111].

Nickel Spiked Alumina – 0 ppm

For the eight experimental peaks of the blank nickel spiked alumina sample, the top eighteen elements and their individual SIF are shown in Table 38. It is expected that Al I or Al II be the top emitter for each peak. For peaks 305.02 nm to 306.60 nm, Al I has an individual SIF in the top five emitters. Peaks 302.55 nm and 304.24 nm do have a singly-ionized aluminum emitter, but its transition has very small SIF less than $1.0 * 10^{-7}$.

With the individual SIF and their emitters, the elements are ordered for the no prior knowledge analyses with Al I ordered third and Al II ninth (Table 39). The smallest BIC value is 38.62 which means the optimal set of ions for the blank nickel doped alumina is five: {Cr II, Th II, Al I, Bi I, Ir II}. With the addition of the neutral emitters of the singly-ionized emitters in the optimal set, the set becomes {Al I, Bi I, Cr I, Cr II, Ir I, Ir II, Th I, Th II}.

Table 38: Ni-spiked alumina spectral peaks (0 ppm) with each peak's top emitters and individual SIF values.

302.55 nm		304.24 nm		305.02 nm		305.47 nm		305.72 nm		305.87 nm		306.44 nm		306.60 nm	
Elem	**SIF**	**Elem**	**SIF**	**Elem**	**SIF**	**Elem**	**SIF**	**Elem**	**SIF**	**Elem**	**SIF**	**Elem**	**SIF**	**Elem**	**SIF**
Bi I	0.661	Ir II	0.206	Th II	0.306	Al I	0.138	Al I	0.503	Cr II	0.083	Al I	0.2160	Co II	0.1378
W I	0.046	W I	0.118	Os I	0.137	Os I	0.137	Th II	0.156	Os I	0.077	U II	0.2088	Th II	0.1227
Th II	0.034	Os II	0.117	Al I	0.096	Y II	0.089	Ta II	0.139	Th II	0.066	Mo I	0.0789	Cr II	0.1194
Co II	0.030	Os I	0.102	Ni I	0.092	Zr II	0.086	Ni I	0.061	Al I	0.066	Yb II	0.0734	Er II	0.0851
Er II	0.021	U II	0.081	Er II	0.091	Cr II	0.075	Hf I	0.039	Zr II	0.065	Cr II	0.0537	Al I	0.0754
Cr II	0.021	Re I	0.053	U II	0.070	Re I	0.069	Ni II	0.027	Ni I	0.065	Pt I	0.0531	Mn I	0.0620
Zr II	0.018	Ta II	0.041	Ni II	0.041	Hf II	0.055	Co I	0.015	Ca II	0.060	Zr II	0.0411	V II	0.0556
Co I	0.015	Cr II	0.029	Ta I	0.038	Co I	0.054	Fe I	0.009	Ti I	0.052	Nb II	0.0336	Mo I	0.0530
Hf II	0.015	Co I	0.028	Cr II	0.028	Mn I	0.047	Cr II	0.009	Co I	0.049	Ni I	0.0324	V I	0.0489
Ir I	0.013	Ru I	0.026	Co I	0.019	Ni I	0.044	Rh I	0.006	V II	0.043	Co I	0.0315	Nb II	0.0480
Mn I	0.012	Yb II	0.024	Hf I	0.018	Fe I	0.034	Fe II	0.005	Mn I	0.041	Mn I	0.0268	Fe I	0.0450
Mo I	0.011	Dy II	0.024	Mn I	0.015	Mn II	0.031	Re I	0.004	Re I	0.041	Ru I	0.0216	Mn II	0.0410
U II	0.011	Mo I	0.022	Mn II	0.011	Ni II	0.028	Mn I	0.004	V I	0.040	Fe I	0.0195	Ni II	0.0373
Dy II	0.011	Mn I	0.021	V II	0.008	Tm II	0.028	V II	0.004	Dy II	0.034	Mn II	0.0177	Cr I	0.0256
Nb II	0.011	Cu II	0.020	V I	0.007	Fe II	0.017	V I	0.004	Fe I	0.031	Ni II	0.0167	Fe II	0.0230
Ta I	0.010	Th II	0.017	W I	0.006	V II	0.017	Zr II	0.003	Ce II	0.030	Cr I	0.0114	Ru I	0.0072
Ce II	0.010	Fe I	0.016	Y II	0.006	Cr I	0.016	Mn II	0.003	Ni II	0.029	Hf II	0.0110	Os I	0.0039
Fe I	0.009	Ni II	0.015	Fe II	0.006	V I	0.014	Ti II	0.002	Mn II	0.027	Re I	0.0106	Ti II	0.0026

Table 39: No prior BIC ordering of Ni-spiked alumina – 0 ppm.

Emitter	BIC
Cr II	62.10
Cr II, Th II	48.22
Cr II, Th II, Al I	44.09
Cr II, Th II, Al I, Bi I	40.35
Cr II, Th II, Al I, Bi I, Ir II	38.62
Cr II, Th II, Al I, Bi I, Ir II, U II	39.96
Cr II, Th II, Al I, Bi I, Ir II, U II, Co II	41.92
Cr II, Th II, Al I, Bi I, Ir II, U II, Co II, Al II	44.12

Given the prior knowledge of the blank nickel spiked alumina sample, the optimal set of emitters for the qualitative prior knowledge is two (Table 40). They are Al I and Al II. Quantitative prior knowledge of the molar concentration for the elements in the alumina sample results in the same set of emitters as the qualitative prior analyses {Al I, Al II}. Neutral and singly-ionized aluminum are the two elements common to all three types of prior knowledge.

Table 40: Prior knowledge BIC ordering of NI-spiked alumina – 0 ppm.

Emitter	BIC
Al I	265.46
Al I, Al II	151.83
Al I, Al II, O I	153.91
Al I, Al II, O I, O II	155.98

Posterior SIF

From the optimal set of emitters, the number of combinations of the eight experimental peaks is 288,000. Figure 38 shows the posterior SIF of the combinations for all three knowledge analyses. For the no prior analyses, peaks 305.72 nm and 306 .44 nm have no spectral interferences and assigns these peaks to Al I which is seen in the qualitative and quantitative analyses. Peaks 302.55 nm and 304.24 nm in the qualitative and quantitative assign these peaks to Al II but with the no prior knowledge analyses, Al II is not present. No prior knowledge assigns Bi I and Ir II to peaks 302.55 nm and 304.24 nm respectively. Peaks 305.02 nm, 305.47 nm, 305. 87 nm, and 306.60 nm have main contributions from Al I but have spectral interferences from Cr II in the no prior knowledge analyses. Line assignment of peaks 305.72 nm and 306.44 nm with Al I agrees with all three knowledge analyses which means that these peaks can be confidently used for line assignment.

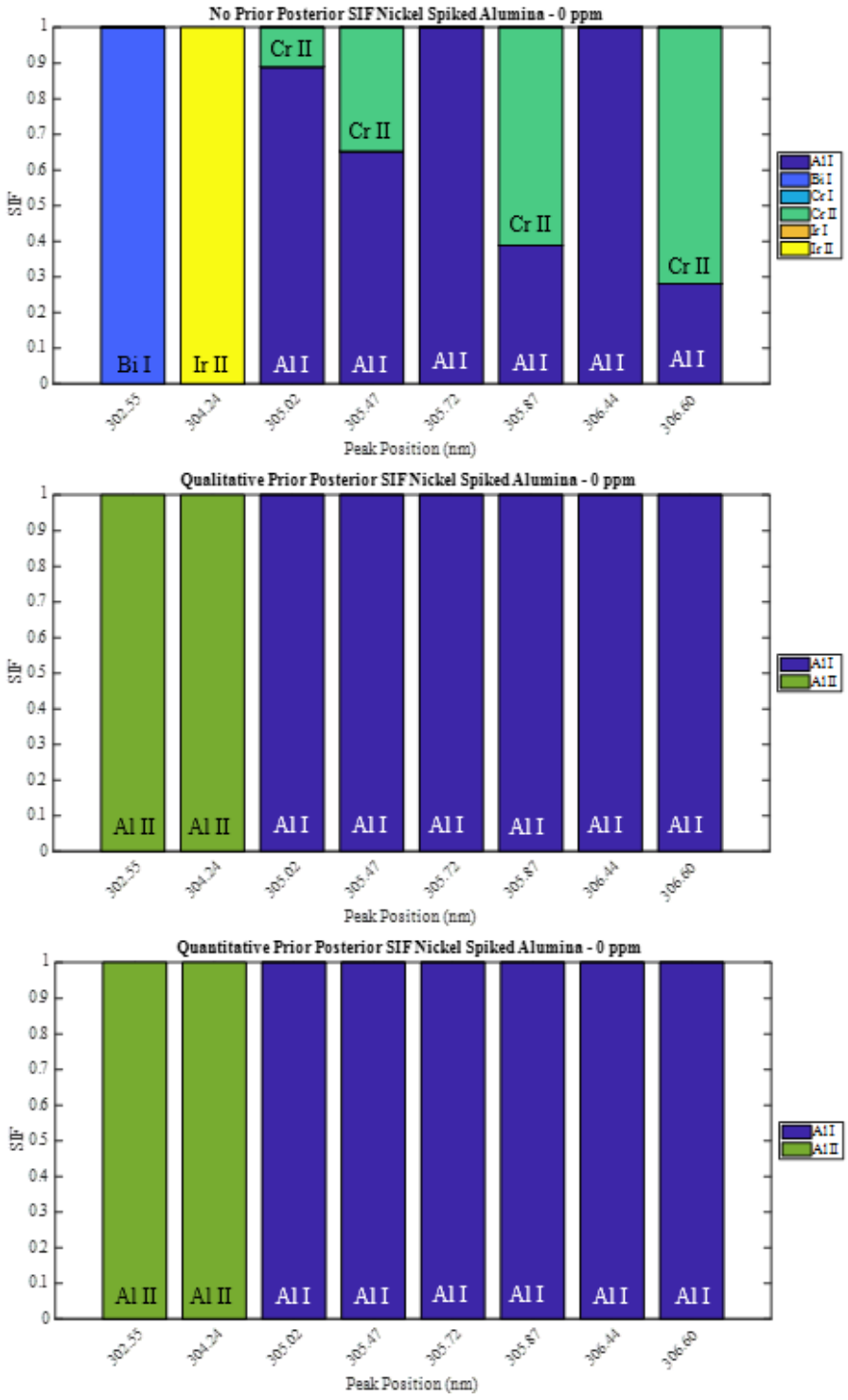

Figure 38: Posterior SIF for Ni-spiked alumina – 0 ppm (Top) No Prior (Middle) Qualitative Prior (Bottom) Quantitative Prior

Nickel Spiked Alumina – 1000 ppm

For the thirteen experimental peaks of the 1000 ppm nickel spiked alumina sample, the top eighteen elements and their individual SIF for five peaks are shown in Table 41. It is expected that Al I, Al II, Ni I, and Ni II be one of the top emitters for each peak. Peaks 301.20 nm, 301.91 nm, 302.45 nm, 303.47 nm, and 303.79 have either neutral or singly-ionized nickel as an emitter of the peak. This is expected as these peaks were not present in the blank nickel spiked alumina samples. Peaks 305.02 nm, 305.47 nm, 305.72 nm, 305.87 nm, 306.44 nm, and 306.60 nm have both aluminum and nickel ions present within the top five emitters. Peaks 302.55 nm and 304.24 nm have small SIF values for both Ni II and Al I.

Table 41: Ni-spiked alumina spectral peaks (1000 ppm) with each peak's top emitters and individual SIF values.

301.20 nm		302.45 nm		303.79 nm		305.72 nm		306.44 nm	
Elem	**SIF**	**Elem**	**SIF**	**Elem**	**SIF**	**Elem**	**SIF**	**Elem**	**SIF**
Ta II	0.419	Ni I	0.090	Ni I	0.427	Al I	0.408	Al I	0.228
Ni I	0.337	Cr II	0.064	Ta II	0.129	Ta II	0.292	U II	0.160
Th II	0.077	Co II	0.057	U II	0.118	Th II	0.116	Mo I	0.083
Zr I	0.054	Zr II	0.054	Dy II	0.059	Ni I	0.084	Ni I	0.058
Co II	0.019	Er II	0.054	Fe I	0.057	Ni II	0.022	Pt I	0.056
U II	0.016	Th II	0.053	Ni II	0.038	Hf I	0.016	Cr II	0.051
Fe I	0.011	Co I	0.042	Mn II	0.031	Co I	0.012	Yb II	0.045
Cu II	0.009	Ti I	0.041	Re I	0.031	Fe I	0.009	Zr II	0.043
Mn I	0.009	Rh I	0.041	Cr II	0.030	Cr II	0.006	Nb II	0.035
Re I	0.009	Mn I	0.039	Fe II	0.025	Rh I	0.005	Co I	0.033
Mn II	0.008	Re I	0.039	Mn I	0.018	Re I	0.004	Mn I	0.031
Cr II	0.006	Ru I	0.038	V I	0.009	Fe II	0.004	Mn II	0.028
Fe II	0.005	Mn II	0.035	Ru I	0.008	Mn I	0.004	Fe I	0.025
Cu I	0.004	Cu I	0.033	Cr I	0.007	Mn II	0.003	Ru I	0.025
Ta I	0.004	Fe I	0.033	Ce II	0.006	V II	0.003	Ni II	0.017

Optimal Set of Emitters

For the no prior analyses, of the nickel spiked alumina 1000 ppm by weight, the optimal set of emitters is determined to be {Al I, Bi I, Ir I, Ir II, Mn I, Ni I, Th II}. Neutral nickel and neutral aluminum are the only two elements present in the sample composition. Singly-ionized aluminum is ordered tenth but was not included because the smallest BIC value of 55.80 did not include it.

Table 42: No prior BIC ordering of Ni-spiked alumina – 1000 ppm.

Emitter	BIC
Mn I	100.21
Mn I, Ni I	73.01
Mn I, Ni I, Th II	67.31
Mn I, Ni I, Th II, Bi I	61.65
Mn I, Ni I, Th II, Bi I, Al I	57.73
Mn I, Ni I, Th II, Bi I, Al I, Ir II	55.80
Mn I, Ni I, Th II, Bi I, Al I, Ir II, Co II	57.63
Mn I, Ni I, Th II, Bi I, Al I, Ir II, Co II, Ta II	59.76
Mn I, Ni I, Th II, Bi I, Al I, Ir II, Co II, Ta II, U II	61.93
Mn I, Ni I, Th II, Bi I, Al I, Ir II, Co II, Ta II, U II, Al II	64.49

The greedy search ordering of the emitters for the qualitative prior knowledge analyses was Ni II, Ni I, Al I, and Al II. Based on the lowest BIC score of 72.25, the optimal set of emitters is {Al I, Ni I, Ni II} which does not include Al II. Singly-ionized aluminum is the next ordered element thus if the analyses included more emitters than the smallest amount, Al II would be included.

Table 43: Qualitative prior BIC ordering of Ni-spiked alumina – 1000 ppm.

Emitter	BIC
Ni II	127.53
Ni II, Ni I	78.24
Ni II, Ni I, Al I	72.25
Ni II, Ni I, Al I, Al II	74.81

The optimal set of emitters for the quantitative prior knowledge of the nickel spiked aluminum 1000 ppm is {Al I, Al II, Ni I, Ni II}. All of the elements present in the sample composition are needed to explain the thirteen peaks in the spectral region of interest. There are two elements, Al I and Ni I, which are common to the no prior, qualitative prior, and quantitative prior analyses.

Table 44: Quantitative prior BIC ordering of Ni-spiked alumina – 1000 ppm.

Emitter	BIC
Ni II	210.019
Ni II, Al I	125.706
Ni II, Al I, Ni I	88.817
Ni II, Al I, Ni I, Al II	85.149

Posterior SIF

Eight of the thirteen experimental peaks for the no prior knowledge have one elemental assignment for their posterior SIF (Figure 39 top). Peaks 301.91 nm, 302.55 nm, 303.47 nm, and 304.24 nm have one contributor of Mn I, Bi I, Th II, and Ir II respectively. Nickel I is the sole

emitter for 301.20 nm and 303.79 nm. There are other peaks that have neutral nickel as an emitter, but these peaks are interfered. Peaks 302.45 nm, 305.02 nm, 305.47 nm, and 305.87 nm have more than one emitter resulting in interference. Neutral nickel causes small interferences of peak 305.02 nm and 305.47 nm with Th II and Al I respectively. Peak 302.45 nm has a main emitter of Ni I with large interferences from Mn I and Th II. Peak 305.87 nm also has a main emitter of Ni I with large interference from Th II and Al I. Peak 306.60 nm has large interferences from Al I and Mn I with the main contribution from Th II.

In Figure 39, the middle graph shows the qualitative prior posterior SIF for the nickel doped alumina 1000 ppm by weight. Eight of the thirteen peaks have one emitter. Peaks 301.20 nm, 302.45 nm, and 303.79 nm come from Ni I emissions. Singly-ionized nickel is the sole contributor to peaks 302.55 nm, 303.47 nm, and 304.24 nm. Peak 301.91 nm has a main emitter of Ni II with a small interference from Ni I. The assignment of this peak can be contributed to nickel because both possible emitters come from nickel. Neutral aluminum can be found in peaks 305.02 nm to 306.60 nm with 305.72 nm and 306.44 nm having no spectral interferences. Neutral nickel is the main contributor to peaks 305.02 nm and 305.87 nm with large interferences from Al I. Aluminum I is the main emitter for peaks 305.47 nm and 306.60 nm with large interferences from Ni I and Ni II respectively.

Eight peaks in the quantitative prior posterior SIF have a SIF of 100% (Figure 39 bottom). Peak 301.20 was assigned Ni I. Peaks 303.47 nm, and 304.24 nm have the sole contribution from Ni

II. Peaks 305.47 nm, 305.72nm, 306.44nm, and 306.60 nm are assigned Al I. Neutral and singly-ionized nickel create spectral interferences in peaks 301.91 nm and 303.79. Although these peaks have interferences, the assignment of peak 301.91 nm and 303.79 nm can be assigned to nickel due to both nickel emitters being possible emitters of the peaks. There are three peaks common to all three knowledge analyses which have 100% SIF assignment. Peaks 302.55 nm, 305.02 nm, and 305.87 nm have very small interferences. The main contributor to peak 302.55 nm is Ni II with a small interference from Al I. Peaks 305.02 nm and 305.87 nm have a main emitter of Al I with a small interference from Ni I. Peaks 301.20 nm, 305.72 nm, and 306.44 nm can be used for assignment of Ni I, Al I, and Al I respectively.

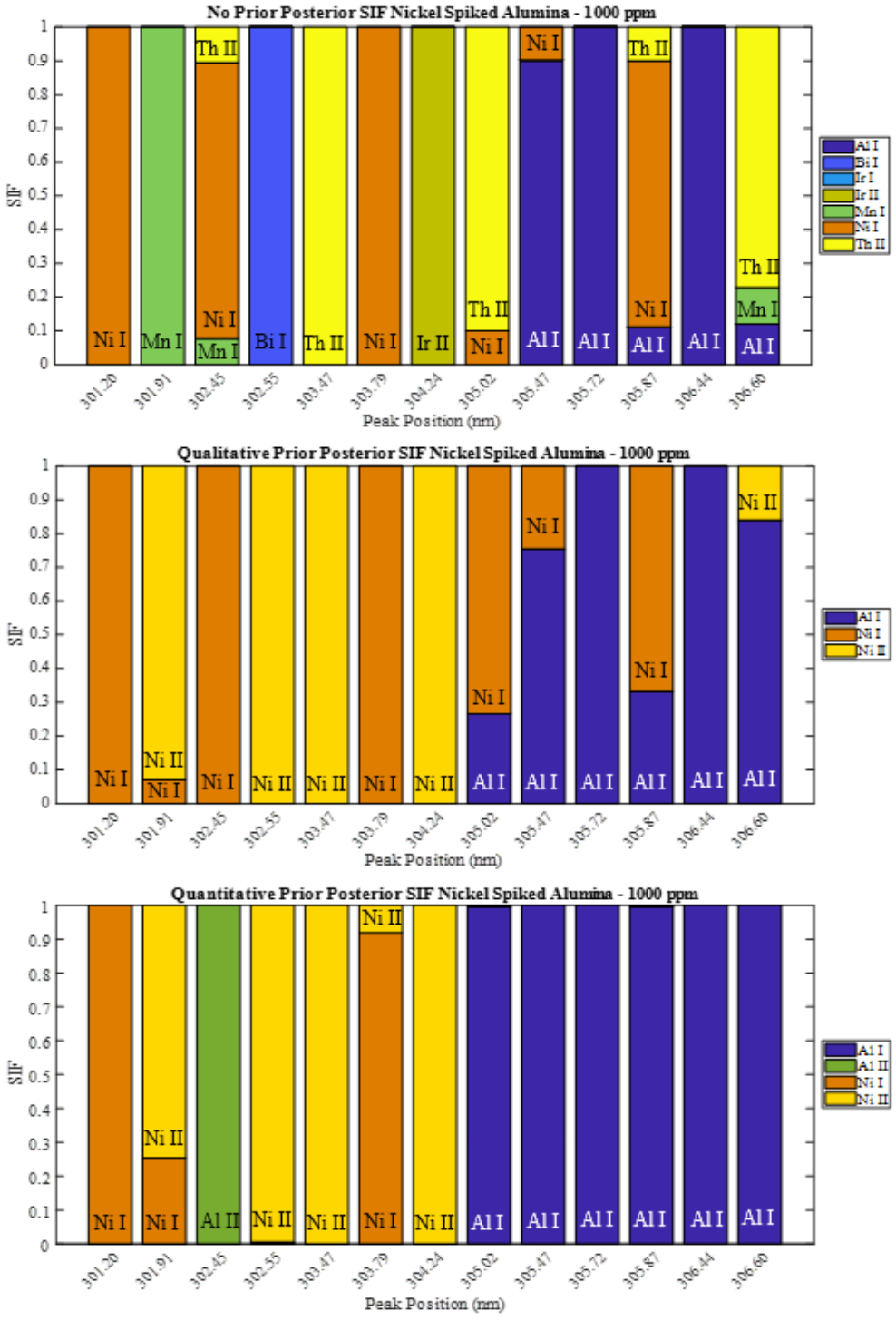

Figure 39: Posterior SIF for Ni-spiked alumina – 1000 ppm (Top) No Prior (Middle) Qualitative Prior (Bottom) Quantitative Prior.

Nickel Spiked Alumina – 2000 ppm

For the thirteen experimental peaks of the 2000 ppm nickel spiked alumina sample, the top eighteen elements and their individual SIF for five peaks are shown in Table 45. It is expected that Al I, Al II, Ni I, and Ni II be one of the top emitters for each peak. Peaks 301.20 nm, 301.91 nm, 302.45 nm, 303.47 nm, and 303.79 have either neutral or singly-ionized nickel as an emitter of the peak. This is expected as these peaks were not present in the blank nickel spiked alumina samples. Peaks 305.02 nm, 305.47 nm, 305.72 nm, 305.87 nm, 306.44 nm, and 306.60 nm have both aluminum and nickel ions present within the top five emitters. Peaks 302.55 nm and 304.24 nm have small SIF values for both Ni II and Al I.

Table 45: Ni-spiked alumina spectral peaks (2000 ppm) with each peak's top emitters and individual SIF values.

301.20 nm		302.45 nm		303.79 nm		305.72 nm		306.44 nm	
Elem	**SIF**	**Elem**	**SIF**	**Elem**	**SIF**	**Elem**	**SIF**	**Elem**	**SIF**
Ta II	0.419	Ni I	0.090	Ni I	0.427	Al I	0.408	Al I	0.228
Ni I	0.337	Cr II	0.064	Ta II	0.129	Ta II	0.292	U II	0.160
Th II	0.077	Co II	0.057	U II	0.118	Th II	0.116	Mo I	0.083
Zr I	0.054	Zr II	0.054	Dy II	0.059	Ni I	0.084	Ni I	0.058
Co II	0.019	Er II	0.054	Fe I	0.057	Ni II	0.022	Pt I	0.056
U II	0.016	Th II	0.053	Ni II	0.038	Hf I	0.016	Cr II	0.051
Fe I	0.011	Co I	0.042	Mn II	0.031	Co I	0.012	Yb II	0.045
Cu II	0.009	Ti I	0.041	Re I	0.031	Fe I	0.009	Zr II	0.043
Mn I	0.009	Rh I	0.041	Cr II	0.030	Cr II	0.006	Nb II	0.035
Re I	0.009	Mn I	0.039	Fe II	0.025	Rh I	0.005	Co I	0.033
Mn II	0.008	Re I	0.039	Mn I	0.018	Re I	0.004	Mn I	0.031
Cr II	0.006	Ru I	0.038	V I	0.009	Fe II	0.004	Mn II	0.028
Fe II	0.005	Mn II	0.035	Ru I	0.008	Mn I	0.004	Fe I	0.025
Cu I	0.004	Cu I	0.033	Cr I	0.007	Mn II	0.003	Ru I	0.025
Ta I	0.004	Fe I	0.033	Ce II	0.006	V II	0.003	Ni II	0.017

Optimal Set of Emitters

The greedy search ordering of the elements for the no prior analyses of the nickel spiked alumina 2000 ppm by weight is the same order as the 1000 ppm. The optimal set of emitters for the no prior knowledge are {Al I, Bi I, Ir I, Ir II, Mn I, Ni I, Th II} as the BIC of the ordered elements are identical to the 1000 ppm.

Table 46: No prior BIC ordering of Ni-spiked alumina – 2000 ppm.

Emitter	BIC
Mn I	100.21
Mn I, Ni I	73.01
Mn I, Ni I, Th II	67.31
Mn I, Ni I, Th II, Bi I	61.65
Mn I, Ni I, Th II, Bi I, Al I	57.73
Mn I, Ni I, Th II, Bi I, Al I, Ir II	55.80
Mn I, Ni I, Th II, Bi I, Al I, Ir II, Co II	57.63
Mn I, Ni I, Th II, Bi I, Al I, Ir II, Co II, Ta II	59.76
Mn I, Ni I, Th II, Bi I, Al I, Ir II, Co II, Ta II, U II	61.93
Mn I, Ni I, Th II, Bi I, Al I, Ir II, Co II, Ta II, U II, Al II	64.49

The optimal set of emitters for the qualitative prior knowledge for the 2000 ppm nickel spiked alumina are also identical to the 1000 ppm qualitative prior knowledge. Singly-ionized aluminum is still not included in the optimal set and the smallest number of emitters to explain the experimental spectrum is three: {Al I, Ni I, Ni II}.

Table 47: Qualitative prior BIC ordering of Ni-spiked alumina – 2000 ppm.

Emitter	BIC
Ni II	127.53
Ni II, Ni I	78.24
Ni II, Ni I, Al I	72.25
Ni II, Ni I, Al I, Al II	74.81

The ordering of the quantitative prior knowledge of the nickel spiked aluminum 2000 ppm is Ni II, Al I, Ni I, and Al II. The BIC value for the set of emitters is very similar to the quantitative prior knowledge analyses of the nickel spiked alumina 1000 ppm and the optimal set of emitters needed to explain the experimental spectrum of thirteen peaks is {Al I, Al II, Ni I, Ni II}. The common emitters to all three knowledge analyses are Al I and Ni I.

Table 48: Quantitative prior BIC ordering of Ni-spiked alumina – 2000 ppm.

Emitter	BIC
Ni II	209.77
Ni II, Al I	133.89
Ni II, Al I, Ni I	97.00
Ni II, Al I, Ni I, Al II	94.74

Posterior SIF

The posterior SIF for the no prior knowledge and qualitative prior knowledge analyses of the nickel doped alumina 2000 ppm have the same SIF values as the 1000 ppm (Figure 40 top and middle). For the no prior knowledge and qualitative prior knowledge analyses, eight peaks have

no spectral interferences and five have interferences that range from small to large. The experimental peaks with no interferences can be used for line assignment. The peaks with spectral interferences should be carefully evaluated by the user for LIBS line assignment.1

For the quantitative prior posterior SIF of the nickel spiked alumina 2000 ppm, there are nine peaks with a SIF of 100% (Figure 40 bottom). Neutral nickel is the sole emitter of peak 301.20 nm. Peaks 302.55 nm and 303.47 nm are produced by Ni II. Peak 302.45 nm has one emitter, Al II. Neutral aluminum is the sole contributor to peaks 305.47 nm, 305.72 nm, 306.44 nm, and 306.60 nm. Peaks 301.91 nm and 303.79 nm have spectral interferences between the neutral and singly-ionized nickel. The LIBS spectral line assignment of those two peaks are considered an emission from nickel. Peaks 305.02 nm and 305.87 nm have spectral interferences. The main contributor to these peaks is Al I with a minor interference from Ni I. There are three peaks common to all three knowledge analyses which have 100% SIF assignment. Peaks 301.20 nm, 305.72 nm, and 306.44 nm can be used for assignment of Ni I, Al I, and Al I respectively.

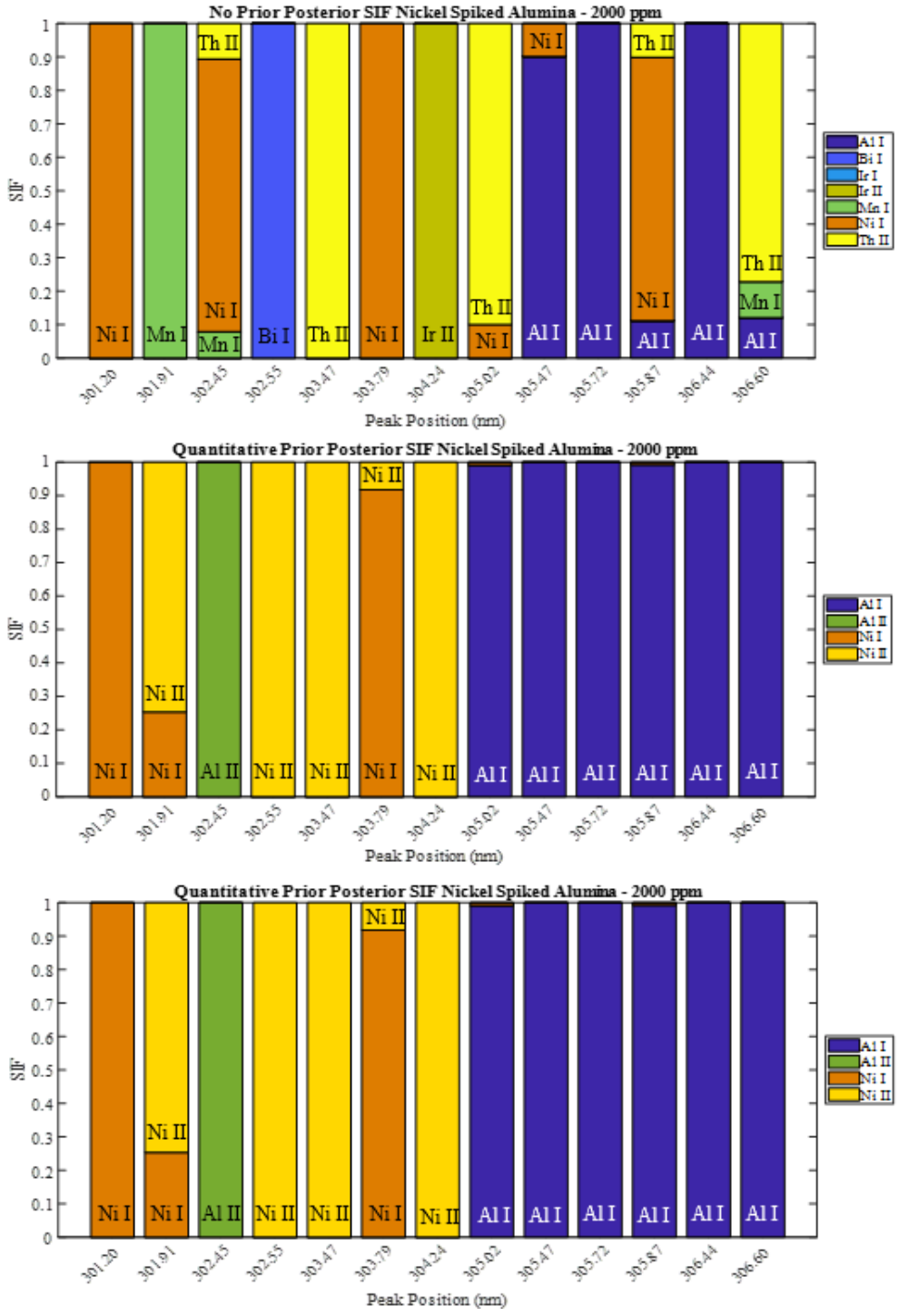

Figure 40: Posterior SIF for Ni-spiked alumina – 2000 ppm (Top) No Prior (Middle) Qualitative Prior (Bottom) Quantitative Prior.

Comparison of Varied Nickel Spiked Alumina Samples

Comparison of the peaks from the 0 ppm, 1000 ppm, and 2000 ppm nickel spiked alumina samples, results in thirteen peaks in the spectral region of 300 nm to 307 nm. The blank nickel spiked alumina samples no prior knowledge results are different from the 1000 ppm and 2000 ppm because the peaks 301.20 nm, 301.91 nm, and 303.78 nm peaks that are attributed to nickel are absent. From the blank, peaks 305.02 nm, 305.47 nm, 305.72 nm, 306.44 nm, and 306.60 nm are aluminum emissions but could be interfered by nickel. Table 49 shows the quantitative results for the SIF of the three concentrations.

Table 49: Quantitative posterior SIF of Ni-spiked alumina[111].

Peak (nm)	301.20	301.91	302.45	302.55	303.47	303.79	304.24	305.02	305.47	305.72	305.87	306.44	306.60
Emitter	0ppm												
Al I	-	-	-	-	-	-	0	1	1	1	1	1	1
Al II	-	-	1	-	-	-	1	-	-	-	-	-	-
	1000ppm												
Al I	0	0	0	0	0	0	0	0.996	1	1	0.996	1	1
Al II	0	0	1	0.005	0	0	0	0	0	0	0	0	0
Ni I	1	0.254	0	0	0	0.919	0	0.004	0	0	0.004	0	0
Ni II	0	0.746	0	0.995	1	0.081	1	0	0	0	0	0	0
	2000ppm												
Al I	0	0	0	0	0	0	0	0.992	1	1	0.992	1	1
Al II	0	0	1	0	0	0	0	0	0	0	0	0	0
Ni I	1	0.253	0	0	0	0.919	0	0.008	0	0	0.008	0	0
Ni II	0	0.747	0	1	1	0.081	1	0	0	0	0	0	0

From Table 49, two different cases are seen. The peaks at 305.47 nm, 305.72 nm, 306.44 nm, and 306.60 nm are one case. The presence of nickel does not affect these peaks' individual SIF values. The other case involves the peaks at 305.02 nm and 305.87 nm where the main contributor is Al I. The interference from Ni I transitions can be seen as the Ni I concentration

increases from 0% to 0.4% to 0.8% with the concentrations of 0 ppm, 1000 ppm, and 2000 ppm respectively. As the nickel concentration and SIF increases, the Al I SIF decreases for peaks 305.02 nm and 305.87 nm. The possible interference of nickel for the aluminum is not apparent for the first case of peaks which can be used for aluminum line assignment. The second case where the concentration of nickel and the SIF values are proportional should not be used for aluminum peak assignment.

Variance of Statistical Interference Factor

The reproducibility of the quantitative posterior SIF was evaluated for NIST SRM 616 samples of twenty-five replicates. A subset of nineteen peaks was used to show the variance of the posterior SIF values obtained for elements present within the SRM 616 sample composition with quantitative prior knowledge. Peaks were chosen that included strontium, aluminum, calcium, iron, gallium, sodium, potassium, and silicon as these elements were present in SRM 616 and in higher concentrations. Table 50 shows the nineteen peaks, their emitter, and six replicate posterior SIF values. Replicates of SRM 616 varied in detected peaks, intensities, and optimal set of emitters. Replicate 6 was absent of peaks 227.49 nm and 243.84 nm which resulted in a posterior SIF assignment of 0. Peak 237.24 nm was present but did not have any aluminum transitions present within the experimental peak's width resulting in a posterior SIF of 0. A 95% confidence interval was calculated to determine the probability that the population mean of the posterior SIF of each individual peak in the subset lies within a specific range.

Table 50: Six replicate posterior SIFs for NIST SRM 616 nineteen-peak subset.

Emitter	Peak	Rep 1	Rep 2	Rep 3	Rep 4	Rep 5	Rep 6
Sr I	227.49	0.4611	0.2129	0.125	0.2524	0.3366	0
Al I	237.27	0.2133	0.1923	0.1494	0.2036	0.9842	0
Si I	243.84	0.0343	0.0146	0.0044	0.005	0.0319	0
Ga I	250.02	0.9914	0.5449	0.9987	0.999	0.991	0.9996
Al I	257.49	0.5363	0.3251	0.2558	0.4099	0.4444	0.9533
Ca I	299.47	0.0673	0.5379	0.1548	0.3156	0.8435	0.9078
Ca I	299.74	0.2371	0.373	0.0642	0.1052	0.523	0.0734
Al I	305.69	0.9217	0	0.7033	0.8876	0.8606	0
Al I	308.21	0.7685	0.7237	0	0.8965	0.7191	0.7862
Ca II	317.91	0.2717	0.2979	0.3113	0.34	0.2372	0.3966
Fe I	387.79	0.0301	0	0.0954	0.088	0.0344	0.0444
Si I	482.26	0.0019	0.000486	0.0033	0.0117	4.16E-08	0.0042
Fe II	507.99	0.002461	0	0.0057	0.000448	0.005	0.002424
Fe I	549.84	0.0279	0.0345	0.0069	0.0103	0.0505	0.0648
Si II	566.92	0.0541	0	0.1962	0.0849	0.107	0.0716
Na I	615.45	0.1736	0.3005	0.6295	0.6936	0.3367	0.4284
Ca I	657.27	0.9992	0.1828	0.3728	0.4854	0.1701	0.2837
Sr I	723.16	0.6367	0	0.5164	0.6692	0.5937	0
K I	766.54	0.9998	0.9997	0.9993	0.9994	0.9998	0.9998

Figure 41 shows the 95% confidence interval of the nineteen-peak subset's posterior SIF. Peaks 257.49 nm, 299.48 nm and 766.54 nm had a posterior SIF of 1 for every replicate which resulted in 100% probability. Peaks 237.27 nm, 305.69 nm, 507.99, and 615.45 nm had the largest confidence intervals resulting from replicates that were missing peaks or not having the emitter's transition present within the experimental peak.

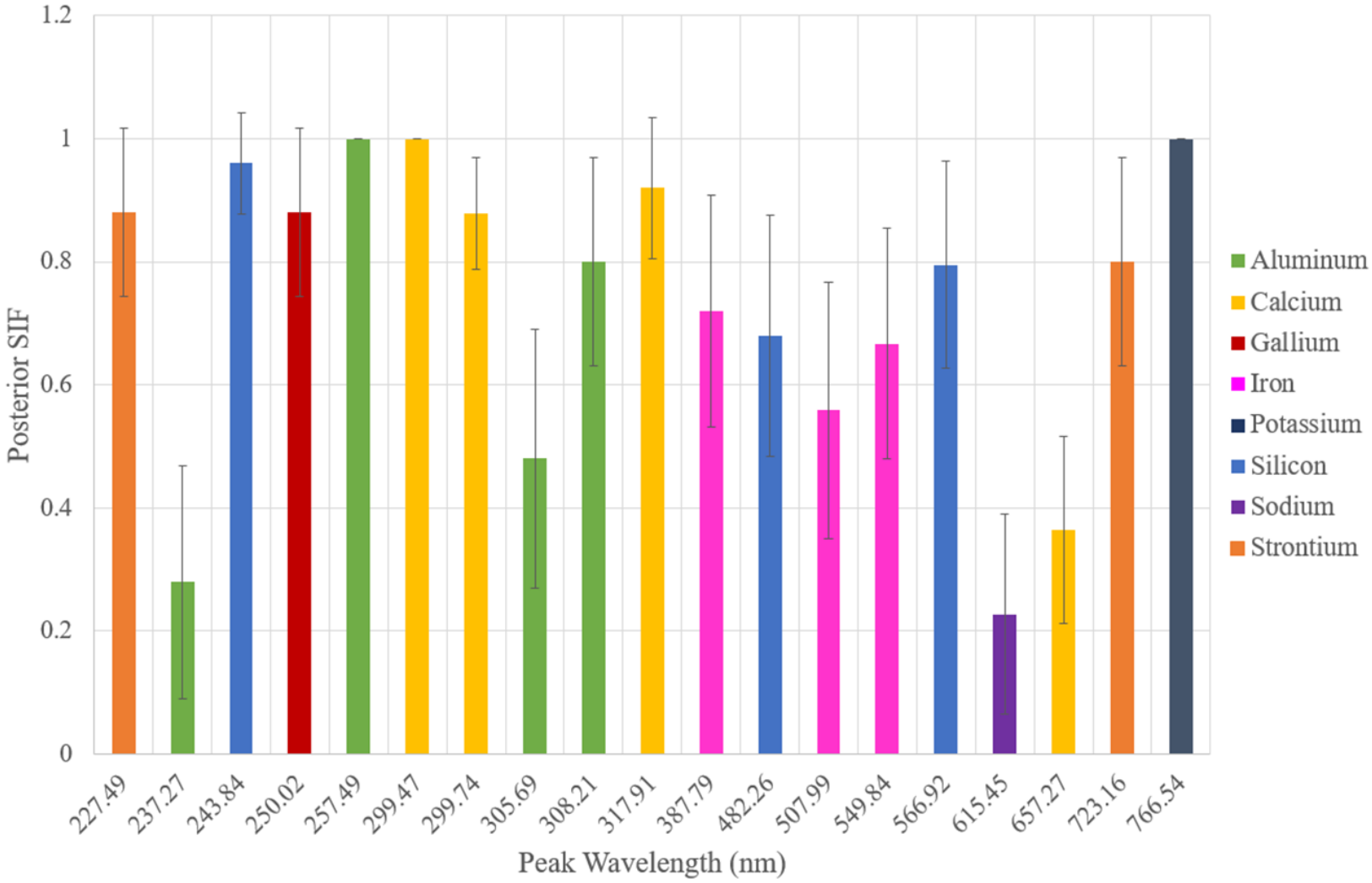

Figure 41: Confidence interval for NIST SRM 616 nineteen-peak subset.

A confidence interval greater than 1 for the posterior SIF means that the peaks 227.49 nm, 243.84 nm, 250.02 nm, and 317.91 nm average values fluctuate and have more variability which causes the wider confidence intervals. The sample size for the replicates was 25 which is small which could also generate wider confidence intervals.

A chi-square hypothesis test of variance was conducted to evaluate the variance between the twenty-five replicates posterior SIF values. The chi-square equation is defined as the test statistic t:

$$\boldsymbol{t = \frac{(n-1)s^2}{\sigma_0^2}} \quad \textbf{(66)}$$

Where n is the sample size, s the replicate standard deviation, and σ_0 the population variance. The null hypothesis was that the replicate variance and population variance were equal and the alternative hypothesis that the replicate and population variances were unequal which is a two-tailed test. Given the nineteen peaks and their emitter, the population mean was $2.27 * 10^{-3}$ and the sample set 25. The significance level tested was $\alpha = 0.05$. The chi-square test statistic t was 0.82 for the nineteen-peak subset of SRM 616 which was compared to the $\chi^2_{\alpha=0.05/2} = 31.526$[126]. The null hypothesis was not rejected because the test statistic is less than table value which means that the variance found within the replicates is statistically equal to the population variance. A p-value was calculated for the chi-square hypothesis test of variance which determines the probability of obtaining a test statistic greater than or equal to what was observed,

and was $6.02 * 10^{-10}$. This means that there is very little variability between replicates' emitters and their posterior SIF values which leads to confidence and replicability of the posterior SIF.

CHAPTER 7: CONCLUSION

The purpose of this study was to develop a statistical interference factor (SIF) to quantify spectral interferences in optical emission spectroscopy (OES) for elemental analysis for identification purposes. The SIF algorithm combines the fundamentals of plasma emission of optical emission spectroscopy with a Bayesian analysis. Characteristics of OES of little to no sample preparation, real-time analysis, and small sample size requirement make it attractive in determining the elemental profile of a sample. This method is unique to OES in that it can analyze a single unknown spectrum without the need for reference spectra. The use of the SIF algorithm will allow users to quickly identify spectral interferences to judge which spectral lines can be confidently used for analysis.

The pure silicon sample was analyzed with no prior and qualitative prior knowledge of the sample composition. This analysis lead to silicon being the main emitter for 60% of the experimental peaks. The qualitative and no prior knowledge analyses for silicon had the same main contributor 67.5%. The effect of a minor element on the posterior SIF was analyzed by nickel spiked at different concentrations alumina samples. Peaks attributed only to aluminum had no spectral interferences and were not affected by the presence of nickel in the sample. The interference of Ni I to Al I increased with the nickel concentration for peaks 305.02 nm and 305.87 nm by 0.4% and 0.8% for 1000 ppm and 2000 ppm respectively. More complex samples with trace interfering elements were evaluated for the NIST SRM 600 glass series for no prior, qualitative prior, and quantitative prior knowledge of the sample composition.

Knowledge of the sample composition for NIST SRM 610, had the main contributor the same 66.27% whereas all prior knowledge analyses of SRM 610 had 40.02%. The lower match between all prior knowledge analyses results from the different optimal set of emitters between all analyses. SRM 612 had a smaller match between the main emitter of all three knowledge analyses with 36.91% than 610. The qualitative and quantitative prior knowledge of the concentrations affected the individual SIF which produced different optimal set of emitters to explain the spectrum. The emitter with the highest SIF for all three prior knowledge analyses occurred 34.38% for SRM 614. The elemental profile between the qualitative and quantitative was different in that Th II was not needed to explain the quantitative experimental spectrum. The number of certified reference elements added to SRM 616 was much smaller than the other glass 600 series which influenced the optimal set of emitters. The optimal set of emitters was very different plus the concentrations affected the individual SIF which provides the information needed to calculate the combinations of the emitters with the highest likelihood. NIST SRM 1243 had many experimental peaks. The posterior SIF had the same emitter for 23.14% of all three prior knowledge analyses due to differences in the no prior and prior knowledge. No prior knowledge of SRM 1243 needed ninety emitters to explain the spectrum because so many emitters had at least one contributing transition to the experimental spectrum. The optimal set of emitters and the prior knowledge affect the combinations of emitters which results in different elemental profiles in the three knowledge analyses as the samples become more complex in number of peaks and elements in the sample composition. The variance of the posterior SIF for twenty-five replicates of SRM 616 was consistent throughout all replicates. This leads to

confidence and reproducibility in the posterior SIF results from day to day fluctuations. This work estimates the error rates of the uncertainty of elemental profiles of optical emission spectroscopy which strengthen OES as a forensic analytical tool. By providing a quantification of the spectral interference error, a more accurate analysis can be obtained and lead to confidence in the elemental profile of an unknown sample.

Future work

Commercial systems don't usually allow for the plasma temperature to be estimated. Measurement of the excitation temperature would provide more accurate results and show how temperature affects the matching factor and the transition probability with the upper energy level of an emitter. Optimization of the posterior SIF would provide more top combinations of emitters for a sample. As of now, when there are more than four-hundred peaks only the top 100,000 combinations can be calculated. Spectral interferences can arise in the combinations with low likelihoods and the addition of more combinations would result in more accurate analysis. The posterior SIF is dependent on the optimal set of emitters to explain the experimental spectrum. Further studies of the same set of emitters would evaluate any variance in the posterior SIF of different prior knowledge analyses.

REFERENCES

1. Nicolodelli, G., et al. "Quantification of total carbon in soil using laser-induced breakdown spectroscopy: a method to correct interferences lines." *Appl. Opt.* 53.10 (2014): 2170-2176.
2. Martin, M.Z., et al. "Analysis of preservative-treated wood by multivariate analysis of laser-induced breakdown spectroscopy spectra." *Spectrochim. Acta, Part B* 60.7-8 (2005): 179-1185.
3. Wan, X. and Wang, P. "Analysis of heavy metals in organisms based on an optimized quantitative LIBS." *Optik* 126.19 (2015): 1930-1934.
4. Rehse, S.J., H. Salimnia and A.W. Miziolek. "Laser-induced breakdown spectroscopy (LIBS): an overview of recent progress and future potential for biomedical applications." *J. Med. Eng. Technol.* 36.2 (2012): 77-89.
5. Singh, V.K., et al. "Importance of laser-induced breakdown spectroscopy for ahrd tissues (bone, teeth) and other calcified tissue materials." *Laers in Medical Science* 30.6 (2014): 1763-1778.
6. Grifoni, E., et al. "Applying LIBS to metals processing." *Spectroscopy* 30.11 (2015): 20-31.
7. Sanghapi, H. C. A. K.; Jain, J.; Bolshakov, A.; Lopano, C.; Mcintyre, D.; Russo, R. “Determination of elemental composition of shale rocks by laser induced breakdown spectroscopy.” *Spectrochim. Acta, Part B* **2016**, *122*, 9-14.

8. Bridge, C.M., et al. "Characterization of automobile float glass with laser-induced breakdown spectroscopy and laser ablation inductively coupled plasma mass spectrometry." *Appl. Spectrosc.* 60.10 (2006): 1181-1187.

9. Trejos, T., A. Flores and J.R. Almirall. "Micro-spectrochemical analysis of document paper and gel inks by laser ablation inductively coupled plasma mass spectrometry and laser induced breakdown spectroscopy." *Spectrochim. Acta, Part B* 65.11 (2010): 884-895.

10. Jantzi, S.C. and J.R. Almirall. "Characterization and forensic analysis of soil samples using laser-induced breakdown spectroscopy (LIBS)." *Anal. Bioanal. Chem.* 400.10 (2011): 3341-3351.

11. Boumans, P.W.J.M.. *Inductively Coupled Plasma Emission Spectroscopy, Part 1: Methodolgy, Instrumentation and Performance*. Chichester: John Wiley & Sons, 1987.

12. Hou, Z., et al. "A hybrid quantification model and its application for coal analysis using laser induced breakdown spectroscopy." *J. Anal. At. Spectrom.* 31.3 (2016): 722-736.

13. Rabb, S.A., et al. "Problems, possibilities and limitations of inductively coupled plasma atomic emission spectrometry in the determination of platinum, palladium and rhodium in samples with different matrix composition." *Spectrochim. Acta, Part B* 65.2 (2010): 130-136.

14. *ICP-MS_Review*. 28 October 2016. 24 June 2018. <www.biochem.pepperdine.edu/dokuwiki/doku.php?id=chem331:icp-ms_review>.

15. Zhang, X. and M. Cresswell. *Inorganic Controlled Release Technology*. New York: Butterworth-Heinemann, 2015.

16. Petrova, P., et al. “Problems, Possibilities and Limitations of Inductively Coupled Plasma Atomic Emission Spectrometry in the Determination of Platinum, Palladium and Rhodium in Samples with Different Matrix Composition.” *Spectrochimica Acta Part B: Atomic Spectroscopy*, vol. 65, no. 2, 2010, pp. 130–136.,

17. Boevski, I.I., et al. "Inductively coupled plasma atomic emission spectrometry - accuracy of analytical results and detection limits in the determination of trace elements in soils and sediments." *Eurasian J. Anal. Chem.* 3.1 (2008): 19-33.

18. Song, Yong-III L. and Joseph Sneddon. *Laser-induced breakdown spectrometry*. New York: Nova Science Publishers, 2000.

19. Miziolek, A.W., V. Palleschi and I. Schechter. *Laser-induced breakdown spectroscopy (LIBS): fundamentals and applications*. Cambridge: Cambridge University Press, 2006.

20. Fan, C.H., J. Sun and J.P. Longtin. "Breakdown threshold and localized electron density in water induced by ultrashort laser pulses." *J. Appl. Phys.* 91.4 (2002): 2530-2536.

21. Gerhard, C., et al. "Quantitative analyses of glass via laser-induced breakdown spectroscopy in argon." *Spectrochim. Acta, Part B* 101.1 (2014): 32-45.

22. Cremers, D.A. and L.J. Radziemski. *Handbook of Laser-Induced Breakdown Spectroscopy*. Chichester: John Wiley & Sons, 2013.

23. Kaiser, J., et al. "Trace elemental analysis by laser-induced breakdown spectroscopy - biological applications." *Surf. Sci. Rep.* 67.11-12 (2012): 233-243.

24. Hussain, T. and M.A. Gondal. "Laser induced breakdown spectroscopy (LIBS) as a rapid tool for material analysis." *J. Phys. Conf. Ser.* 439 (2013): 12050-12062.

25. Radziemski, L.J., et al. "Time-resolved laser-induced breakdwon spectrometry of aerosols." *Anal. Chem.* 55.8 (1983): 1246-1252.

26. McLauglin, R.P., et al. "Note: A portable laser induced breakdown spectroscopy instrument for rapid sampling and anlysis of silicon-containing aerosols." *Rev. Sci. Instrum.* 87.5 (2016).

27. Connors, B., D. Day and A. Somers. "Application of handheld laser-induced breakdown spectroscopy (LIBS) to geochemical analysis." *Appl. Spectrosc.* 70.5 (2016): 810-815.

28. Lee, Y., et al. "Laser-ablation sampling for accurate analysis for sulfur in edible salts." *Appl. Spectrosc.* 71.4 (2017): 651-658.

29. Arnquist, I.J., T.E. Kreschollek and J.A. Holcombe. "Simultaneous electrothermal vaporization and nebulizer sample introduction system for inductively coupled plasma mass spectrometry." *Spectrochim. Acta, Part B* 66.3 (2011): 255-260.

30. Prakash, V., et al. "Correlation of the Material Composition and Transistional Phases During Stress, on Cyclic Fatigue of Three Different Ni-ti Rotary File System." *Biosci. Biotechnol. Res. Asia* 13.4 (2016): 2037-2044.

31. Brenner, I.B. and A.T. Zander. "Review: Axially and radially viewed inductively coupled plasmas - a critical review." *Spectrochim. Acta, Part B.* 55.8 (2000): 1195-1240.

32. Lorenzen, C.J., et al. "Applications of laser-induced emission spectral analysis for industrial process and quality control." *J. Anal. At. Spectrom.* 7.6 (1992): 1029-1035.

33. Yu, K.-Q., et al. "Laser-Induced Breakdown Spectroscopy Coupled with Multivariate Chemometrics for Variety Discrimination of Soil." *Sci. Reports* (2016): 1-10.

34. Demtröder, W. *Laser Spectroscopy*. Vol. 1. Berlin: Springer, 2008.

35. Griem, H.R. *Spectral Line Broadening by Plasmas*. New York: Academic Press, 1974.

36. Larson, G.F. and V.A. Fassel. "Line broadening and radiative recombination background interferences in inductively coupled plasma-atomis emission spectroscopy." *Appl. Spectrosc.* 33.6 (1979): 592-599.

37. Gornushkin, I. "Line broadening mechanisms in the low pressure laser-induced plasma." *Spectrochim. Acta, Part B* 54.8 (1999): 1207-1217.

38. Moreno, J. C., et al. "Doppler-Shifted Line Profiles from Spherically Expanding Plasmas."*Journal of the Optical Society of America B*, vol. 9, no. 3, 1992, pp. 339–343., doi:10.1364/josab.9.000339.

39. Griem, H. "Doppler-shifted line profiles from spherically expanding plasmas." *J. Opt. Soc. Am.* 9.3 (1992): 339-343.

40. Ochkin, V.N. *Spectroscopy of Low Temperature Plasma*. Weinheim: Wiley-VCH, 2009.

41. Muñoz, J., et al. "Using the van der Waals broadening of spectral atomic lines to measure the gas temperature of an argon-helium microwave plasma at atmospheric pressure." *Spectrochim. Acta, Part B* 64.2 (2009): 167-172.

42. Ali, A.W. and H.R. Griem. "Theory of resonance broadening of spectral lines by atom-atom impacts." *Phys. Rev.* 140.4A (1965): A1044-A1049.

43. Stollberg, C., et al. "Revisiting the stark width and shift of He II Pα." *Emitters* 6.2 (2018): 23-35.

44. Surmick, D.M. and C.G. Parigger. "Electron density determination of aluminum laser-induced plasma." *J. Phys. B: At., Mol. Opt. Phys.* 6.23 (2015): 115701-115707.

45. Konjević, N. "Plasma broadening and shifting of non-hydrogenic spectral lines: present status and applications." *Phys. Rep.* 316.6 (1999): 339-401.

46. Sharaparev, N.Y. "New possibilities of using the voigt profile." *Russian Physics Journal* 59.12 (2017): 2004-2011.

47. Yi, R., et al. "Investigation of the self-absorption effect using spatially resolved laser-induced breakdown spectrocopy." *J. Anal. At. Spectrom.* 31 (2016): 961-967.

48. Kramida, A., et al. "NIST Atomic Spectra Database, ver. 5.5.2." (2018). online. <http://physics.nist.gov/asd>.

49. Kurucz, R. and B. Bell. "1995 Atomic Line Data." Cambridge: Smithsonian Astrophysical Observatory, n.d. <http://www.cfa.harvard.edu/amp/ampdata/kurucz23/sekur.html>.

50. Harrison, G.R. and F.M. Phelps. *Massachusetts Institute of Technology wavelength tables*. Cambridge: MIT Press, 1969.

51. Kelly, R. "Kelly Atomic Line Database." 2005.

52. Zhang, S., et al. "Review: Laser induced plasma temperature." *Spectrochim. Acta, Part B* 97.2 (2014): 13-33.

53. Boiteux, H. *Flame Spectroscopy*. New York: John Wiley , 1965.

54. Apruzese, J.P., et al. "The physics of radiation transport in dense plasmas." *Phys. Plasmas* 9.5 (2002): 2411-2419.

55. Cristoforetti, G., et al. "Local thermodynamic equilibrium in laser-induced breakdown spectroscopy: beyond the McWhirter criterion." *Spectrochim. Acta, Part B* 65 (2010): 86-95.

56. Cristoforetti, G., E. Tognoni and L.A. Gizzi. "Review: Thermodynamic equilibrium states in laser-induced plasmas: from the general case to laser-induced breakdown spectroscopy plasmas." *Spectrochimc. Acta, Part B* 90 (2013): 1-22.

57. Chance, K. and R.V. Martin. *Spectroscopy and Radiative Transfer of Planetary Atmospheres*. Oxford: Oxford University Press, 2017.

58. Boumans, P.W.J.M.. *Theory of Spectrochemical Excitation*. New York: Plenum Press, 1966.

59. Charfi, B. "Theoretical calculation of population on excited level of emitting atomic species in water plasma." *Physics Procedia* 2.3 (2009): 1481-1487.

60. Griem, H.R. *Principles of Plasma Spectroscopy*. Cambridge: Cambridge University Press, 1997.

61. Christen, T., F. Kassubek and R. Gati. "Radiative Heat Transfer and Effective Transport Coefficients." Belmiloudi, A. *Heat Transfer- Mathematical Modelling, Numerical Methods and Information Technology*. New York: InTech, 2011. 102-120.

62. Unnikrishnan, V.K., et al. "Measurements of plasma temperature and electron density in laser-induced copper plasma by time-resolved spectroscopy of neutral emitters and ion emissions." *Pramana* 74.6 (2010): 983-993.

63. Bye, C.A. and A. Scheeline. "Saha-Boltzmann statistics for determination of electron temperature and density in spark discharges using an Echelle/CCD system." *Appl. Spectrosc.* 47.12 (1993): 2022-2030.

64. Liao, L. and J. He. "Discussion on laser-induced plasma diagnostics under condition of optically thick." *Optik* 127.11 (2016): 4878-4880.

65. Gornushkin, I. "Determination of the maximum temperature at the center of an optically thick laser-induced plasma using self-reversed spectral lines." *Appl. Spectrosc.* 58.9 (2004): 1023-1031.

66. Yang, J., et al. "A calibration-free laser-induced breakdown spectroscopy (CF-LIBS) quantitative analysis method based on the auto-selection of an internal reference line and optimized estimation of plasma temperature." *Appl. Spectrosc.* 72.1 (2017): 129-140.

67. Li, J., et al. "Evaluation of the self-absorption reduction of minor elements in laser-induced breakdown spectroscopy assisted with laser-stimulated absorption." *J. Anal. At. Spectrom.* 32.11 (2017): 2189-2193.

68. Tognoni, E., et al. "Combination of the ionic-to-atomic line intensity ratios from two test elements for the diagnostic of plasma temperature and electron number density in inductively coupled plasma atomic emission spectroscopy." *Spectrochim. Acta, Part B* 62.5 (2007): 435-443.

69. Xiao, X., X. Hua and Y. Wu. "Comparison of temperature and composition measurement by spectroscopic methods for argon-helium arc plasma." *Optics and Laser Technology* 66 (2015): 138-145.

70. Camacho, J., et al. "Optical emission studies of nitrogen plasma generated by IR CO2 laser pulses." *J. Phys. B: At. Mol. Opt. Phys.* 40.24 (2007): 4537-4590.

71. Aguilera, J.A. and C. Aragón. "Characterization of laser-induced plasma during its expansion in air by optical emission spectroscopy: observation of strong explosion self-similar behavior." *Spectrochim. Acta, Part B* 63.9 (2008): 893-916.

72. Goddard, B.J. "Materials analysis using laser-based spectroscopic techniques." *Transactions of the Institute of Measurement and Control* 13.3 (1991): 128-139.

73. Nekahi, A. and M. Farzaneh. "Excitation temperature determination of an arc formed over an ice surface using optical emission spectroscopy." *IEEE Transactions on Dielectrics and Electrical Insulation* 18.6 (2011): 1829-1834.

74. Burton, L.L. and M.W. Blades. "A simple method for calculating deviations from local thermodynamic equilibrium in the inductively coupled plasma." *Spectrochim. Acta, Part B* 45.1-2 (1990): 139-144.

75. Gornushkin, I.B., et al. "Effects of non-uniformity of laser induced plasma on plasma temperature and concentrations determined by the Boltzmann plot method: implications from plasma modeling." *J. Anal. At. Spectrom.* 25.10 (2010): 1643-1653.

76. Zafar, A., et al. "A temporally and spatially resolved electron density diagnostic method for the edge plasma based on Stark broadening." *Review of Scientific Instruments* 87.11 (2016): 11E505-1 - 11E505-3.

77. National Resarch Council. *Strengthening Forensic Science: A Path Forward*. Washing,DC: National Academies Press, 2009.

78. Hübert, W. and G. Ankerhold. "Elemental misinterpretation in automated analysis of LIBS spectra." *Anal. Bioanal. Chem.* 400.10 (2011): 3273-3278.

79. Lajunen, L.H.J. *Spectrochemical analysis by atomic absorption and emission*. Cambridge: Royal Society of Chemistry, 2004.

80. Larson, G.F. and V.A. Fassel. "Comparison of interelement effects in a microwave single electrode plasma and in a radio frequency inductively coupled plasma." *Anal. Chem.* 48 (1976): 1161-1166.

81. 83. Hahn, D.W. and N. Omenetto. "Laser-induced breakdown spectroscopy (LIBS), part II: review of instrumental and methodological approaches to material analysis and applications to different fields." *Appl. Spectrosc.* 66.4 (2012): 347-419.

82. Kuba, J. *Coincidence tables for atomic spectroscopy; principal lines for emission spectral analysis with coincidences from 2,000 to 10,000 Å.* Amsterdam: Elsevier Pub. Co., 1965.

83. Boumans, P.W.J.M. "Detection limit including selectivity as a criterion for line selection in trace analysis using inductively coupled plasma-atomic emission spectrometry (ICP-AES) - a tutorial treatment of a fundamental problem of AES." *Spectrochim. Acta, Part B* 42.6 (1987): 819-840.

84. Baloyi, J.N. "Spectral Interferences in ICP-OES." *Analytical Challenges in Metallurgy*. Randburg, 2006.

85. Fassel, V.A., J.M. Katzenberger and R.K. Winge. "Effectiveness of interference filters for reduction of stray light effects in atomic emission spectrometry." *Appl. Spectrosc.* 33.1 (1979): 1-5.

86. Goode, S.R. and S.R. Crouch. "Practical method for the determination of stray radiant energy in atomic emission spectrometers." *Anal. Chem.* 46.1 (1974): 181-182.

87. Ruscic, B. "Uncertainty quantification in thermochemistry, benchmarking electonic structure computations, and active thermochemical tables." *Int. J. Quantum Chem.* 114 (2014): 1097-1101.

88. Ellison, S.L.R. and A. Williams. *Quantifying uncertainty in analytical measurement*. Ed. 3rd. Eurachem, 2012.

89. Saffaj, T. and B. Ihssane. "Uncertainty profiles for the validation of analytical methods." *Talanta* 85.3 (2011): 1535-1542.

90. Andersen, J.E.T. "On the development of quality assurance." *TrAC Trends in Analytical Chemistry* 60 (2014): 16-24.Boumans, P.W.J.M. "Detection limits and spectral interferences in atomic emission spectrometry." *Anal. Chem.* 66.8 (1994): 459a-467a.

91. Winge, R.K., et al. "ICP emission spectrometry: on the selection of analytical lines, line coincidence tables, and wavelength tables." *Appl. Spectrosc.* 36 (1982): 210-221.

92. Boumans, P.W.J.M. and A.H.M. Van Ham-Heijms. "Simulation of atomic spectra - II. mutual spectral interferences of rare earth elements in the inductively coupled plasma." *Spectrochim. Acta, Part B* 46.14 (1991): 1863-1883.

93. Thomsen, V., D. Schatzlein and D. Mercuro. "Interelement corrections in spectrochemistry." *Spectroscopy* 21.7 (2006): 32-40.

94. Boumans, P.W.J.M., J.A. Tielrooy and F.J.M.J. Maessen. "Mutual spectral interferences of rare earth elements in inductively coupled plasma atomic emission spectrometry. I. rational line selection and correction procedure." *Spectrochim. Acta, Part B* 43 (1988): 173-199.

95. Boumans, P.W.J.M.. "Line interference, line selection, and true detection limit in inductively coupled plasma emission spectrometry." *Spectrochim. Acta, Part B* 45.10 (1990): 1121-1138.

96. Andrade, J.M., et al. "Classical univariate calibration and partial least squares for quantitative analysis of brass samples by laser-induced breakdown spectroscopy." *Spectrochim. Acta, Part B* 65.8 (2010): 658-663.

97. Gornushkin, I.B., et al. "Identification of solid materials by correlation analysis using a microscopic laser-induced plasma spectrometer." *Anal. Chem.* 71.22 (1999): 5157-5164.

98. Anzano, J.M., et al. "Laser-induced plasma spectroscopy for characterization of archaeological material." *Can. J. Anal. Sci. Spectrosc.* 47 (2002): 134-140.

99. Anzano, J.M., et al. "Laser-induced plasma spectroscopy for plastic identification." *Polym. Eng. Sci.* 40 (2000): 2423-2429.

100. Press, W.H. *Numerical Recipes: the Art of Scientific Computing*. New York: Cambridge University Press, 2007.

101. Jurado-López, A. and L. de Castro. "Rank correlation of laser-induced breakdown spectroscopic data for the identification of alloys used in jewelry manufacture." *Spectrochim. Acta, Part B* 58.7 (2003): 1291-1299.

102. Labutin, T.A., S.M. Zaytsev and A.M. Popov. "Automatic identification of emission lines in laser-induced plasma by correlation of model and experimental spectra." *Anal. Chem.* 85.4 (2013): 1985-1990.

103. Chappell, J., M. Martinez and M. Baudelet. "Statistical evaluation of spectral interferences in LIBS." *Spectrochim. Acta Part B* (2018) [manuscript in review].

104. MATLAB and Signal Processing Toolbox Release R2018a, The MathWorks, Inc., Natick, Massachusetts, United States.

105. Ida, T., M. Ando and H. Toraya. "Extended pseudo-Voigt function for approximating the Voigt profile." *J. Appl. Cryst.* 33.6 (2000): 1311-1316.

106. Kim, J.H. "Chi-square goodness-of-fit testing randomly censored data." *Ann. Statist*. 21.3 (1993): 1621-1639.

107. NIST/SEMATECH e-Handbook of Statistical Methods, http://www.itl.nist.gov/divd898/handbook/

108. Pořĭka, P., et al. "Detection of fluorine using laser-induced breakdown spectroscopy and Raman spectroscopy." *J. Anal. At. Spectrosc.* 32.10 (2017): 1966-1974.

109. Labutin, T.A., S.M. Zaytsev and A.M. Popov. "Automatic identification of emission lines in laser-induced plasma by correlation of model and experimental spectra." *Anal. Chem.* 85.4 (2013): 1985-1990.

110. Gelman, A., et al. *Bayesian Data Analysis*. New York: CRC Press, 2003.

111. Kalyanaraman, J., et al. "Uncertainty quantification via bayesian inference using sequential monte carlo methods for CO2 adsorption process." *AlChE Journal* 62.9 (2016): 3352-3368.

112. Kennedy, M.C. and A. O'Hagan. "Bayesian calibration of computer models." *Journal of the Royal Statistical Society: Series B (Statistical Methodology)* 63.3 (2001): 425-464.

113. Lesaffre, E. and A.B. Lawson. *Bayesian Biostatistics*. Chichester: Wiley, 2012.

114. Schwarz, G. "Estimating the dimension of a model." *Ann. Statist.* 6 (1978): 461-464.

115. Rust, R.T., et al. "Model selection criteria: an investigation of relative accuracy, posterior probabilities, and combinations of criteria." *Management Science* 41 (1995): 322-333.

116. National Institute of Standards and Technology Standard Reference Materials Program (2012) *Certificate of Analysis, Standard Reference Material 610, Trace Elements in Glass*, NIST, Gaithersburg, MD, USA, https://www-s.nist.gov/srmors/certificates/610.pdf

117. National Institute of Standards and Technology Standard Reference Materials Program (2012) *Certificate of Analysis, Standard Reference Material 612, Trace Elements in Glass*, NIST, Gaithersburg, MD, USA, https://www-s.nist.gov/srmors/certificates/612.pdf

118. National Institute of Standards and Technology Standard Reference Materials Program (2012) *Certificate of Analysis, Standard Reference Material 614, Trace Elements in Glass*, NIST, Gaithersburg, MD, USA, https://www-s.nist.gov/srmors/certificates/614.pdf

119. National Institute of Standards and Technology Standard Reference Materials Program (2012) *Certificate of Analysis, Standard Reference Material 616, Trace Elements in Glass*, NIST, Gaithersburg, MD, USA, https://www-s.nist.gov/srmors/certificates/616.pdf

120. National Institute of Standards and Technology Standard Reference Materials Program (2012) *Certificate of Analysis, Standard Reference Material 1243, Ni-Cr-Co Alloy UNS N07001*, NIST, Gaithersburg, MD, USA, https://www-s.nist.gov/srmors/certificates/1243.pdf

121. Pandey, S.J., et al. *Spectrochim. Acta Part B* 148 (2018): 99-104.

122. Navidi, W.; Monk, B.. *Essential Statistics*. New York: McGraw-Hill, 2014.